Density Model for Seals (*Phocidae*) for the U.S. East Coast: Supplementary Report

Model Version 5.1

Duke University Marine Geospatial Ecology Laboratory*

2023-05-27

Citation

When citing our methodology or results generally, please cite Roberts et al. (2016, 2023). The complete references appear at the end of this document. We are preparing a new article for a peer-reviewed journal that will eventually replace those. Until that is published, those are the best general citations.

When citing this model specifically, please use this reference:

Roberts JJ, Yack TM, Cañadas A, Fujioka E, Halpin PN, Barco SG, Boisseau O, Chavez-Rosales S, Cole TVN, Cotter MP, Cummings EW, Davis GE, DiGiovanni Jr. RA, Garrison LP, Gowan TA, Jackson KA, Kenney RD, Khan CB, Lockhart GG, Lomac-MacNair KS, McAlarney RJ, McLellan WA, Mullin KD, Nowacek DP, O'Brien O, Pabst DA, Palka DL, Quintana-Rizzo E, Redfern JV, Rickard ME, White M, Whitt AD, Zoidis AM (2022) Density Model for Seals (*Phocidae*) for the U.S. East Coast, Version 5.1, 2023-05-27, and Supplementary Report. Marine Geospatial Ecology Laboratory, Duke University, Durham, North Carolina.

Copyright and License

Model Version History

Version	Date	Description
1	2015-01-22	Initial version.
2	2015-01-23	Added latitude as a predictor variable, to try to obtain a more realistic distribution along the east coast.
3	2015-01-24	Split the data into two seasons (Sep-May, Jun-Aug), based on the NOAA harbor seal stock assessment report.
3.1	2015-03-06	Updated the documentation. No changes to the model.
3.2	2015-05-14	Updated calculation of CVs. Switched density rasters to logarithmic breaks. No changes to the model. Model released as part of a scheduled update to the U.S. Navy Marine Species Density Database (NMSDD). Omitted from Roberts et al. (2016) journal publication, which only concerned cetaceans.

Version	Date	Description
4	2018-04-14	Began update to Roberts et al. (2015) model. Introduced new surveys from AMAPPS, NARWSS, UNCW, VAMSC, and the SEUS NARW teams. Updated modeling methodology. Refitted detection functions and spatial models from scratch using new and reprocessed covariates. Model released as part of a scheduled update to the U.S. Navy Marine Species Density Database (NMSDD).
5	2022-06-20	This model is a major update over the prior version, with substantial additional data, improved statistical methods, and an increased spatial resolution. It was released as part of the final delivery of the U.S. Navy Marine Species Density Database (NMSDD) for the Atlantic Fleet Testing and Training (AFTT) Phase IV Environmental Impact Statement. Several new collaborators joined and contributed survey data: New York State Department of Environmental Conservation, TetraTech, HDR, and Marine Conservation Research. We incorporated additional surveys from all continuing and new collaborators through the end of 2020. (Because some environmental covariates were only available through 2019, certain models only extend through 2019.) We increased the spatial resolution to 5 km and, at NOAA's request, we extended the model further inshore from New York through Maine. We reformulated and refitted all detection functions and spatial models. We updated all enviromental covariates to newer products, when available, and added several covariates to the set of candidates. For models that incorporated dynamic covariates, we estimated model uncertainty using a new method that accounts for both model parameter error and temporal variability.
5.1	2023-05-27	Completed the supplementary report documenting the details of this model. Corrected the 5 and 95 percent rasters so that they contain the value 0 where the taxon was asssumed absent, rather than NoData. Nothing else was changed.

1 Survey Data

Four species of earless seals (*Phocidae*) inhabit or visit U.S. waters of the western North Atlantic: harbor seal, gray seal, harp seal, and hooded seal (Hayes et al. 2019; Hayes et al. 2021; Hayes et al. 2022; Haverkamp et al. 2023). 73% of the sightings contributed by the collaborating institutions had the taxonomic identification "unidentified seal". The remaining 27% were harbor and gray seals; no harp or hooded seals were reported. Because of the small proportion of fully-identified sightings and the substantial overlap in harbor and gray seal habitats, we could not attempt to classify unidentified seals into one species or another with environmental covariates. Accordingly, we modeled all four species together as a guild. We excluded sightings of hauled-out seals; density estimates given by this model are for seals in the water.

We built this model from data collected between 1998-2020 (Table 1, Figure 1). In keeping with our primary strategy for the 2022 modeling cycle, we excluded data prior to 1998 in order to utilize biological covariates derived from satellite ocean color observations, which were only available for a few months before 1998. The model was split into summer and winter seasons. For summer, we excluded data after 2019 in order to utilize zooplankton and micronekton biomass estimates from SEAPODYM (Lehodey et al. 2008), which preliminary modeling indicated were were effective spatial covariates but were only available through 2019.

Seals are small and difficult to detect from long distances or in poor conditions. Accordingly, we excluded all surveys that did not target seals, as well as aerial surveys flown at altitudes higher than 750 ft., which species experts within our collaboration determined was the maximum altitude they were likely to be reliably detected. Although detections at higher altitudes were possible, we lacked the counts needed to fit detection functions unless we pooled surveys flown at lower altitudes, which species experts determined would be inappropriate. Some surveys flown at 1000 ft. utilized a belly camera to address this problem, but the camera data were not available for this project.

Finally, we restricted this model to survey transects collected in sea states of Beaufort 3 or less, owing to the difficulty in modeling detectability of seals in rougher sea states. We also excluded transects with poor weather or visibility for surveys that reported those conditions.

Table 1: Survey effort and observations considered for this model. Effort is tallied as the cumulative length of on-effort transects. Observations are the number of groups and individuals encountered while on effort. Off effort observations and those lacking an estimate of group size or distance to the group were excluded.

Institution	Program	Period	Effort	Observations		
			1000s km	Groups	Individuals	Mean Group Size
Aerial Surveys						
NEFSC	AMAPPS	2010-2019	55	530	1,151	2.2
NEFSC	NARWSS	2003-2016	274	791	1,803	2.3
NEFSC	Pre-AMAPPS	1999-2008	37	146	261	1.8
NJDEP	NJEBS	2008-2009	9	1	1	1.0
SEFSC	AMAPPS	2010-2020	91	0	0	
SEFSC	MATS	2002-2005	27	0	0	
VAMSC	MD DNR WEA	2013-2015	11	0	0	
	Total		**504**	**1,468**	**3,216**	**2.2**
Shipboard Surveys						
MCR	SOTW Visual	2012-2019	6	1	1	1.0
NEFSC	AMAPPS	2011-2016	8	9	9	1.0
NEFSC	Pre-AMAPPS	1998-2007	9	210	234	1.1
NJDEP	NJEBS	2008-2009	7	3	4	1.3
SEFSC	AMAPPS	2011-2016	10	0	0	
SEFSC	Pre-AMAPPS	1998-2006	18	0	0	
	Total		**57**	**223**	**248**	**1.1**
	Grand Total		**561**	**1,691**	**3,464**	**2.0**

Table 2: Institutions that contributed surveys used in this model.

Institution	Full Name
MCR	Marine Conservation Research
NEFSC	NOAA Northeast Fisheries Science Center
NJDEP	New Jersey Department of Environmental Protection
SEFSC	NOAA Southeast Fisheries Science Center
VAMSC	Virginia Aquarium & Marine Science Center

Table 3: Descriptions and references for survey programs used in this model.

| Program	Description	References
AMAPPS	Atlantic Marine Assessment Program for Protected Species	Palka et al. (2017), Palka et al. (2021)
MATS	Mid-Atlantic Tursiops Surveys	
MD DNR WEA	Aerial Surveys of the Maryland Wind Energy Area	Barco et al. (2015)
NARWSS	North Atlantic Right Whale Sighting Surveys	Cole et al. (2007)
NJEBS	New Jersey Ecological Baseline Study	Geo-Marine, Inc. (2010), Whitt et al. (2015)
Pre-AMAPPS	Pre-AMAPPS Marine Mammal Abundance Surveys	Mullin and Fulling (2003), Garrison et al. (2010), Palka (2006)
SOTW Visual	R/V Song of the Whale Visual Surveys	Ryan et al. (2013)
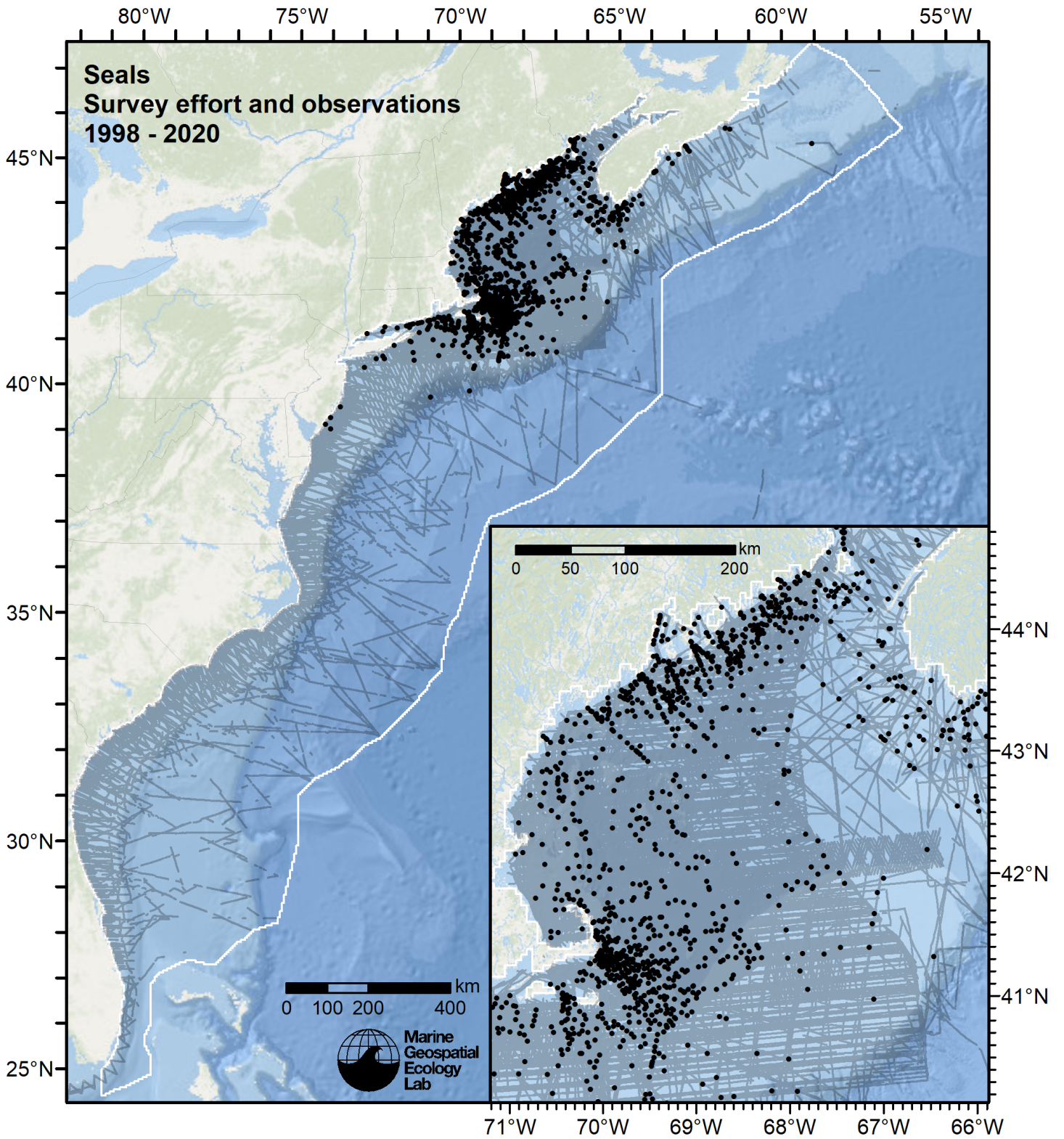
Figure 1: Survey effort and seals observations available for density modeling, after detection functions were applied, and excluded segments and truncated observations were removed.

2 Detection Functions

2.1 Without a Taxonomic Covariate

We fitted the detection functions in this section to pools of species with similar detectability characteristics but could not use a taxonomic identification as a covariate to account for differences between them. We usually took this approach after trying the taxonomic covariate and finding it had insufficient statistical power to be retained. We also resorted to it when the focal taxon being modeled had too few observations to be allocated its own taxonomic covariate level and was too poorly known for us to confidently determine which other taxa we could group it with.

2.1.1 Seals

2.1.1.1 Aerial Surveys
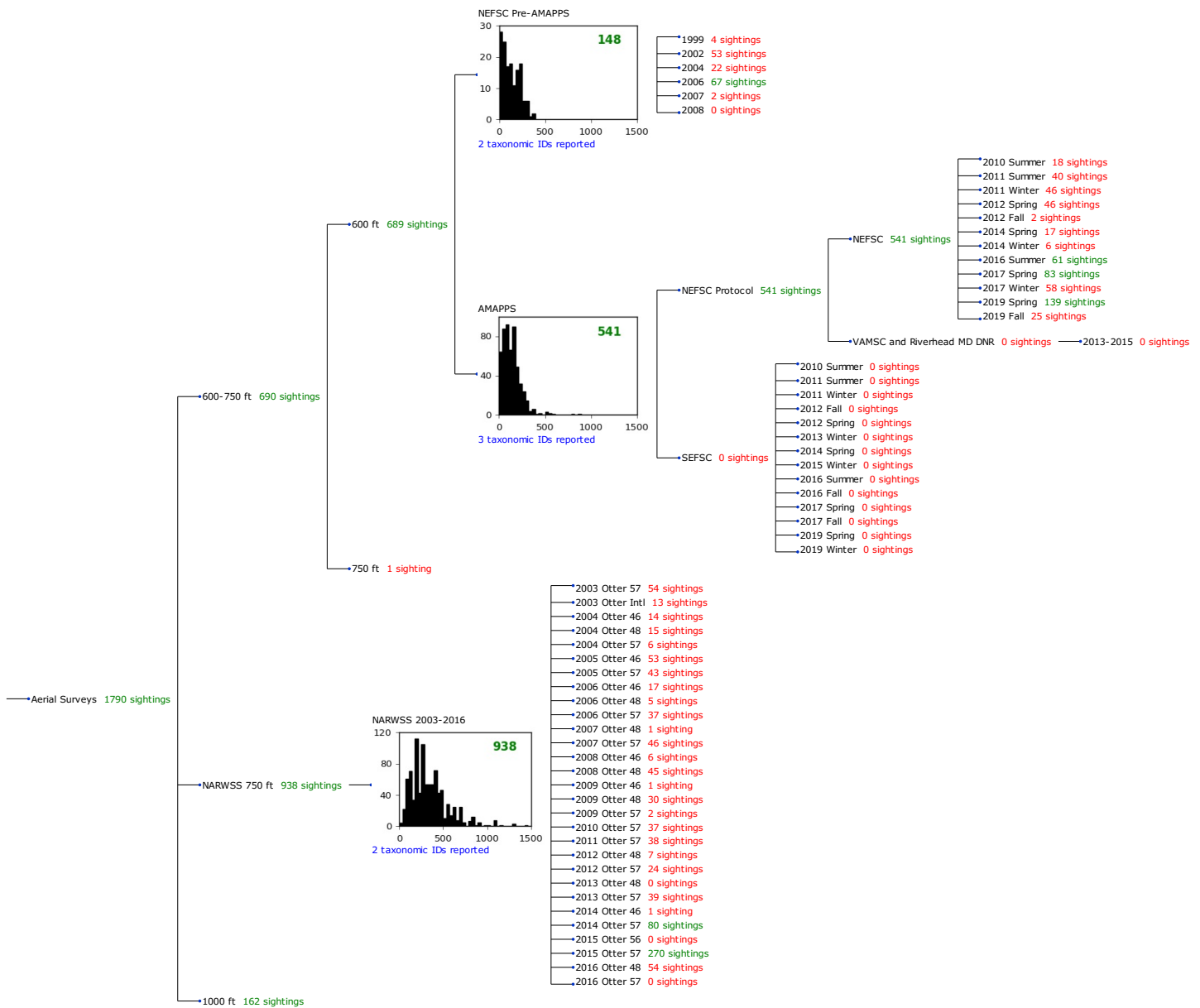
Figure 2: Detection hierarchy for aerial surveys, showing how they were pooled during detectability modeling, for detection functions that pooled multiple taxa but could not use a taxonomic covariate to account for differences between them. Each histogram represents a detection function and summarizes the perpendicular distances of observations that were pooled to fit it, prior to truncation. Observation counts, also prior to truncation, are shown in green when they met the recommendation of Buckland et al. (2001) that detection functions utilize at least 60 sightings, and red otherwise. For rare taxa, it was not always possible to meet this recommendation, yielding higher statistical uncertainty. During the spatial modeling stage of the analysis, effective strip widths were computed for each survey using the closest detection function above it in the hierarchy (i.e. moving from right to left in the figure). Surveys that do not have a detection function above them in this figure were either addressed by a detection function presented in a different section of this report, or were omitted from the analysis.

2.1.1.1.1 NEFSC Pre-AMAPPS

After right-truncating observations greater than 350 m, we fitted the detection function to the 146 observations that remained (Table 4). The selected detection function (Figure 3) used a half normal key function with no covariates.

Table 4: Observations used to fit the NEFSC Pre-AMAPPS detection function.

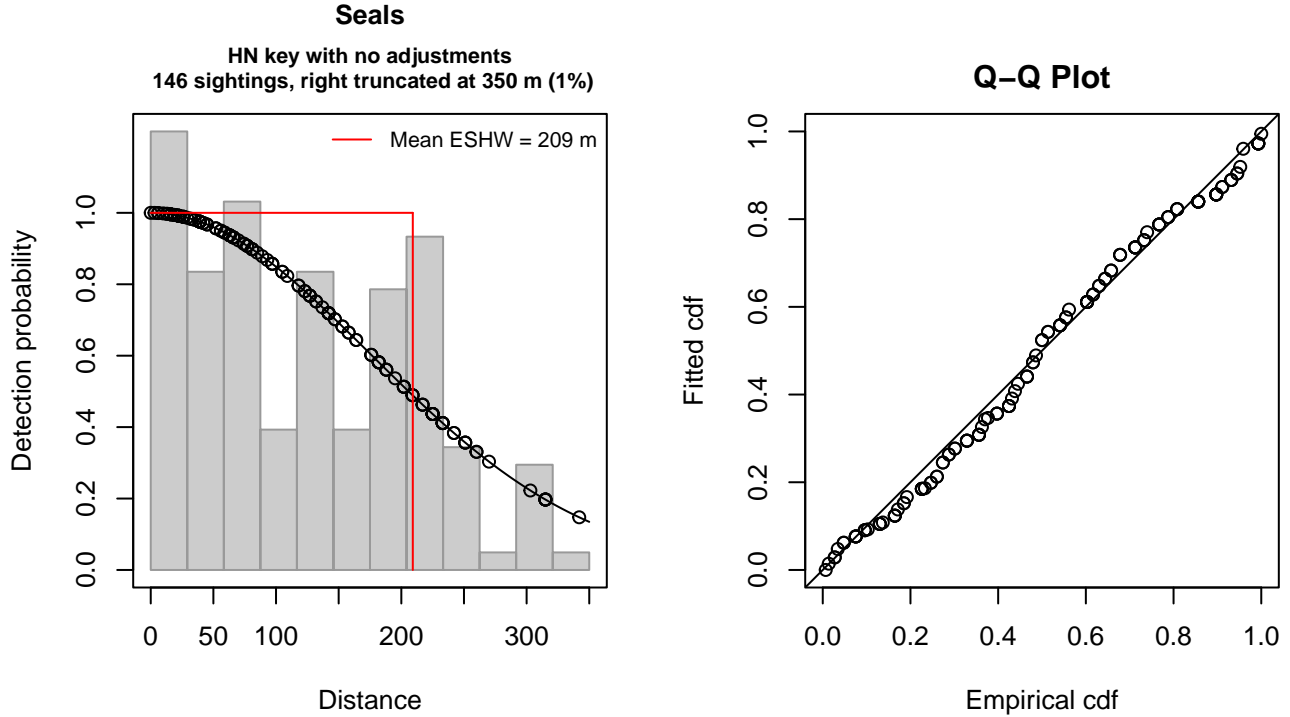| ScientificName	n
Canifornia	12
Phoca vitulina	134
Total	**146**

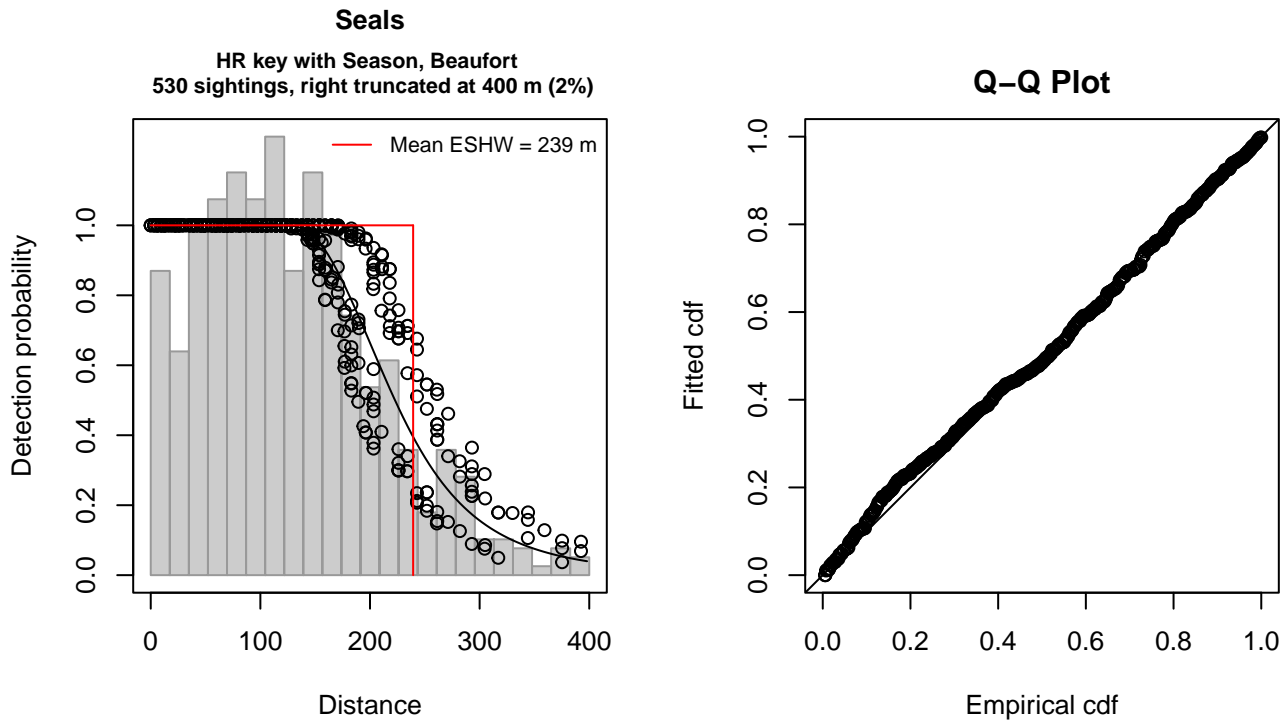Figure 3: NEFSC Pre-AMAPPS detection function and Q-Q plot showing its goodness of fit.

Statistical output for this detection function:

```
Summary for ds object
Number of observations :  146
Distance range         :  0  -   350
AIC                    :  1675.274

Detection function:
 Half-normal key function

Detection function parameters
Scale coefficient(s):
           estimate         se
(Intercept) 5.163593 0.09545195

                   Estimate        SE         CV
Average p         0.5975919  0.04418523 0.07393879
N in covered region 244.3138733 22.15478888 0.09068167

Distance sampling Cramer-von Mises test (unweighted)
Test statistic = 0.111819  p = 0.529986
```

2.1.1.1.2 AMAPPS

After right-truncating observations greater than 400 m, we fitted the detection function to the 530 observations that remained (Table 5). The selected detection function (Figure 4) used a hazard rate key function with Beaufort (Figure 5) and Season (Figure 6) as covariates.

Table 5: Observations used to fit the AMAPPS detection function.

ScientificName	n
Caniformia	409
Halichoerus grypus	98
Phoca vitulina	23
Total	**530**

Figure 4: AMAPPS detection function and Q-Q plot showing its goodness of fit.

Statistical output for this detection function:

```
Summary for ds object
Number of observations :  530
Distance range         :  0  -  400
AIC                    :  6052.007

Detection function:
 Hazard-rate key function

Detection function parameters
Scale coefficient(s):
                      estimate          se
(Intercept)           5.3192500 0.09170451
SeasonWinter, Spring  0.2626905 0.05787642
Beaufort             -0.0552160 0.04227600
```

```
Shape coefficient(s):
            estimate          se
(Intercept) 1.639891 0.1347447


                       Estimate          SE          CV
Average p             0.5895192  0.0169129 0.02868930
N in covered region 899.0377653 36.1214571 0.04017791


Distance sampling Cramer-von Mises test (unweighted)
Test statistic = 0.167977  p = 0.339161
```
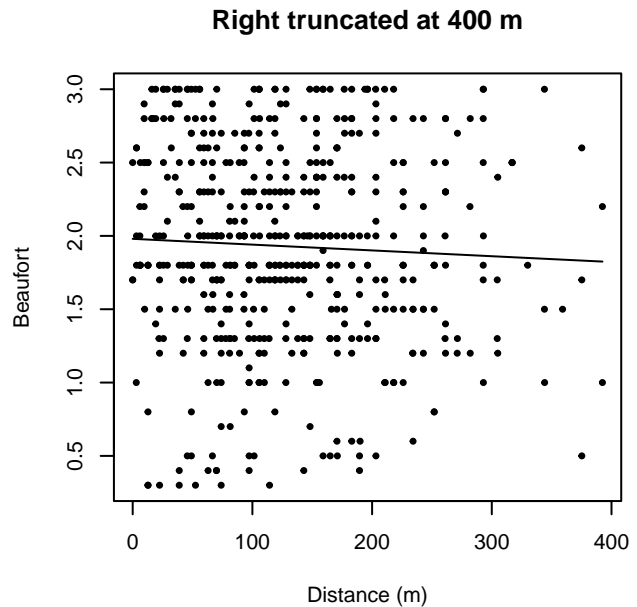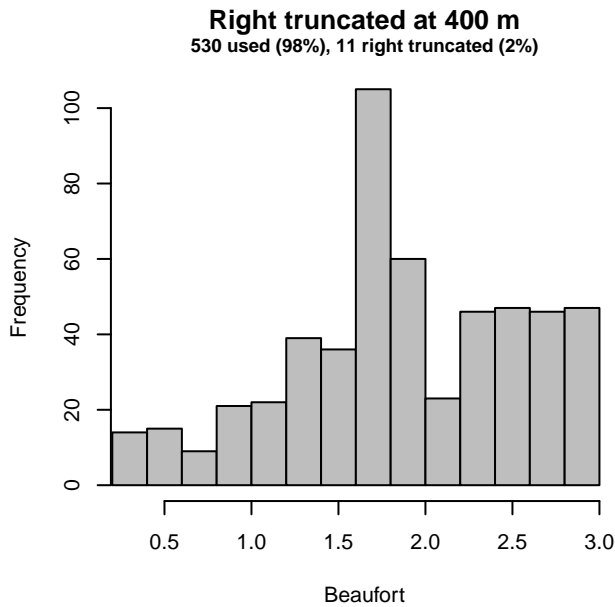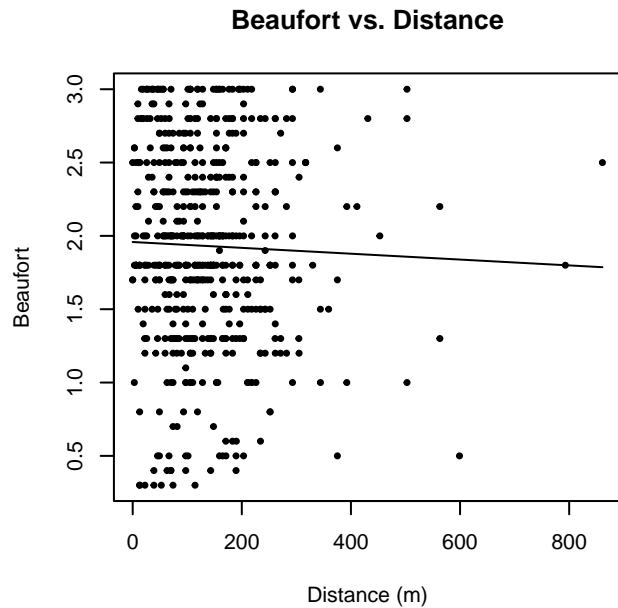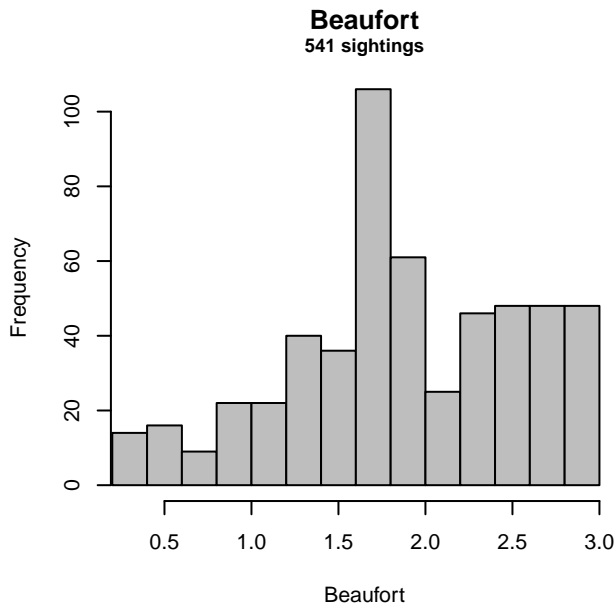

Figure 5: Distribution of the Beaufort covariate before (top row) and after (bottom row) observations were truncated to fit the AMAPPS detection function.
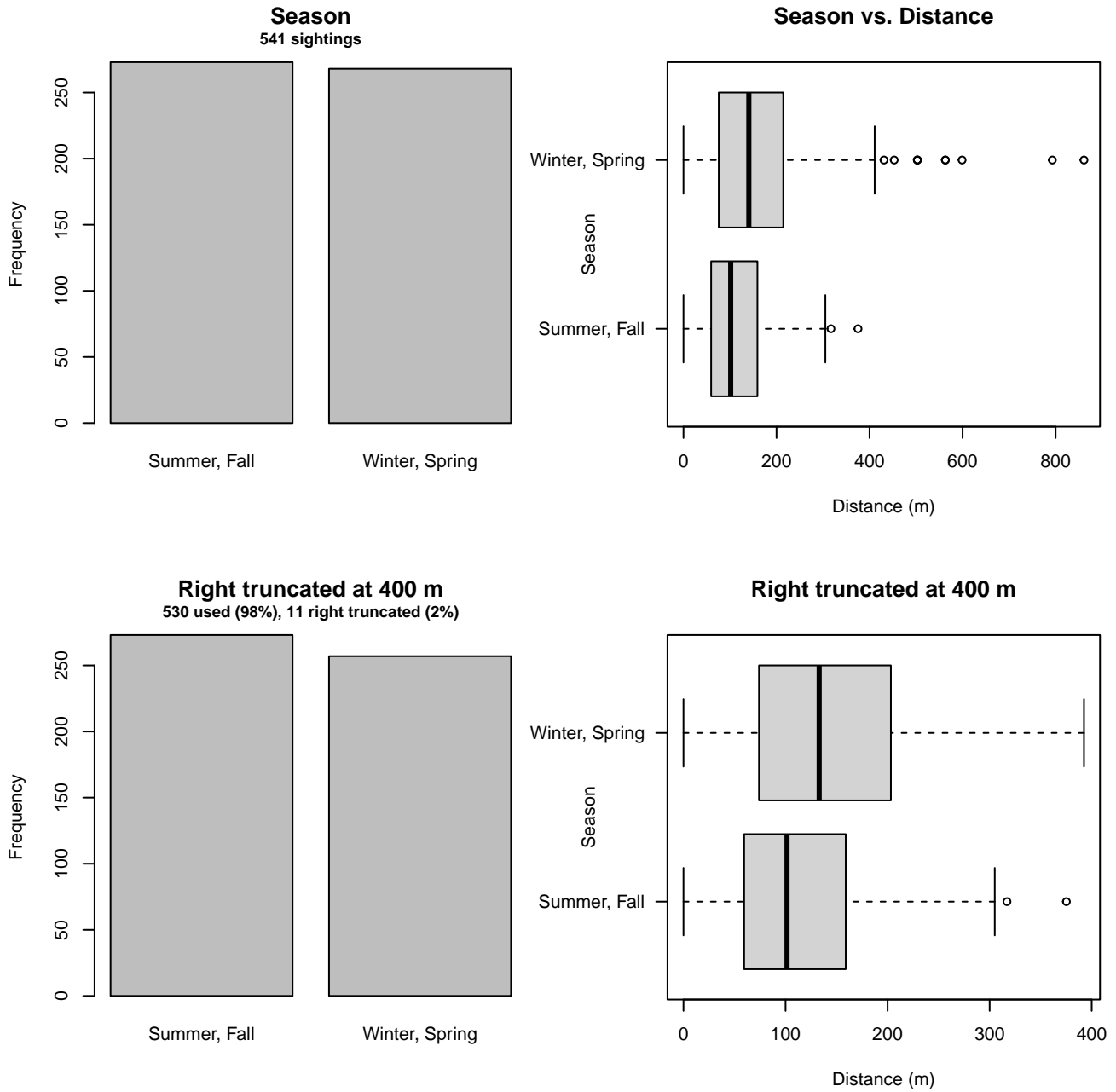
Figure 6: Distribution of the Season covariate before (top row) and after (bottom row) observations were truncated to fit the AMAPPS detection function.

2.1.1.1.3 NARWSS 2003-2016

After right-truncating observations greater than 726 m and left-truncating observations less than 122 m (Figure 8), we fitted the detection function to the 791 observations that remained (Table 6). The selected detection function (Figure 7) used a hazard rate key function with Beaufort (Figure 9), Glare (Figure 10) and Season (Figure 11) as covariates.

Table 6: Observations used to fit the NARWSS 2003-2016 detection function.

ScientificName	n
Caniformia	790
Halichoerus grypus	1
Total	**791**

Seals

HR key with Season, Glare, Beaufort
791 sightings, left trunc. 122 m (10%), right trunc. 726 m (6%
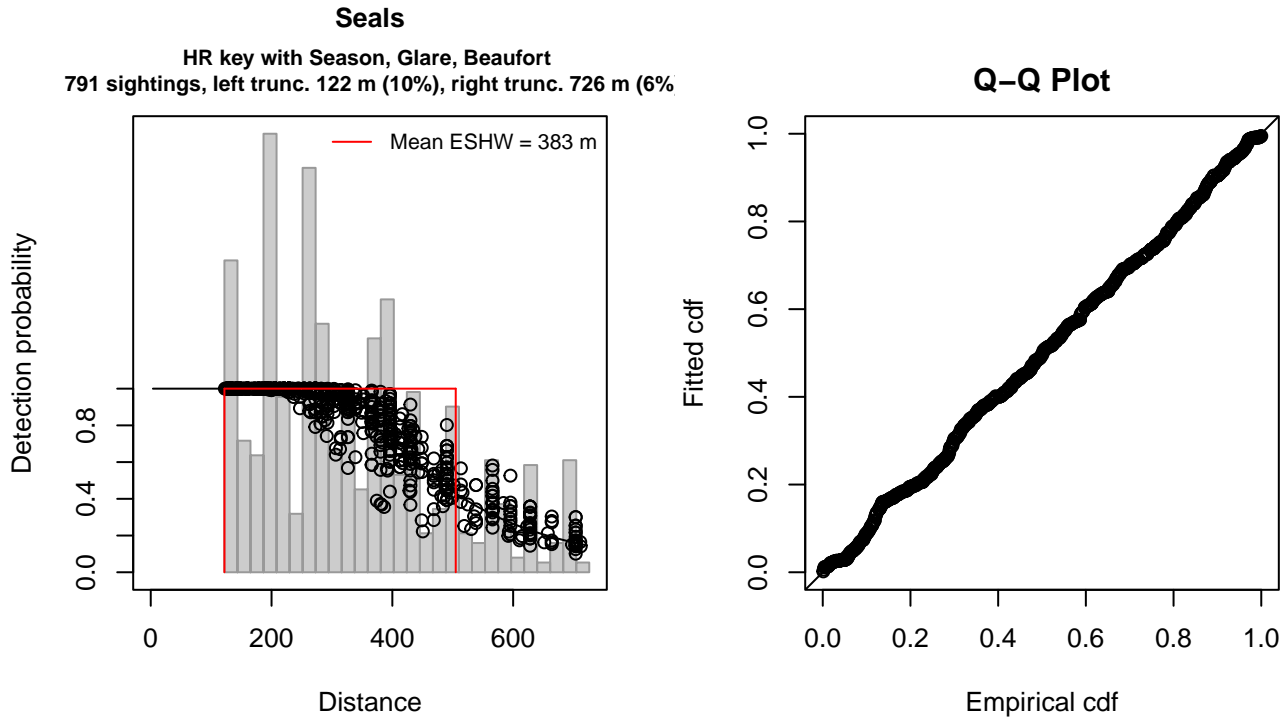
Mean ESHW = 383 m

Q–Q Plot

Figure 7: NARWSS 2003-2016 detection function and Q-Q plot showing its goodness of fit.

Statistical output for this detection function:

```
Summary for ds object
Number of observations :   791
Distance range         :   122  -  726
AIC                    :   9898.116

Detection function:
 Hazard-rate key function

Detection function parameters
Scale coefficient(s):
                          estimate          se
(Intercept)             5.78174069  0.14900322
SeasonSpring, Summer    0.27376636  0.10158234
GlareNone, Slight, Unk. -0.14132145  0.07949858
Beaufort                0.09065059  0.04388884

Shape coefficient(s):
           estimate         se
(Intercept) 1.291485  0.1187187


                    Estimate         SE          CV
Average p          0.6237221  0.02393758  0.03837859
N in covered region 1268.1929272 56.16855810  0.04429023

Distance sampling Cramer-von Mises test (unweighted)
Test statistic = 0.084470  p = 0.666419
```

Left trucated sightings (in red)
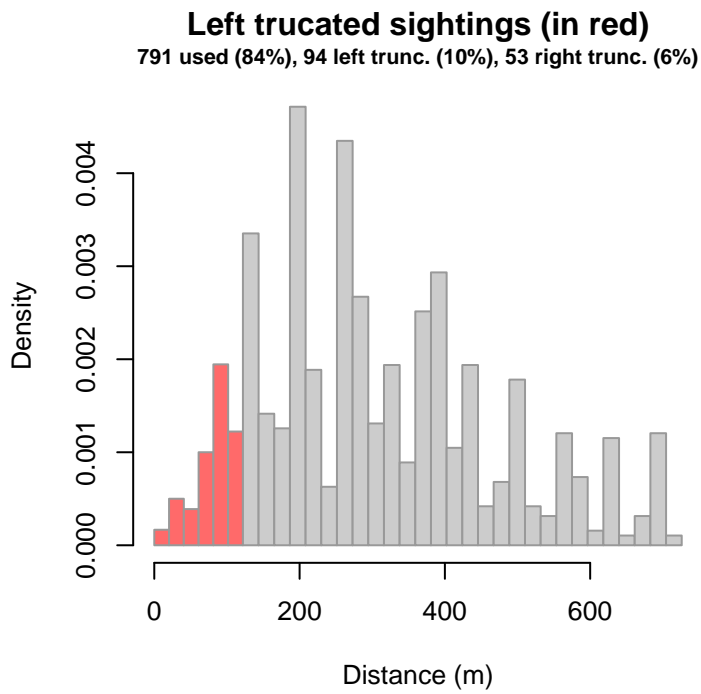791 used (84%), 94 left trunc. (10%), 53 right trunc. (6%)

Figure 8: Density histogram of observations used to fit the NARWSS 2003-2016 detection function, with the left-most bar showing observations at distances less than 122 m, which were left-truncated and excluded from the analysis [Buckland et al. (2001)]. (This bar may be very short if there were very few left-truncated sightings, or very narrow if the left truncation distance was very small; in either case it may not appear red.)
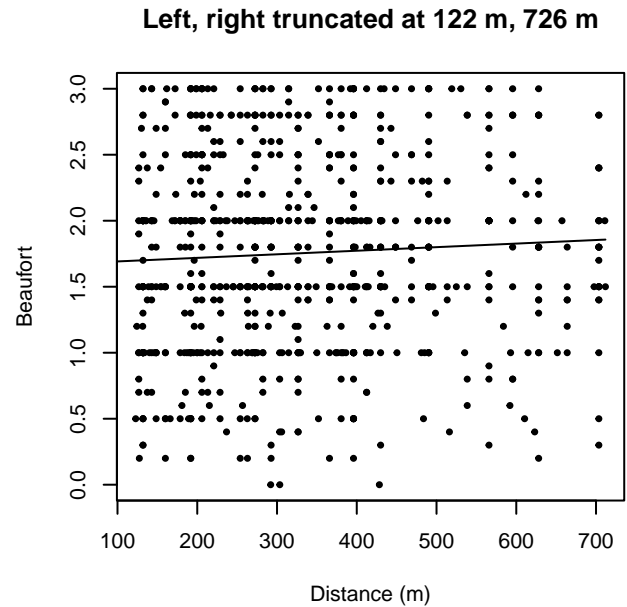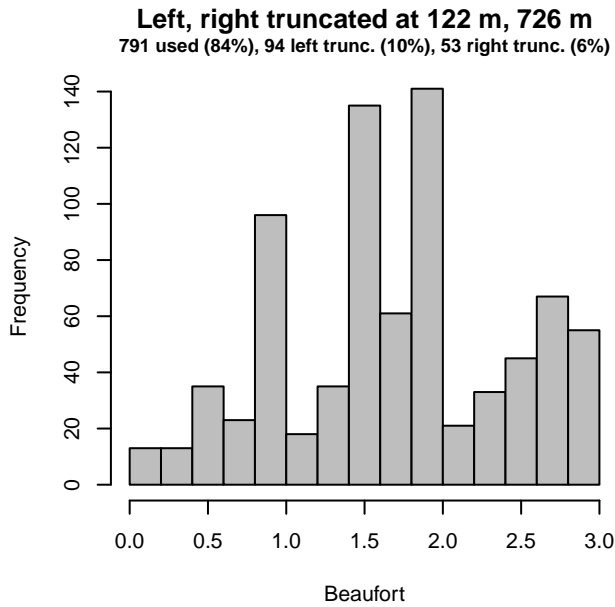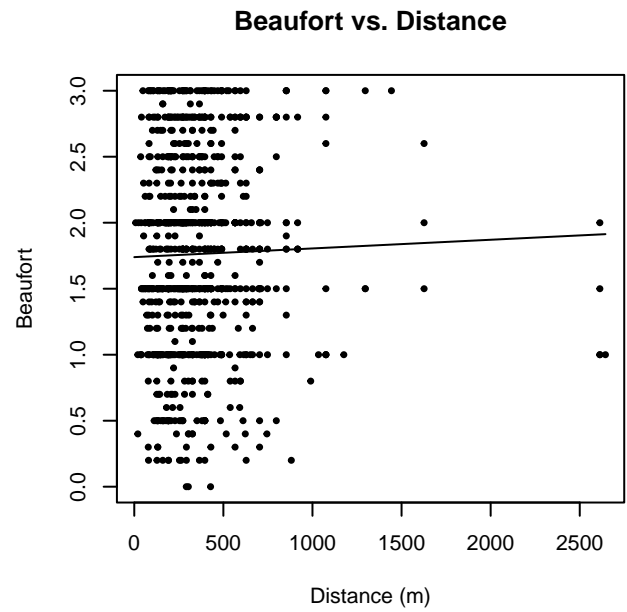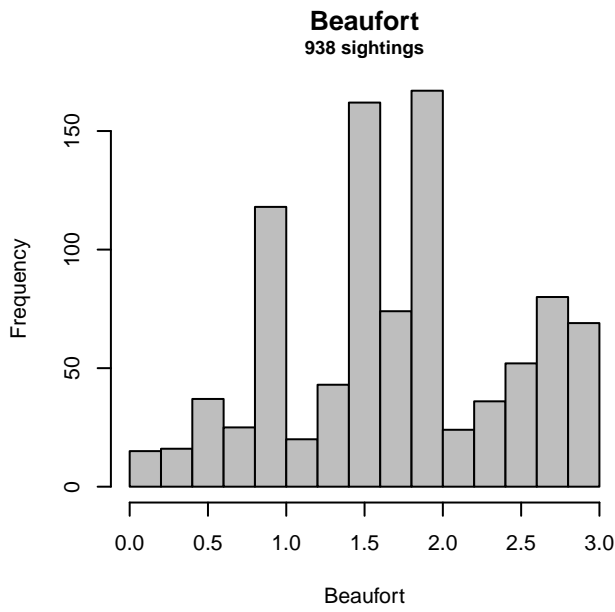
Figure 9: Distribution of the Beaufort covariate before (top row) and after (bottom row) observations were truncated to fit the NARWSS 2003-2016 detection function.
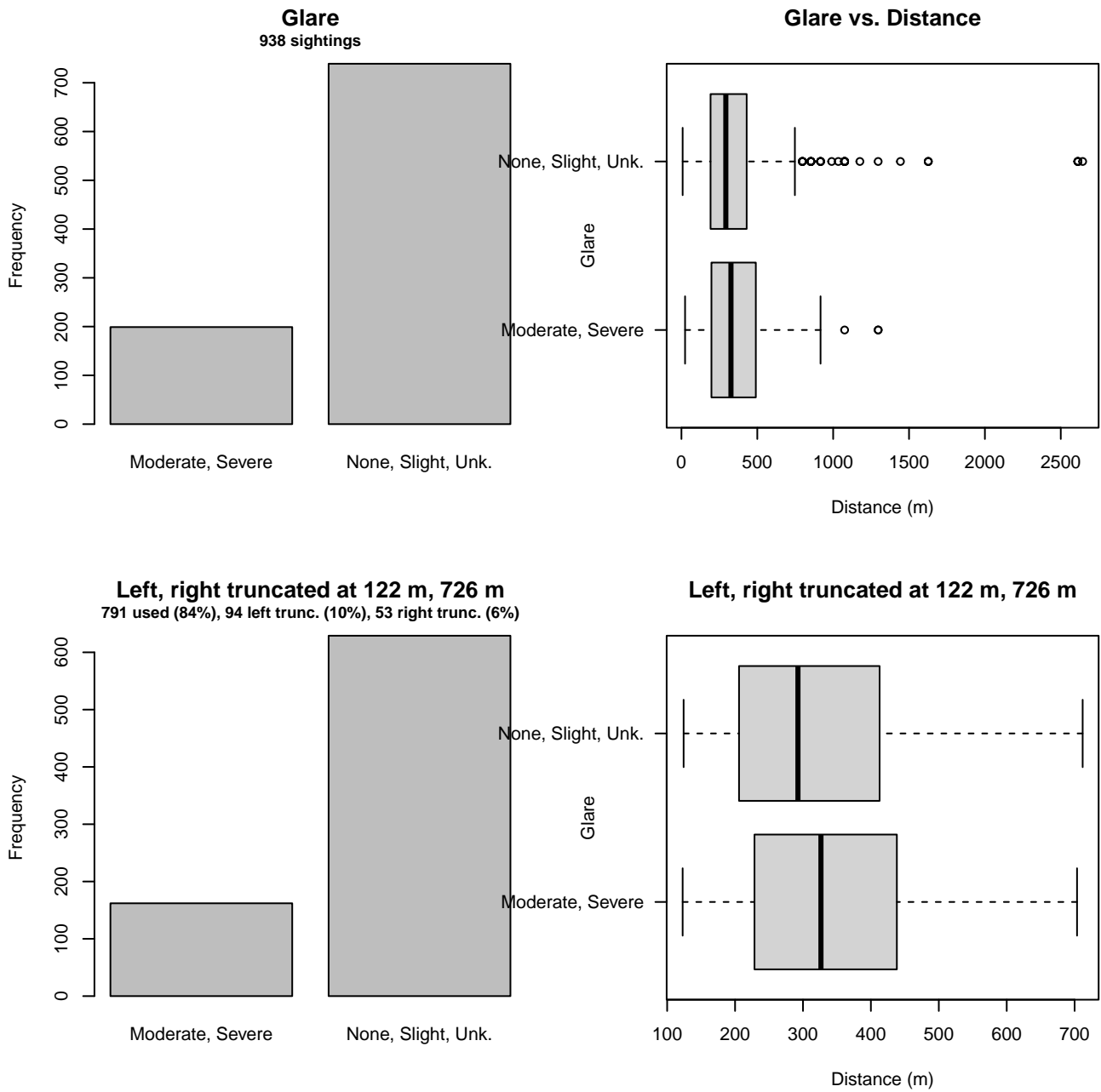
Figure 10: Distribution of the Glare covariate before (top row) and after (bottom row) observations were truncated to fit the NARWSS 2003-2016 detection function.
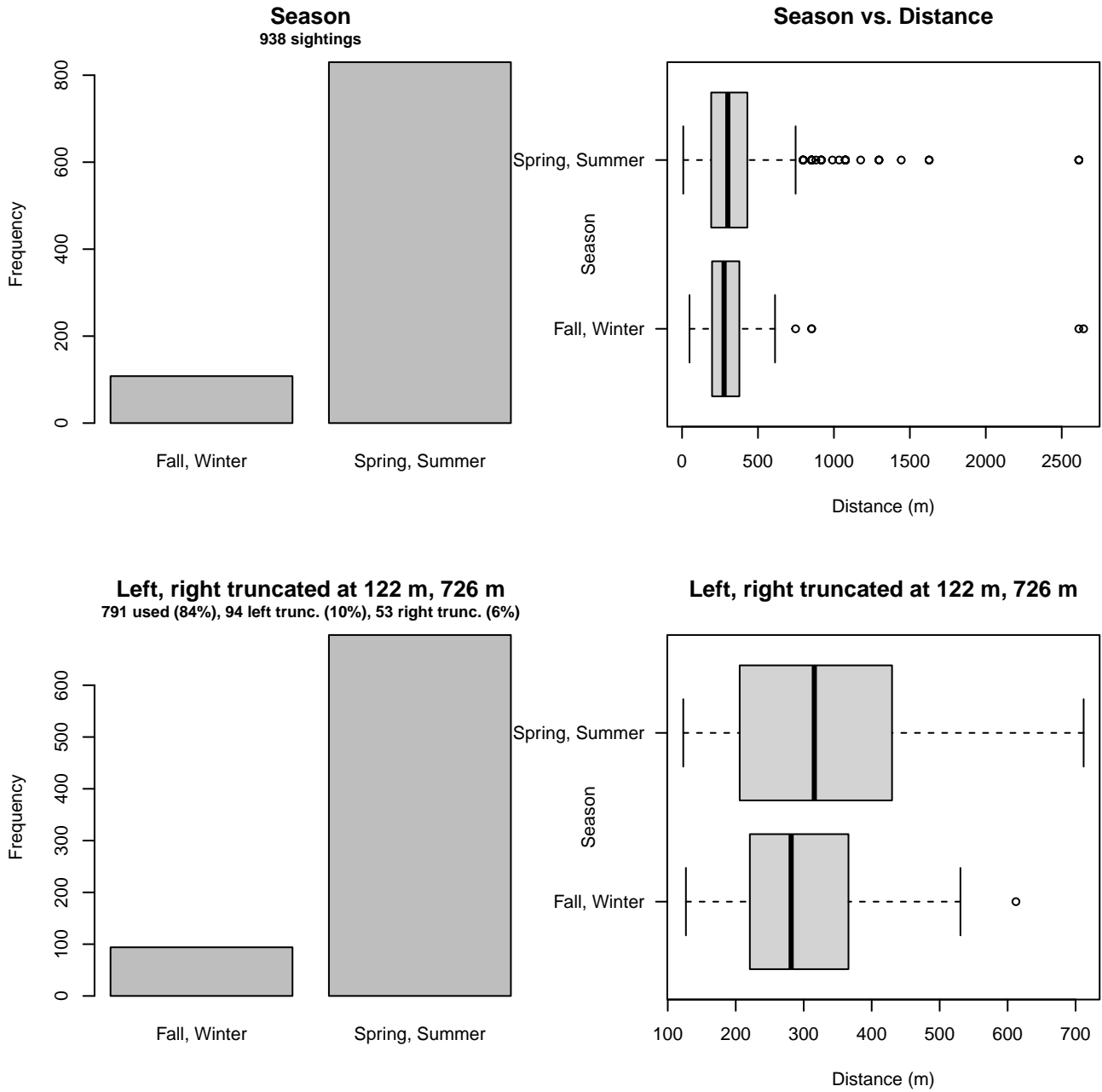
Figure 11: Distribution of the Season covariate before (top row) and after (bottom row) observations were truncated to fit the NARWSS 2003-2016 detection function.
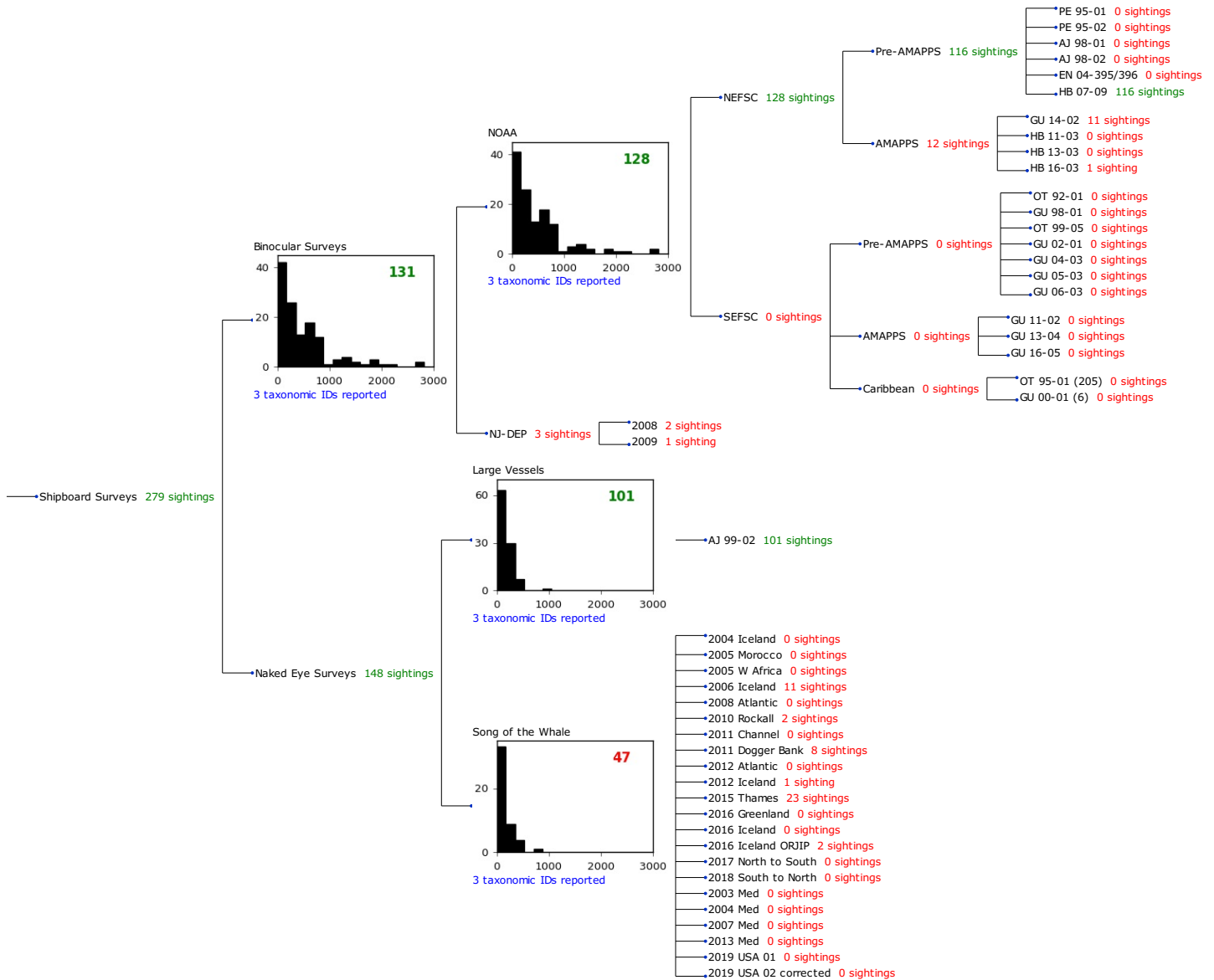
2.1.1.2 Shipboard Surveys

Figure 12: Detection hierarchy for shipboard surveys, showing how they were pooled during detectability modeling, for detection functions that pooled multiple taxa but could not use a taxonomic covariate to account for differences between them. Each histogram represents a detection function and summarizes the perpendicular distances of observations that were pooled to fit it, prior to truncation. Observation counts, also prior to truncation, are shown in green when they met the recommendation of Buckland et al. (2001) that detection functions utilize at least 60 sightings, and red otherwise. For rare taxa, it was not always possible to meet this recommendation, yielding higher statistical uncertainty. During the spatial modeling stage of the analysis, effective strip widths were computed for each survey using the closest detection function above it in the hierarchy (i.e. moving from right to left in the figure). Surveys that do not have a detection function above them in this figure were either addressed by a detection function presented in a different section of this report, or were omitted from the analysis.

2.1.1.2.1 NOAA

After right-truncating observations greater than 1550 m, we fitted the detection function to the 120 observations that remained (Table 7). The selected detection function (Figure 13) used a hazard rate key function with no covariates.

Table 7: Observations used to fit the NOAA detection function.

ScientificName	n
Caniformia	23
Halichoerus grypus	25
Phoca vitulina	72
Total	**120**

Seals

HR key with no adjustments
120 sightings, right truncated at 1550 m (6%)
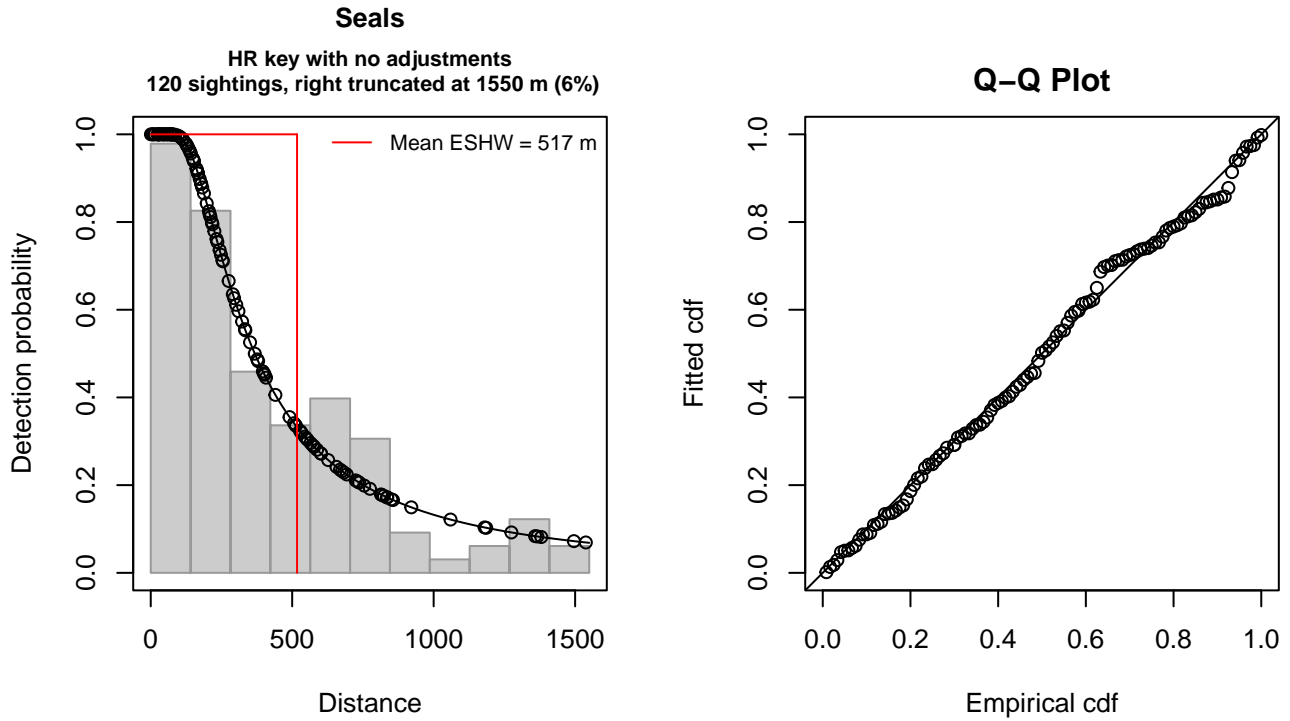

Figure 13: NOAA detection function and Q-Q plot showing its goodness of fit.

Statistical output for this detection function:

```
Summary for ds object
Number of observations :  120
Distance range         :  0  -  1550
AIC                    :  1680.262

Detection function:
 Hazard-rate key function

Detection function parameters
Scale coefficient(s):
            estimate        se
(Intercept) 5.675867 0.2645732

Shape coefficient(s):
            estimate        se
(Intercept) 0.460157 0.2007531


                       Estimate          SE         CV
Average p              0.3336537  0.04850864  0.1453862
N in covered region 359.6543797 58.75704358  0.1633709
```

```
Distance sampling Cramer-von Mises test (unweighted)
Test statistic = 0.048881   p = 0.883041
```

2.1.1.2.2   Binocular Surveys

After right-truncating observations greater than 2000 m, we fitted the detection function to the 126 observations that remained (Table 8). The selected detection function (Figure 14) used a hazard rate key function with no covariates.

Table 8: Observations used to fit the Binocular Surveys detection function.

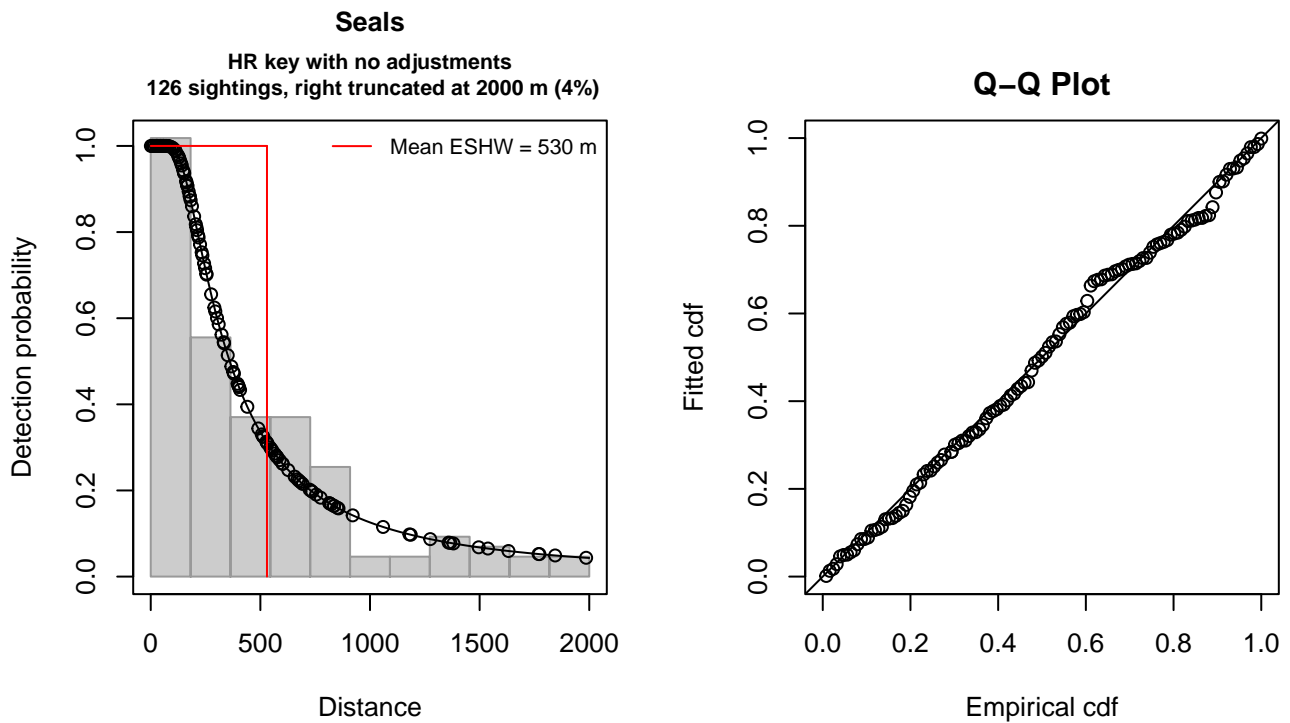| ScientificName	n
Caniformia	25
Halichoerus grypus	25
Phoca vitulina	76
Total	**126**

Figure 14: Binocular Surveys detection function and Q-Q plot showing its goodness of fit.

Statistical output for this detection function:

```
Summary for ds object
Number of observations :  126
Distance range         :  0  -  2000
AIC                    :  1796.3

Detection function:
 Hazard-rate key function

Detection function parameters
Scale coefficient(s):
           estimate        se
(Intercept) 5.657908 0.2456458
```

```
Shape coefficient(s):
            estimate         se
(Intercept) 0.4735328 0.1634037


                    Estimate         SE         CV
Average p            0.2650894  0.03764663 0.1420148
N in covered region 475.3113335 76.64288633 0.1612478


Distance sampling Cramer-von Mises test (unweighted)
Test statistic = 0.048389  p = 0.885993
```

2.1.1.2.3 Large Vessels

After right-truncating observations greater than 450 m, we fitted the detection function to the 99 observations that remained (Table 9). The selected detection function (Figure 15) used a half normal key function with no covariates.

Table 9: Observations used to fit the Large Vessels detection function.

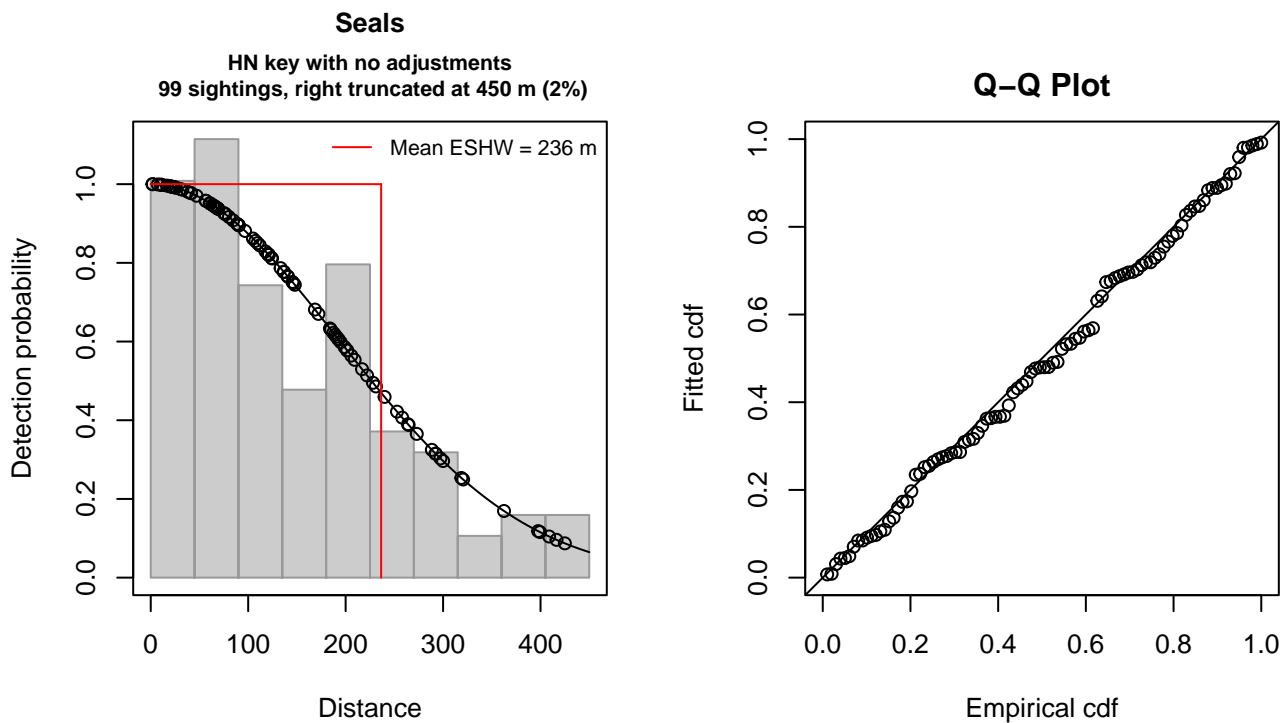| ScientificName	n
Caniformia	1
Halichoerus grypus	20
Phoca vitulina	78
Total	**99**

Figure 15: Large Vessels detection function and Q-Q plot showing its goodness of fit.

Statistical output for this detection function:

```
Summary for ds object
Number of observations :  99
Distance range         :  0  -   450
AIC                    :  1170.991
```

```
Detection function:
 Half-normal key function


Detection function parameters
Scale coefficient(s):
            estimate          se
(Intercept) 5.259396 0.08809049


                      Estimate          SE          CV
Average p            0.5254136   0.04057422 0.07722339
N in covered region 188.4229927 19.54270279 0.10371719


Distance sampling Cramer-von Mises test (unweighted)
Test statistic = 0.031593  p = 0.970648
```

2.1.1.2.4   Song of the Whale

After right-truncating observations greater than 500 m, we fitted the detection function to the 46 observations that remained (Table 10). The selected detection function (Figure 16) used a hazard rate key function with Beaufort (Figure 17) as a covariate.

Table 10: Observations used to fit the Song of the Whale detection function.

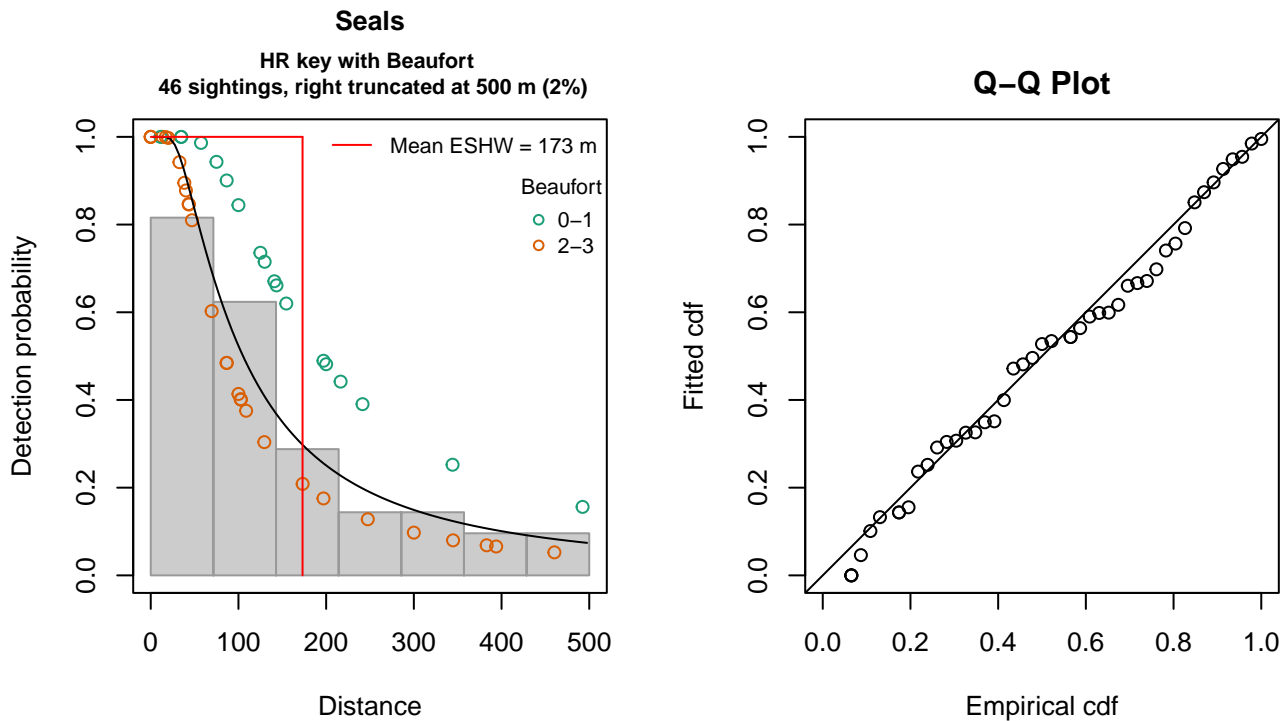| ScientificName	n
Cystophora cristata	1
Halichoerus grypus	34
Phocidae	11
Total	**46**

Figure 16: Song of the Whale detection function and Q-Q plot showing its goodness of fit.

Statistical output for this detection function:

```
Summary for ds object
Number of observations :  46
Distance range          :  0  -  500
AIC                     :  545.5977

Detection function:
 Hazard-rate key function

Detection function parameters
Scale coefficient(s):
              estimate         se
(Intercept)  5.0184244 0.5582498
Beaufort2-3 -0.8312102 0.6555273

Shape coefficient(s):
             estimate         se
(Intercept) 0.4064594 0.2790365

                     Estimate          SE         CV
Average p           0.3153174  0.08308944 0.2635105
N in covered region 145.8847645 42.53075639 0.2915367

Distance sampling Cramer-von Mises test (unweighted)
Test statistic = 0.038395  p = 0.941241
```
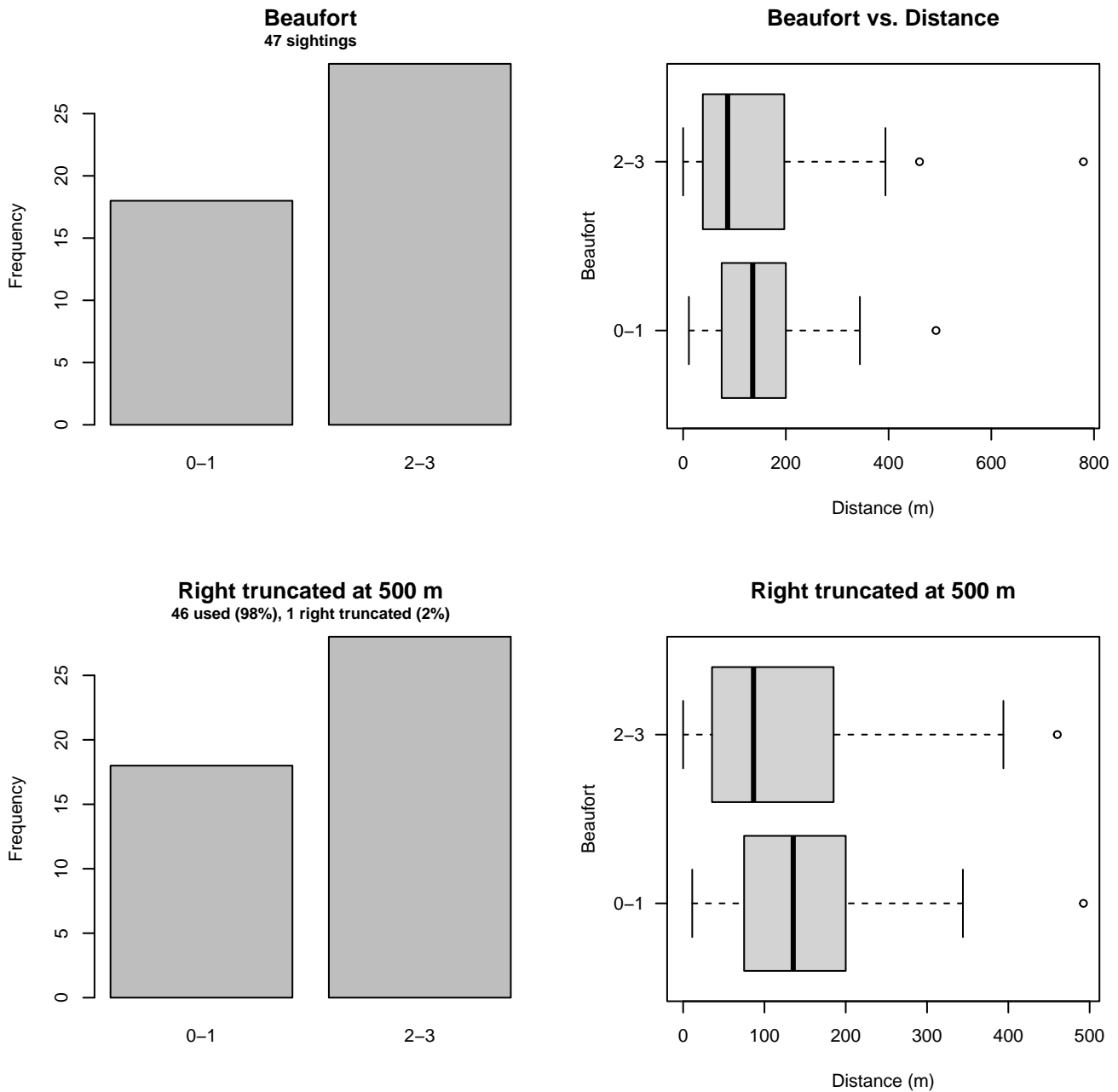
Figure 17: Distribution of the Beaufort covariate before (top row) and after (bottom row) observations were truncated to fit the Song of the Whale detection function.

2.1.2 Seals (second group)

This section contains a single detection function, which was used for aerial surveys flown at 750 ft. Because these surveys did not sight enough seals for a detection function, we pooled surveys from 600 ft in with them, and applied the resulting 600-750 ft detection function only to those flown at 750 ft. (The previous section shows the detection functions applied to the 600 ft surveys, which were only fitted to sightings made on those surveys.)
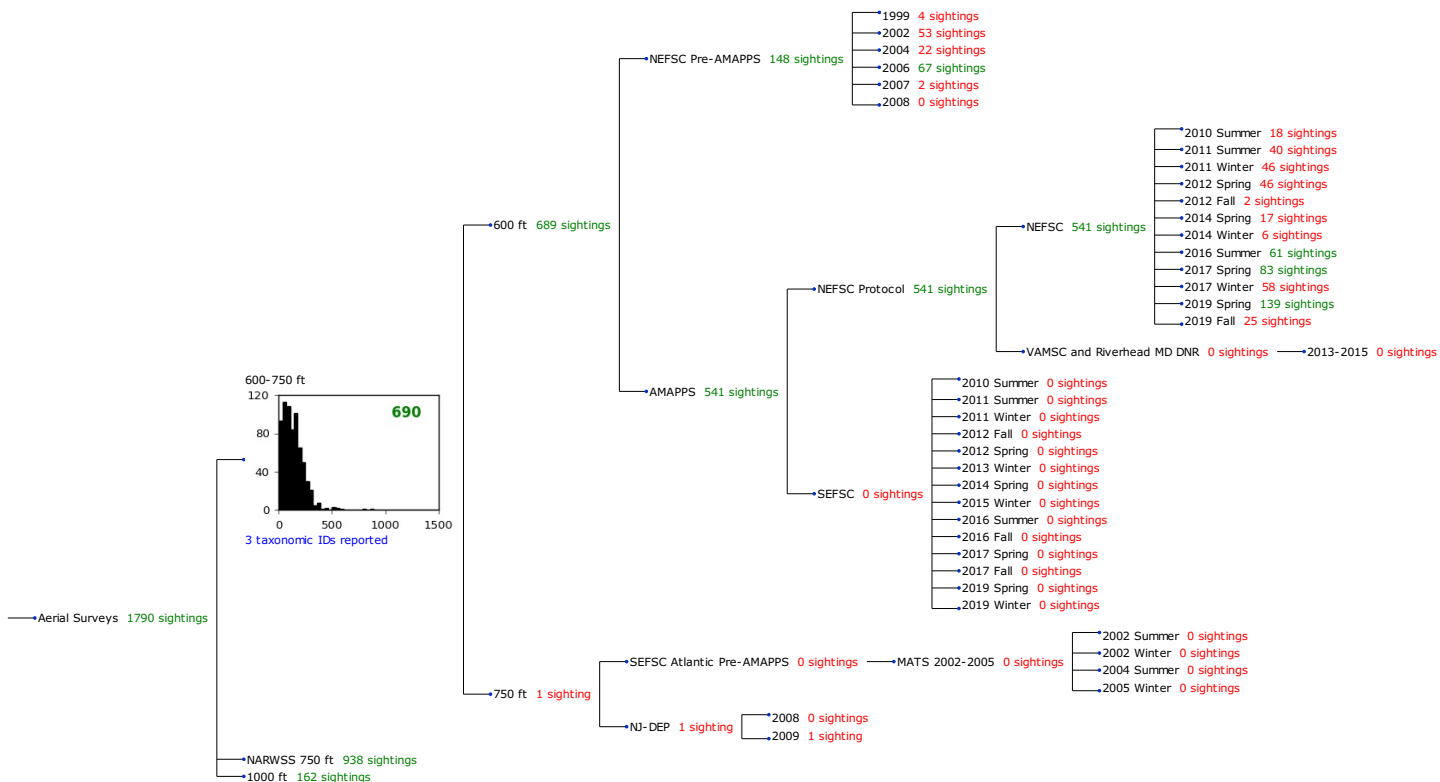
2.1.2.1 Aerial Surveys

Figure 18: Detection hierarchy for aerial surveys, showing how they were pooled during detectability modeling, for detection functions that pooled multiple taxa but could not use a taxonomic covariate to account for differences between them. Each histogram represents a detection function and summarizes the perpendicular distances of observations that were pooled to fit it, prior to truncation. Observation counts, also prior to truncation, are shown in green when they met the recommendation of Buckland et al. (2001) that detection functions utilize at least 60 sightings, and red otherwise. For rare taxa, it was not always possible to meet this recommendation, yielding higher statistical uncertainty. During the spatial modeling stage of the analysis, effective strip widths were computed for each survey using the closest detection function above it in the hierarchy (i.e. moving from right to left in the figure). Surveys that do not have a detection function above them in this figure were either addressed by a detection function presented in a different section of this report, or were omitted from the analysis.

2.1.2.1.1 600-750 ft

After right-truncating observations greater than 400 m, we fitted the detection function to the 679 observations that remained (Table 11). The selected detection function (Figure 19) used a hazard rate key function with no covariates.

Table 11: Observations used to fit the 600-750 ft detection function.

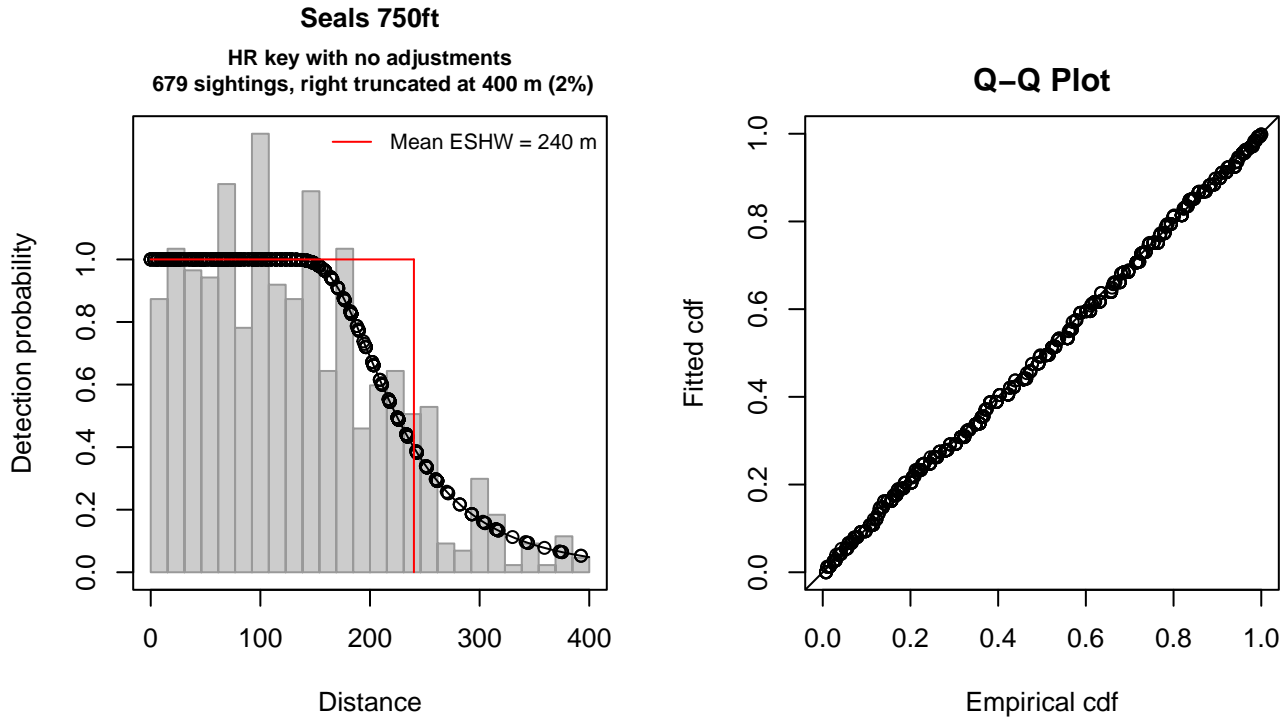| ScientificName	n
Caniformia	423
Halichoerus grypus	98
Phoca vitulina	158
Total	**679**

Figure 19: 600-750 ft detection function and Q-Q plot showing its goodness of fit.

Statistical output for this detection function:

```
Summary for ds object
Number of observations :   679
Distance range         :   0  -  400
AIC                    :   7793.246

Detection function:
 Hazard-rate key function

Detection function parameters
Scale coefficient(s):
            estimate          se
(Intercept) 5.332202 0.03865737

Shape coefficient(s):
            estimate        se
(Intercept) 1.515698 0.114239


                      Estimate         SE          CV
Average p            0.6001397  0.01620359 0.02699970
N in covered region 1131.4032175 41.07288822 0.03630261

Distance sampling Cramer-von Mises test (unweighted)
Test statistic = 0.053921  p = 0.852138
```

3 Bias Corrections

Density surface modeling methodology uses *distance sampling* (Buckland et al. 2001) to model the probability that an observer on a line transect survey will detect an animal given the perpendicular distance to it from the transect line. Distance sampling assumes that detection probability is 1 when perpendicular distance is 0. When this assumption is not met, detection probability is biased high, leading to an underestimation of density and abundance. This is known as the $g_0 < 1$ problem, where g_0 refers to the detection probability at distance 0. Modelers often try to address this problem by estimating g_0 empirically and dividing it into estimated density or abundance, thereby correcting those estimates to account for the animals that were presumed missed.

Two important sources of bias for visual surveys are known as *availability bias*, in which an animal was present on the transect line but impossible to detect, e.g. because it was under water, and *perception bias*, in which an animal was present and available but not noticed, e.g. because of its small size or cryptic coloration or behavior (Marsh and Sinclair 1989). Modelers often estimate the influence of these two sources of bias on detection probability independently, yielding two estimates of g_0, hereafter referred to as g_{0A} and g_{0P}, and multiply them together to obtain a final, combined estimate: $g_0 = g_{0A} \cdot g_{0P}$.

Our overall approach was to perform this correction on a per-observation basis, to have the flexibility to account for many factors such as platform type, surveyor institution, group size, group composition (e.g. singleton, mother-calf pair, or surface active group), and geographic location (e.g. feeding grounds vs. calving grounds). The level of complexity of the corrections varied by species according to the amount of information available, with North Atlantic right whale having the most elaborate corrections, derived from a substantial set of publications documenting its behavior, and various lesser known odontocetes having corrections based only on platform type (aerial or shipboard), derived from comparatively sparse information. Here we document the corrections used for seals.

3.1 Aerial Surveys

Palka et al. (2017) developed a perception bias correction, $g_{0P} = 0.181$, using two team, mark recapture distance sampling (MRDS) methodology (Burt et al. 2014) for aerial surveys conducted in 2010-2014 by NOAA NEFSC during the AMAPPS program. This was the only extant perception bias estimate developed from aerial surveys used in our analysis. (Palka et al. (2021) updated their 2017 cetacean models, but not their seals model.) We applied the Palka et al. (2017) estimate to all aerial survey programs.

We caution that it is possible that perception bias was different on the other aerial programs, as some of them used different personnel or flew at 750 ft. rather than 600 ft. as was done for AMAPPS. Correcting the other programs using NOAA's AMAPPS estimate as we have done is likely to yield less bias than leaving them uncorrected, but we urge all programs to undertake their own efforts to estimate perception bias, as resources allow.

To estimate availability bias corrections, we first needed estimates of mean dive and surface intervals. We used intervals for harbor seals, as they were the most frequently reported species in the sightings that reported a species identification (rather than "unidentified seal"). Vance et al. (2021) tracked 12 offshore foraging trips made by 8 harbor seals in the German Wadden Sea. Over all trips, seals performed a mean of 13 foraging dives per hour (SD=1.6) with an average dive interval of 3.3 min (198 s), which yields 42.9 min submerged per hour, 17.1 min at the surface per hour, and a surface interval of 1.32 min (78.9 s). The researchers reported that "foraging rates during travel to and from offshore sites were comparable to offshore rates," therefore we considered these estimates to be adequate summaries of harbor seal behavior throughout their time spent at sea, rather than just at locations that appeared to be foraging hotspots.

Lesage et al. (1999) reported dive statistics for 11 seals monitored with time-depth recorders in the St. Lawrence estuary in Canada. A total of 61,495 dives were recorded; of these, 46% were to depths >4 m and further analyzed. These dives were classified into five dive types and summeries were computed for each type. Mean dive and surface intervals for the five types ranged from 40.1-167.9 s and 38.6-44.8 s, respectively. Although these times were shorter than those reported by Vance et al., the mean time spent submerged across the five types was 55.1-78.9%, with a weighted mean of 74.2% across all dives, which was similar to Vance et al.'s seals, for which the mean was 71.5%. Given that Lesage et al. reported roughly similar percentages but did not analyze the shallower dives comprising 54% of their dataset, we determined the best course of action was to use the intervals derived from Vance et al.'s results (Table 12).

We estimated availability bias corrections using the Laake et al. (1997) estimator. To estimate time in view, needed by the Laake estimator, we used results reported by Robertson et al. (2015), rescaled linearly for each survey program according to its target altitude and speed. We caution that Robertson's analysis was done for a de Havilland Twin Otter, which may have a different field of view than that of the Cessna 337 Skymaster used by NJDEP, although NJDEP only reported one sighting so the effect on our final results was likely to be insignificant.

To address the influence of group size on availability bias, we applied the group availability estimator of McLellan et al. (2018) on a per-observation basis. Following Palka et al. (2017), who also used that method, we assumed that individuals

in the group dived asynchronously. The resulting g_{0A} corrections ranged from about 0.37 to 1 (Figure 20). We caution that the assumption of asynchronous diving can lead to an underestimation of density and abundance if diving is actually synchronous; see McLellan et al. (2018) for an exploration of this effect and Section 6 for further discussion.

Table 12: Surface and dive intervals for seals used to estimate availability bias corrections.

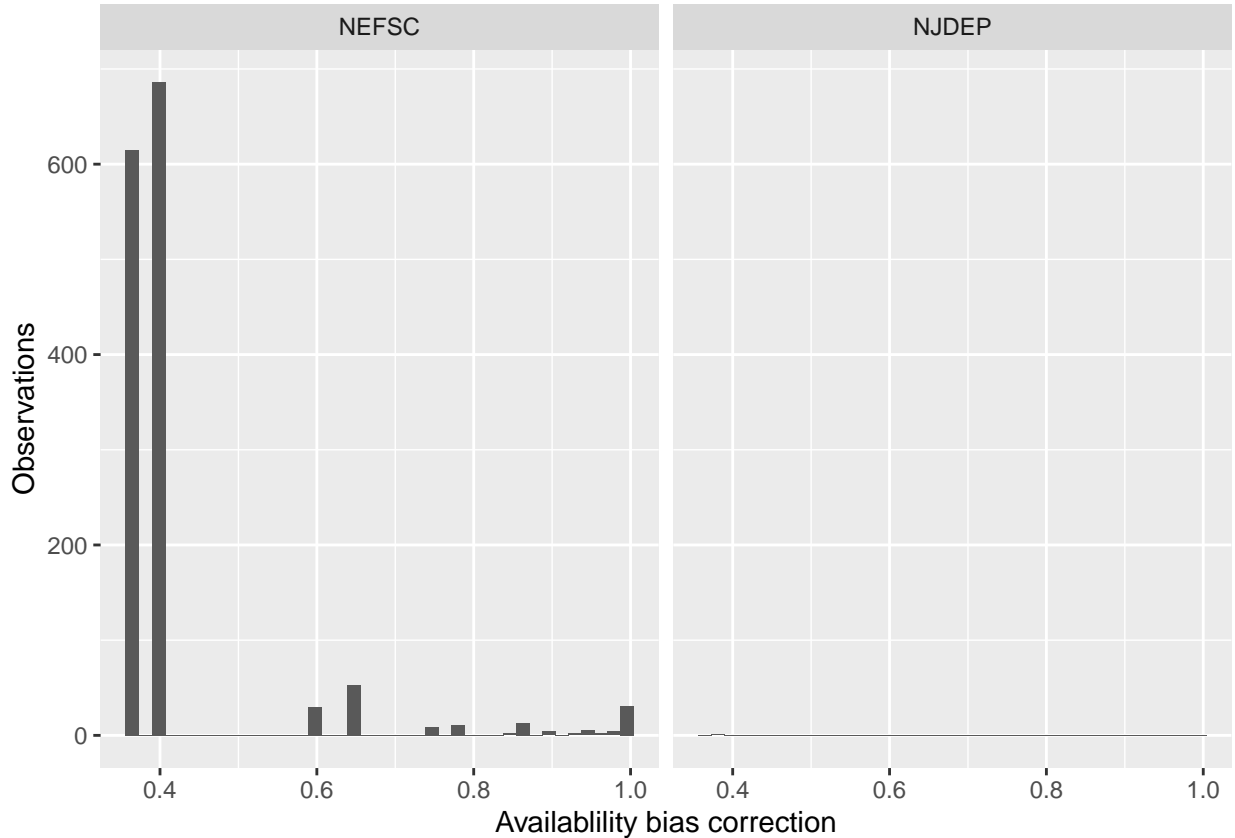| Surface Interval (s)	Dive Interval (s)	Source
198	78.9	Vance et al. (2021)

Figure 20: Availability bias corrections for seals for aerial surveys, by institution.

3.2 Shipboard Surveys

The only boat-based perception bias estimate we could find for harbor seals or gray seals was from Reay (2005), who estimated $g_{0P} = 0.85$ for gray seals in Cardigan Bay (in Wales) sighted by naked eye from small boats (observer height 3 m) using MRDS methods. We applied this estimate to all shipboard surveys. We caution that nearly all of our sightings occurred on NOAA vessels (Table 1 which all had substantially higher observation platforms (9.2-15.1 m) and about half of them searched with high-power (25x150), pedestal-mounted binoculars rather than naked eyes.

Given that the dive interval of this species (Table 12) was short relative to the amount of time a given patch of water remained in view to shipboard observers, we assumed that no availability bias correction was needed ($g_{0A} = 1$).

4 Density Model

Seals are harder than cetaceans for observers to fully identify, particularly on aerial surveys, when a close, extended view of the animals may not be possible. 73% of the sightings reported by our collaborating survey teams were of "unidentified seal". Of the remaining 27% that were identified, 68% were harbor seals and 32% were gray seals. Although harp seals and hooded seals may occasionally occur in U.S. waters, and both strandings and bycatch events have been reported (Byrd et al. 2014; Hayes et al. 2019; Hayes et al. 2022; Haverkamp et al. 2023), NOAA's stock definitions for these species do not extend into the U.S., and no sightings were reported by our collaborators. Accordingly, we based our modeling decisions on what is known about harbor seals and gray seals.

Although both harbor seals and gray seals are often described as non-migratory (Breed et al. 2006; Ampela et al. 2019) and occupy the Gulf of Maine year-round (Haverkamp et al. 2023), they are known to undertake directed seasonal movements that can span hundreds of kilometers (Moxley 2016; Ampela et al. 2019). Both species are known to exhibit strong seasonal changes in haul-out behavior (Pace et al. 2019). Below, we review what is known of the seasonality of the two species in our study area, and then discuss how we approached modeling them together as a guild.

Harbor seals

During pupping season, May-June, the New England harbor seal the population is found primarily in Maine and Canada (Gilbert et al. 2005), where a sizeable fraction of the popuation it is resident year-round (Payne and Selzer 1989). Pupping season is followed by a molting period in July-August (Pace et al. 2019). In late September through late May, harbor seals may be found south of Maine (Payne and Selzer 1989). In winter, significant numbers occur from Cape Cod to Long Island (Gilbert et al. 2005).

South of New York, harbor seals occur regularly, if in lower numbers, from fall through spring. From 1996-2010, Toth et al. (2018) observed harbor seals overwintering at the Great Bay-Mullica River estuary in southern New Jersey and reported that seals consistently arrived in October or November and departed by May, with February-April being the months of highest occupancy. The authors reported a significant interannual increase in the maximum daily abundance of hauled-out seals, assessed as raw counts made on daily surveys, from 100 individuals in the 1996/97 season to 160 in 2010/11.

During fall-spring of 2014/15 through 2020/21, Jones and Rees (2022) observed harbor seals hauled-out in Virginia, along rock armor formations of the Chesapeake Bay Bridge Tunnel, from November through May, with the peak occurring in January, February, or March, depending on the year. These researchers estimated abundance for each of their six survey seasons with a Lincoln-Petersen mark-resight model and reported a minimum, mean, and maximum of 81, 183, and 242 individuals, respectively.

On 2-4 February 2018, Ampela et al. (2019) fitted satellite tags to seven harbor seals captured at the haul-out sites monitored by Jones and Rees (2022). Six conducted local movements at the mouth of Chesapeake Bay for two months, then departed Virginia waters between 29 March and 15 April 2018 and were tracked to southern New England and the Gulf of Maine. Four reached coastal Maine or Canada between 15 April and 15 May. Two reached the south coast of Massachusetts before transmissions ceased on 9 April and 23 May. The seventh, a young-of-the-year less than 1.5 years old (the only such seal tagged), did not depart Virginia waters before transmissions ceased on 26 April. Ampela et al. (2021) tagged an additional two harbor seals on 26 February and 2 March 2020. These seals departed Virginia on 31 and 20 March, respectively, and moved to coastal Maine. Their arrival times were not reported, but final transmission dates were 11 July and 10 June, respectively.

Byrd et al. (2014) summarized harbor seal strandings in North Carolina by month over the period 1997-2008. Strandings were reported at least once in every month except August, but 86% of sightings occurred between January and April, consistent with the seasonality observed for Virginia by Jones and Rees (2022), with a peak in March. The authors examined the spatial distribution of strandings across the North Carolina shoreline and found that south of Cape Lookout, the expected number of strandings was significantly fewer than north of Cape Lookout. The authors also reported that 86% of the North Carolina harbor seals were of immature animals. In Virginia, of the nine seals tagged by Ampela et al., three were adults, five were juveniles, and one was a young-of-the-year, and Ampela et al. (2019) reported that "the Chesapeake Bay and coastal Virginia is seasonal habitat for healthy juvenile and adult harbor seals." (Jones and Rees (2022) did not report on maturity.)

Gray seals

Considerably less is known about gray seals in U.S. waters. In eastern Canada, european hunting had depleted gray seal populations by the mid-1800s, and the gray seal was considered uncommon through the 1950s (Lesage and Hammill 2001). Starting in the 1960s, the population at Sable Island began a period of strong exponential growth, at an annual rate of 12.8%, that was sustained through the 1990s, eventually becoming the largest gray seal colony in the world (Bowen et al. 2003). Since 2007, the growth rate has slowed to 5-7% per annum (den Heyer et al. 2021). In the U.S., hunting had extirpated gray seals by the mid-20th century, but the species gained protection with the passage of the Marine Mammal Protection Act in 1972 (Wood et al. 2020). Since the 1990s, several U.S. gray seal colonies have undergone exponential recovery similar to

that observed at Sable Island (Pace et al. 2019; Wood et al. 2020), and strandings, as well as bycatch rates in the U.S. sink gillnet fishery, have similarly increased (Johnston et al. 2015).

Gray seal pupping season occurs in December-February and is followed by a molting period from March-June (Pace et al. 2019). Lesage and Hammill (2001) report a post-breeding, pre-molting pelagic phase at Sable island that runs from February-April. The pupping and molting periods are followed by a longer foraging period in which time spent hauled-out is reduced and more variable (Pace et al. 2019).

Complicating this are apparent seasonal and diel patterns in haul-out behavior observed at Chatham, Massachusetts, not far from the largest U.S. gray seal colony at Monomoy Island. Here, in 2012-2013, Moxley (2016) tracked 8 gray seals with GPS/GSRM telemetry tags and reported results for the months of June through March. In summer, the seals spent a greater proportion of time hauled-out, made shorter trips to sea that encompassed a smaller area, tended to depart just before sunset or during twilight, and return just prior to dawn. During winter, seals spent less time hauled-out, made much longer trips to much larger areas that ranged far offshore, and tended to depart and arrive evenly throughout the day and night. Moxley identified the month of November as the time the seals switched between these two modes, and hypothesized these behaviors were related to the summer presence and winter absence of predatory white sharks in the area.

In winter, gray seals do not currently appear to travel as far south, at least in as great numbers, as harbor seals. Jones and Rees (2022) reported that gray seals were only occasionally observed in Virginia in winter, and recorded just four sightings in the 2020/21 survey season. Byrd et al. (2014) reported that in North Carolina between 1997-2008, only 12 strandings were reported: 11 in February through May and 1 in August.

Model configuration

Much of the northern half of our study area is occupied year-round by both harbor seals and gray seals. Both species undertake directed seasonal movements within the region and exhbit changes in haul-out behavior. When seasonal changes in behavior such as these are likely to manifest different species-environment relationships, our modeling approach for the 2022 modeling cycle was to split the year into seasonal models. This job was complicated by the species exhibiting different timing in their annual reproduction and molting cycles. After reviewing the available survey data and what is known about the species, we settled on a two season model, with "Summer" running from June-October and "Winter" running from November-May.

We placed the Winter-to-Summer transition at May-June based on June being the month in which most harbor seals will have completed their seasonal migration to traditional breeding grounds in Maine and Canada. We explored placing this transition at April-May instead, but noted very few sightings in May off of coastal Maine, with many sightings still reported east of Cape Cod and the Nantucket Shoals, while June showed many sightings off Maine and fewer east of Cape Cod. This is consistent with Payne and Selzer's (1989) description of the harbor seal occurring in southern New England through late May. We recommend additional surveying of the Maine coastline in May to better assess the density of seals in the water during this month.

We placed the Summer-to-Winter transition at October-November based on November being the first month in which the surveys reported sightings along Long Island and on Moxley's reported change in gray seal behavior from long haul-outs with short foraging excursions to short haul-outs with long excursions. We experimented with placing this transition at September-October, based on Payne and Selzer's (1989) description of the harbor seal occurring in southern New England starting in late September, but Winter models that started in October predicted higher density in the mid-Atlantic in October than in all other months (November-May), which did not accord with the seasonal peaks reported by the studies in New Jersey, Virginia, and North Carolina (see above).

4.1   Summer Model

For the Summer (June-October) season, we split the study area at Chesapeake Bay and assumed seals were absent south of here during these months. In preliminary model development, all of the top scoring models retained a distance to front covariate, indicating higher density near fronts, based on frontal features found in the Gulf of Maine where sightings were plentiful. This relationship caused aberrant predictions of moderate density near Cape Hatteras in June and October, driven by the proximity to the Gulf Stream. To fix the problem, we kept the covariate but shifted the model's southern edge to Chesapeake Bay. We caution that strandings have very occasionally occurred as far south as North Carolina in every month of the year (Byrd et al. 2014), but do not believe this indicates a non-negligible density south of Chesapeake Bay in June-October.

We excluded waters north of Halifax, Nova Scotia from the model, owing to a lack of data in this region. In particular, we lacked adequate data around Sable Island, the largest gray seal colony in the world (Bowen et al. 2003) and were not confident our model would estimate reasonable densities there.

Preliminary modeling suggested that zooplankton biomass estimates from SEAPODYM (Lehodey et al. 2008) were the most effective biological covariate of those we tried. Because this covariate was only available through 2019, and the surveying done in 2020 did not provide critical new information on seal distributions, we excluded 2020 from the model in order to utilize the zooplankton covariate.

The surveys incorporated into the model, spanning 1998-2019, reported over 700 sightings (Figure 21). Most were concentrated along the coast of Maine, including numerous sightings on the surveys that navigated deep inshore, such as into Penobscot Bay. Smaller concentrations occurred off southern Nova Scotia and southeast of Cape Cod.

The model selection procedure was straightforward. When ranked by REML score (Wood 2011), the highest ranked model with climatological covariates slightly outranked that with contemporaneous covariates, and explained slightly more deviance, 47.8% vs. 47.0%. However, predictions from the best climatological-covariate models yielded mean monthly abundances that were clearly too high, so we selected the best contemporaneous-covariate model as our final choice.

The model included two static covariates and three dynamic covariates (Table 13). The functional relationships for depth and distance to shore (Figure 24) indicated a positive effect in waters shallower than 80 m (about 1.9 in $\log_{10}$ scale) and closer than 40 km to shore, consistent with harbor and gray seals being described as coastal species (Payne and Selzer 1989; Lesage and Hammill 2001). The relationship for sea surface temperature (SST) showed a slight peak at about 12.5 °C and a positive effect for waters colder than about 17.5 °C, indicating a strong preference for waters in the northern half of the modeled region. The relationship for distance to SST fronts was positive for waters closer than 20 km to fronts, neutral between 20-40 km, and negative for waters farther than 40 km. This relationship likely relates to a high density of seals present in the vicinity of the Eastern Maine Coastal Current and Western Maine Coastal Current, where fronts regularly occur, as well as off southern Nova Scotia. Finally, the relationship for SEAPODYM's zooplankton biomass was bimodal, with one peak at high values and another at low values. This result was difficult to interpret, and likely reflects seals being present both along the Maine Coast, where SEAPODYM predicted zooplankton biomass was high, and other areas such as east of Cape Cod late in the season, where it was lower. Seals do not consume zooplankton, but we included it in the pool of candidate covariates on the basis that it might serve as a proxy for seals' actual prey.
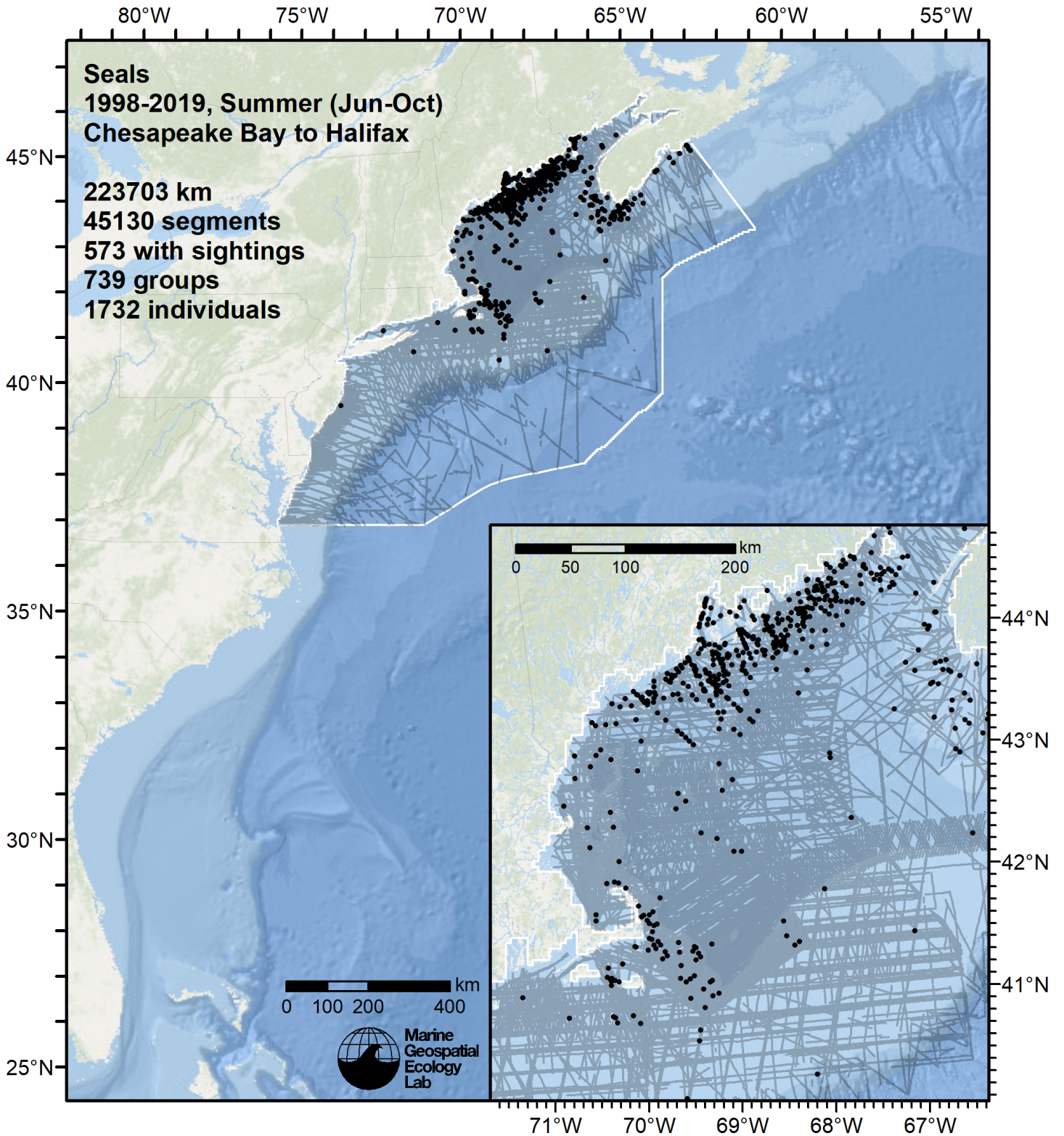
Figure 21: Survey segments used to fit the model for the region Chesapeake Bay to Halifax for Summer. Black points indicate segments with observations.
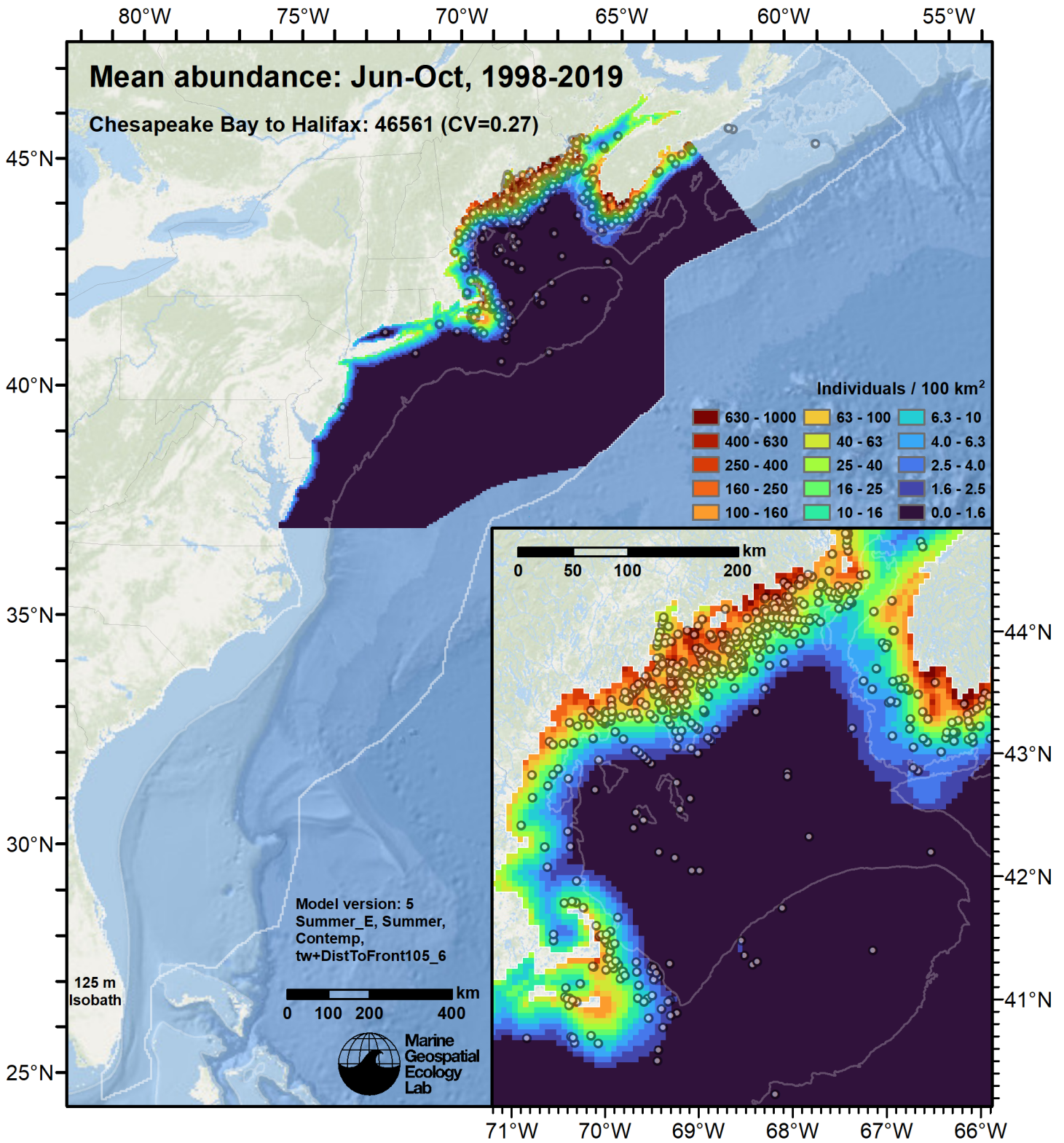
Figure 22: Seals mean density for the indicated period, as predicted by the model for the region Chesapeake Bay to Halifax for Summer. Open circles indicate segments with observations. Mean total abundance and its coefficient of variation (CV) are given in the subtitle. Variance was estimated with the analytic approach given by Miller et al. (2022), Appendix S1, and accounts both for uncertainty in model parameter estimates and for seasonal and interannual variability in dynamic covariates.
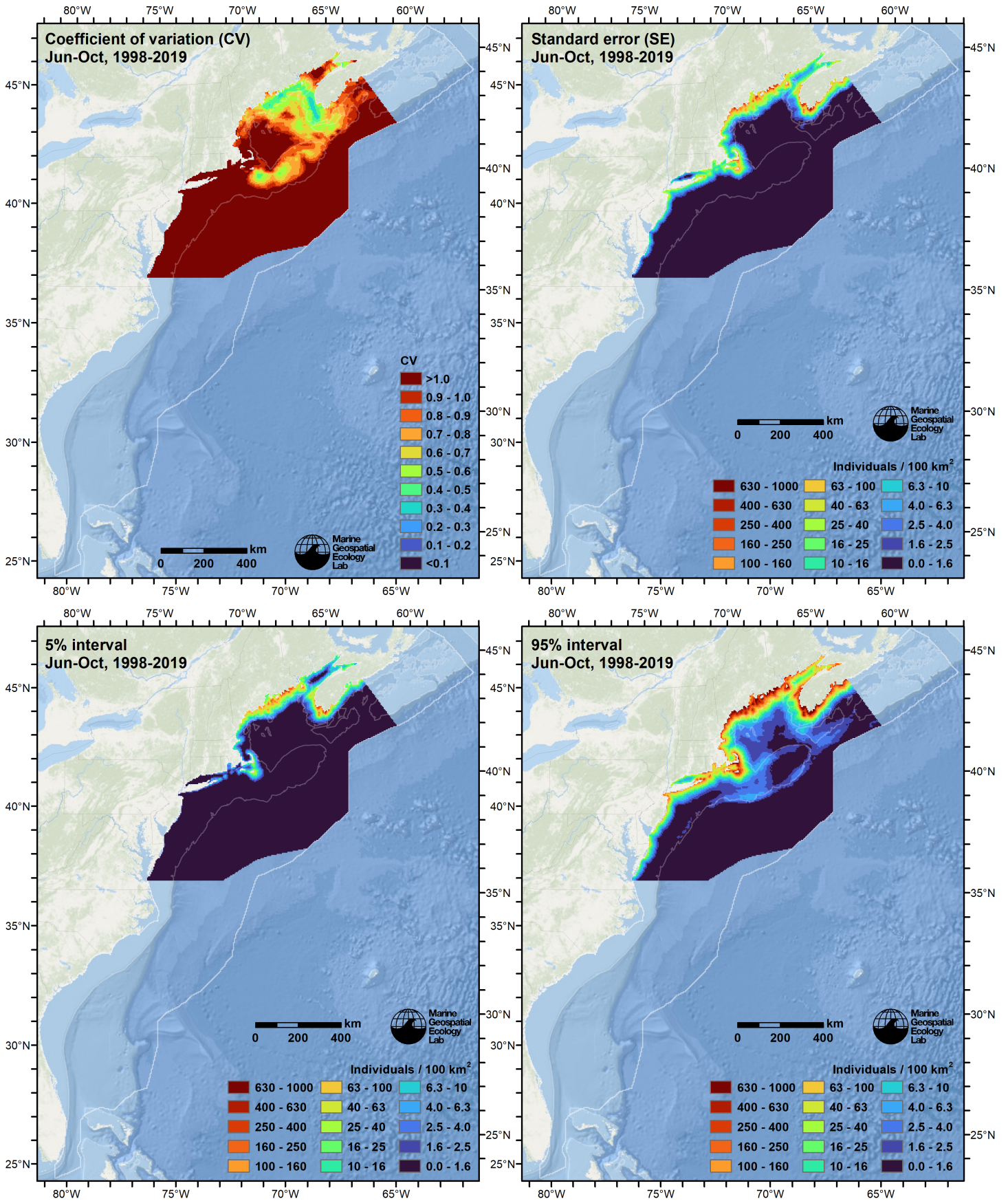
Figure 23: Uncertainty statistics for the seals mean density surface (Figure 22) predicted by the model for the region Chesapeake Bay to Halifax for Summer. Variance was estimated with the analytic approach given by Miller et al. (2022), Appendix S1, and accounts both for uncertainty in model parameter estimates and for seasonal and interannual variability in dynamic covariates.

Statistical output for this model:

```
Family: Tweedie(p=1.451)
Link function: log

Formula:
IndividualsCorrected ~ offset(log(SegmentArea)) + s(pmin(I(DistToShore/1000),
    250), bs = "ts", k = 5) + s(log10(pmax(3, pmin(Depth, 500)))),
    bs = "ts", k = 5) + s(pmax(6, pmin(SST_CMC, 27)), bs = "ts",
    k = 5) + s(pmin(I(DistToFront105/1000), 75), bs = "ts", k = 5) +
    s(pmax(0.2, pmin(Zoo_SEAPODYM, 12)), bs = "ts", k = 5)

Parametric coefficients:
            Estimate Std. Error t value Pr(>|t|)
(Intercept) -18.6552     0.1141  -163.6   <2e-16 ***
---
Signif. codes:  0 '***' 0.001 '**' 0.01 '*' 0.05 '.' 0.1 ' ' 1


Approximate significance of smooth terms:
                                       edf Ref.df       F  p-value
s(pmin(I(DistToShore/1000), 250))    3.793      4 100.290  < 2e-16 ***
s(log10(pmax(3, pmin(Depth, 500))))  1.785      4   4.742 2.15e-05 ***
s(pmax(6, pmin(SST_CMC, 27)))        3.260      4  49.572  < 2e-16 ***
s(pmin(I(DistToFront105/1000), 75))  3.487      4  34.938  < 2e-16 ***
s(pmax(0.2, pmin(Zoo_SEAPODYM, 12))) 3.686      4   8.151 1.38e-06 ***
---
Signif. codes:  0 '***' 0.001 '**' 0.01 '*' 0.05 '.' 0.1 ' ' 1


R-sq.(adj) =  0.0043   Deviance explained =   47%
-REML = 4900.8  Scale est. = 44.488    n = 45130

Method: REML   Optimizer: outer newton
full convergence after 11 iterations.
Gradient range [-0.0007965455,0.0001141972]
(score 4900.793 & scale 44.48757).
Hessian positive definite, eigenvalue range [0.1736985,2004.392].
Model rank =  21 / 21

Basis dimension (k) checking results. Low p-value (k-index<1) may
indicate that k is too low, especially if edf is close to k'.

                                       k'  edf k-index p-value
s(pmin(I(DistToShore/1000), 250))    4.00 3.79    0.51  <2e-16 ***
s(log10(pmax(3, pmin(Depth, 500))))  4.00 1.78    0.55  <2e-16 ***
s(pmax(6, pmin(SST_CMC, 27)))        4.00 3.26    0.54  <2e-16 ***
s(pmin(I(DistToFront105/1000), 75))  4.00 3.49    0.59   0.575
s(pmax(0.2, pmin(Zoo_SEAPODYM, 12))) 4.00 3.69    0.55   0.005 **
---
Signif. codes:  0 '***' 0.001 '**' 0.01 '*' 0.05 '.' 0.1 ' ' 1
```

(a) Seafloor depth (m)

(b) Distance to SST front (km)

(c) Distance to shore (km)

(d) Sea surface temperature (°C)
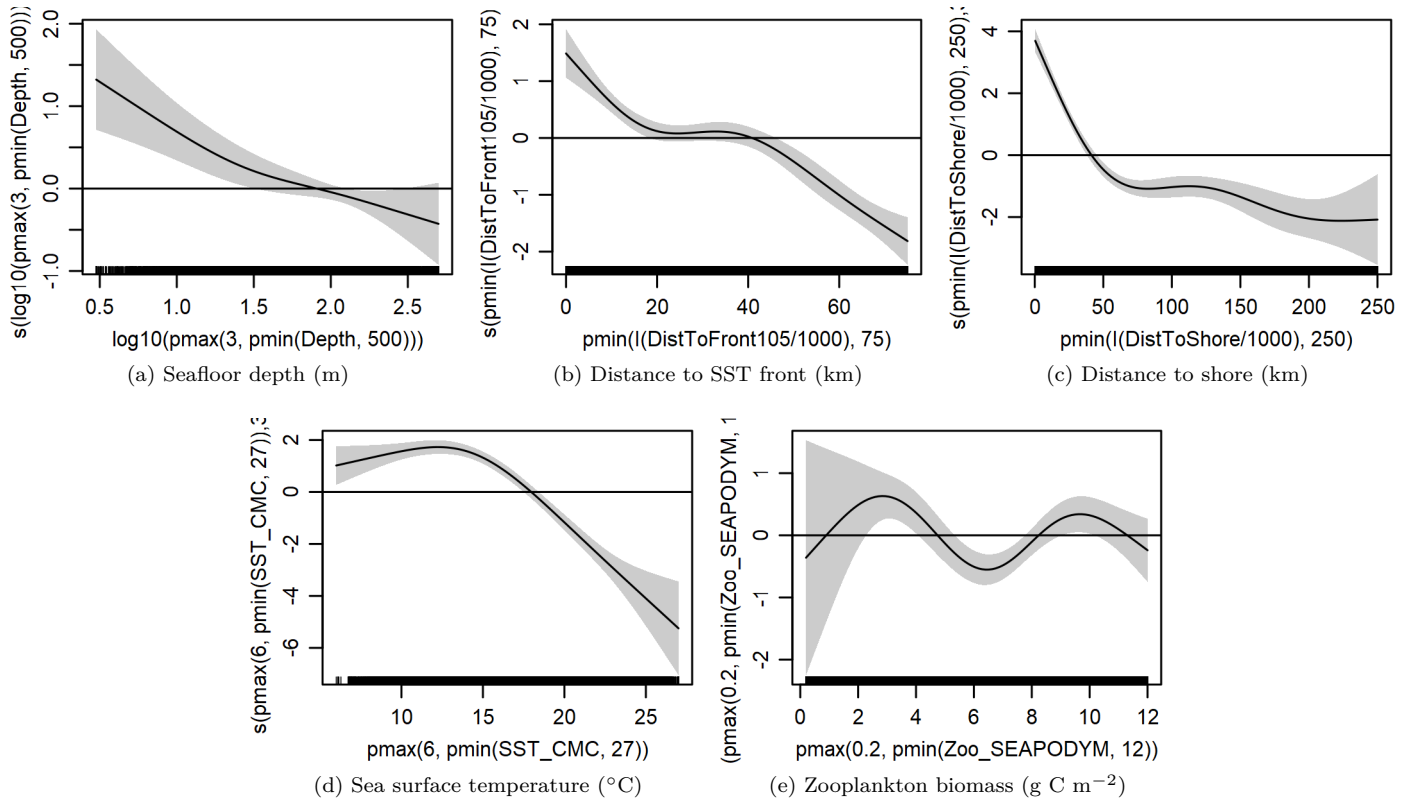
(e) Zooplankton biomass (g C m^{-2})

Figure 24: Functional plots for the final model for the region Chesapeake Bay to Halifax for Summer. Transforms and other treatments are indicated in axis labels. *log10* indicates the covariate was $\log_{10}$ transformed. *pmax* and *pmin* indicate the covariate's minimum and maximum values, respectively, were Winsorized to the values shown. Winsorization was used to prevent runaway extrapolations during prediction when covariates exceeded sampled ranges, or for ecological reasons, depending on the covariate. */1000* indicates meters were transformed to kilometers for interpretation convenience.

Table 13: Covariates used in the final model for the region Chesapeake Bay to Halifax for Summer.

| Covariate	Description
Depth	Depth (m) of the seafloor, from SRTM30_PLUS (Becker et al. (2009))
DistToFront105	Monthly mean distance (km) to the closest sea surface temperature front detected in daily GHRSST Level 4 CMC0.2deg and CMC0.1deg images (Brasnett (2008); Canada Meteorological Center (2012); Meissner et al. (2016); Canada Meteorological Center (2016)) with MGET's implementation of the Canny edge detector (Roberts et al. (2010); Canny (1986))
DistToShore	Distance (km) to shore excluding Bermuda and Sable Island, derived from SRTM30_PLUS (Becker et al. (2009))
SST_CMC	Monthly mean sea surface temperature (°C) from GHRSST Level 4 CMC0.2deg and CMC0.1deg (Brasnett (2008); Canada Meteorological Center (2012); Meissner et al. (2016); Canada Meteorological Center (2016))
Zoo_SEAPODYM	Monthly mean zooplankton biomass expressed in carbon (g C m^{-2}) from SEAPODYM (Lehodey et al. (2008); Lehodey et al. (2015)), provided by E.U. Copernicus Marine Service. doi: 10.48670/moi-00020

4.1.2 Diagnostic Plots
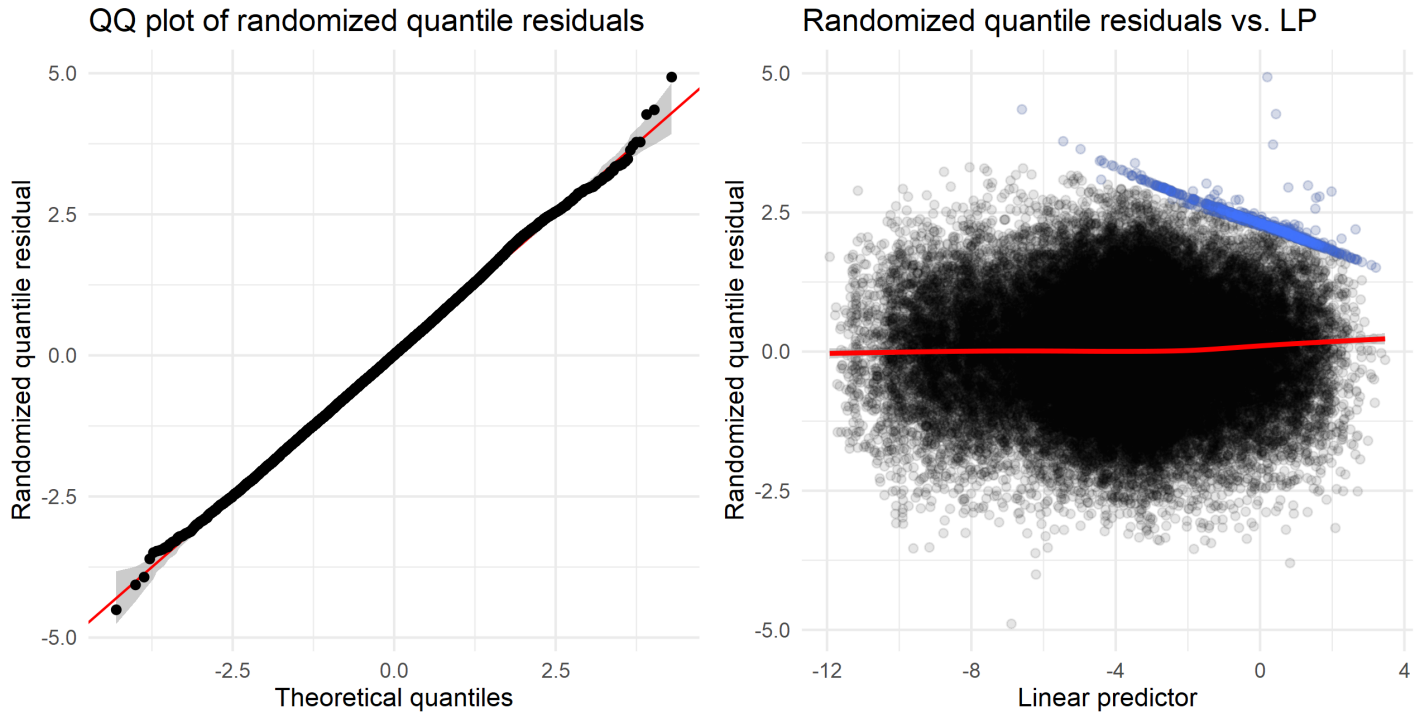
Figure 25: Residual plots for the final model for the region Chesapeake Bay to Halifax for Summer.
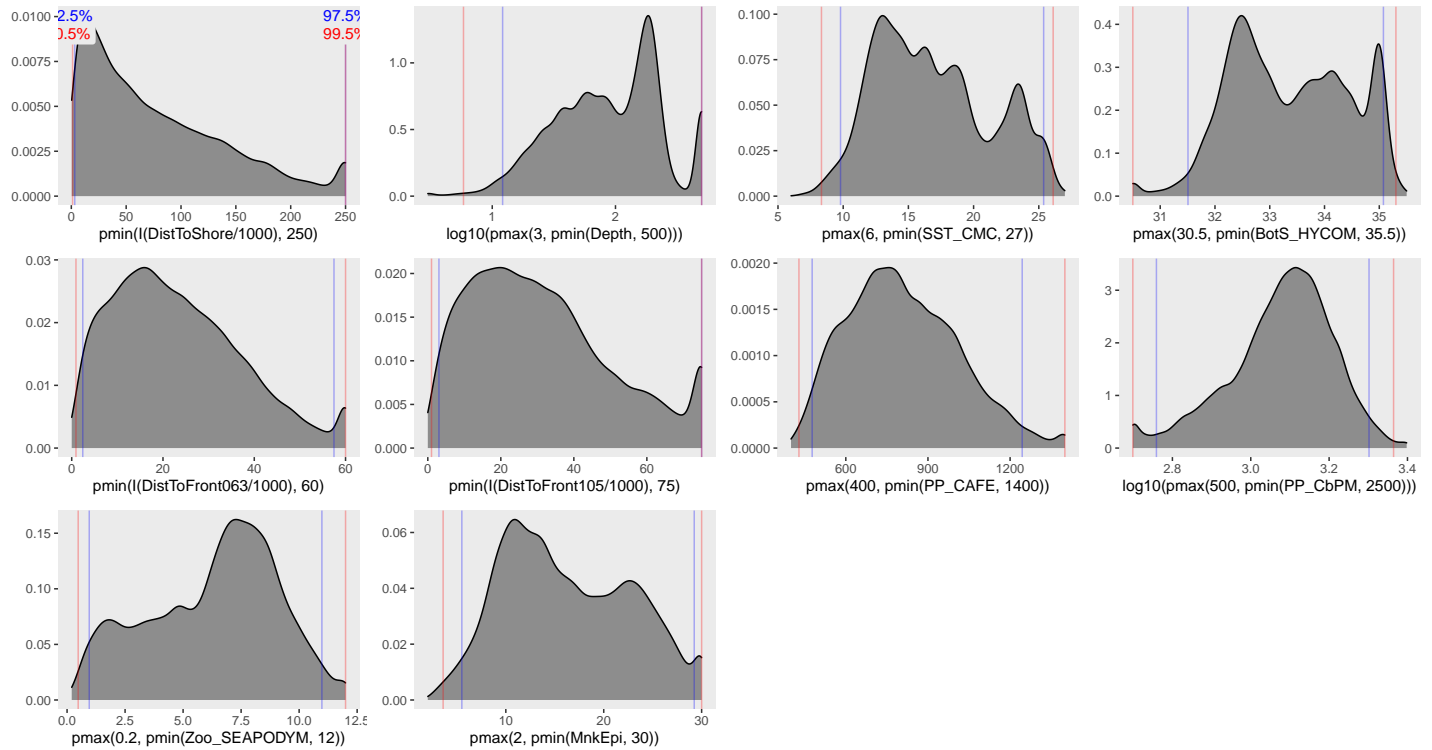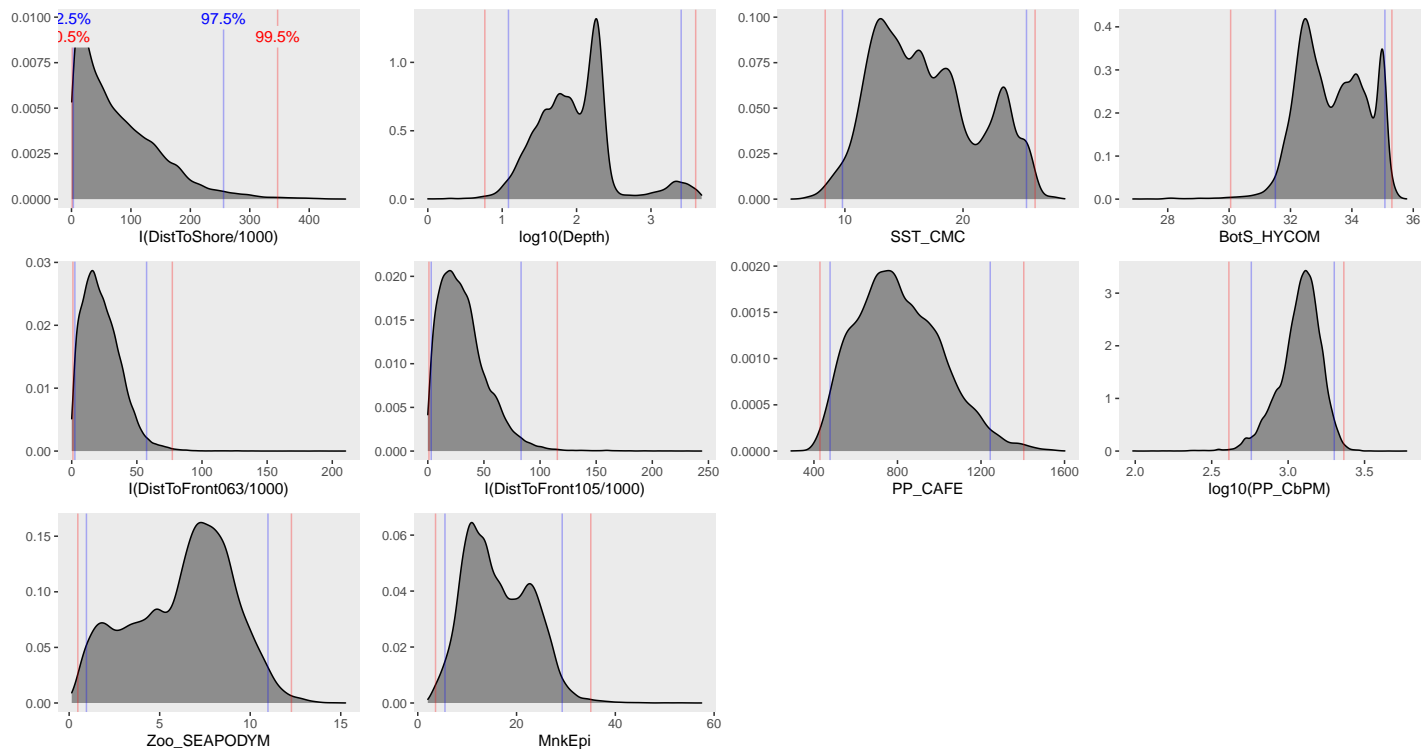
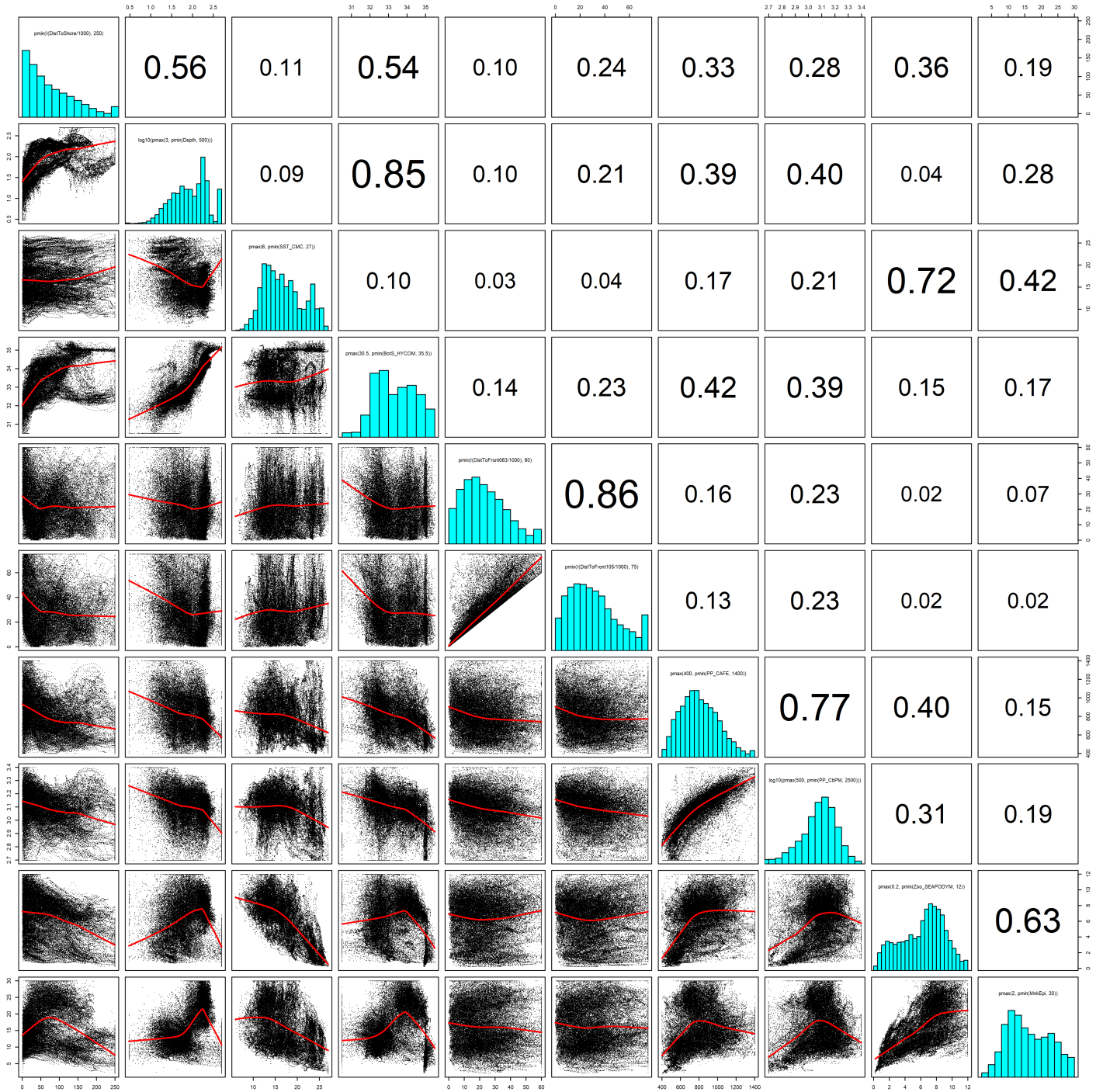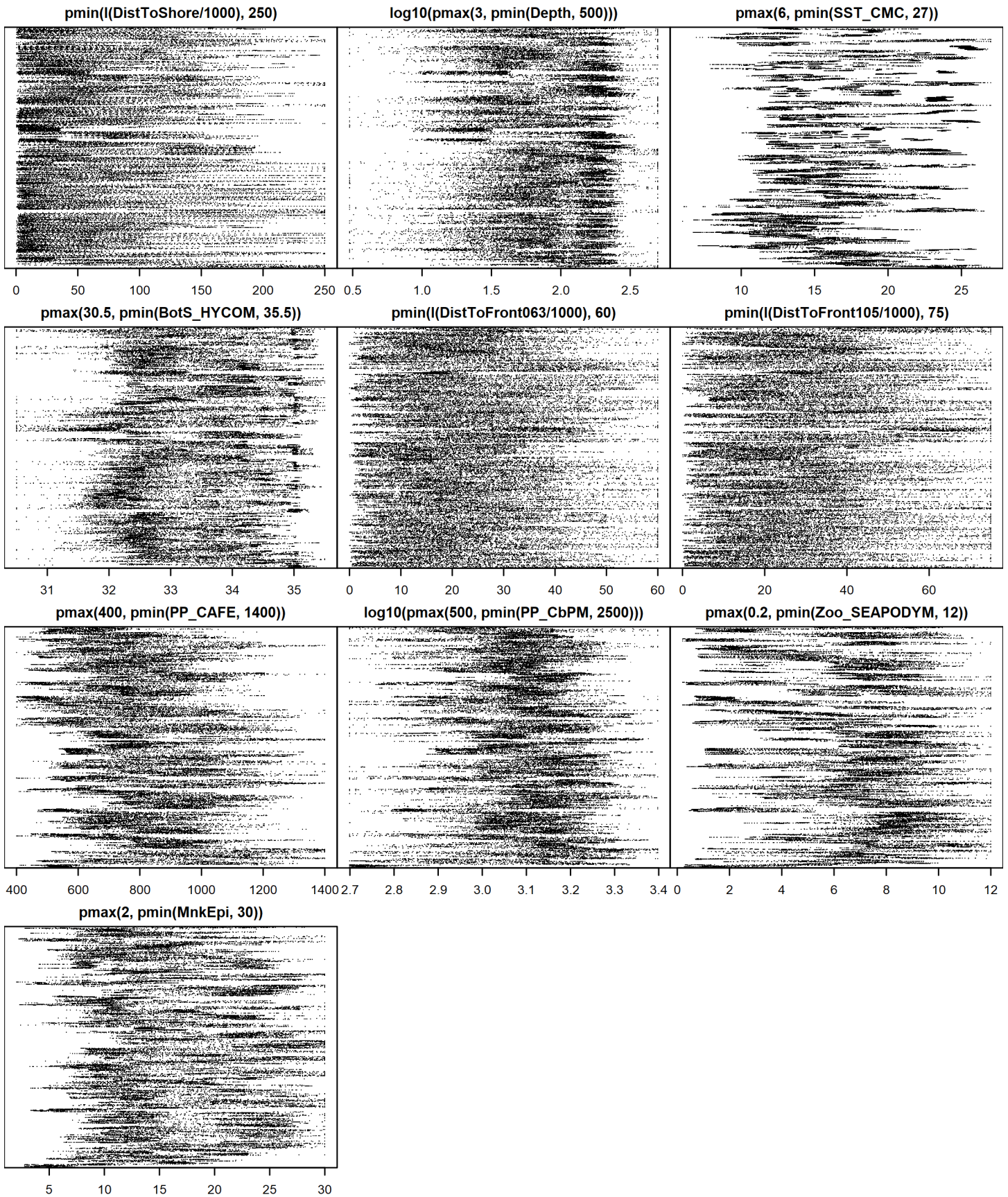Figure 26: Density histograms showing the distributions of the covariates considered during the final model selection step. The final model may have included only a subset of the covariates shown here (see Figure 24), and additional covariates may have been considered in preceding selection steps. Red and blue lines enclose 99% and 95% of the distributions, respectively. Transforms and other treatments are indicated in axis labels. *log10* indicates the covariate was $\log_{10}$ transformed. *pmax* and *pmin* indicate the covariate's minimum and maximum values, respectively, were Winsorized to the values shown. Winsorization was used to prevent runaway extrapolations during prediction when covariates exceeded sampled ranges, or for ecological reasons, depending on the covariate. */1000* indicates meters were transformed to kilometers for interpretation convenience.

Figure 27: Density histograms shown in Figure 26 replotted without Winsorization, to show the full range of sampling represented by survey segments.

38

Figure 28: Scatterplot matrix of the covariates considered during the final model selection step. The final model may have included only a subset of the covariates shown here (see Figure 24), and additional covariates may have been considered in preceding selection steps. Covariates are transformed and Winsorized as shown in Figure 26. This plot is used to check simple correlations between covariates (via pairwise Pearson coefficients above the diagonal) and visually inspect for concurvity (via scatterplots and red lowess curves below the diagonal).

Figure 29: Dotplot of the covariates considered during the final model selection step. The final model may have included only a subset of the covariates shown here (see Figure 24), and additional covariates may have been considered in preceding selection steps. Covariates are transformed and Winsorized as shown in Figure 26. This plot is used to check for suspicious patterns and outliers in the data. Points are ordered vertically by segment ID, sequentially in time.

4.1.3 Extrapolation Diagnostics

4.1.3.1 Univariate Extrapolation

(a) Depth covariate

(b) DistToShore covariate
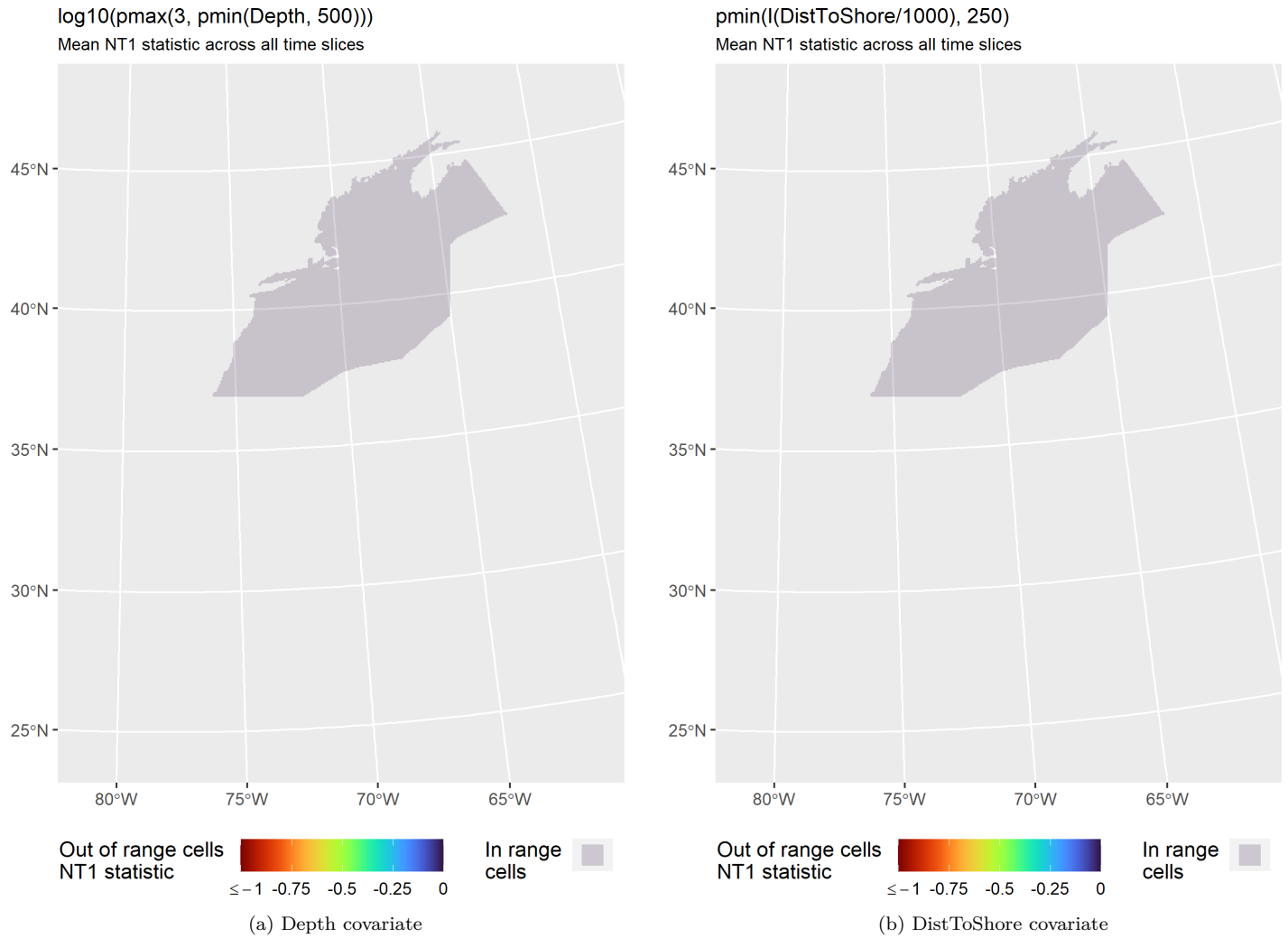
Figure 30: NT1 statistic (Mesgaran et al. (2014)) for static covariates used in the model for the region Chesapeake Bay to Halifax for Summer. Areas outside the sampled range of a covariate appear in color, indicating univariate extrapolation of that covariate occurred there. Areas within the sampled range appear in gray, indicating it did not occur.
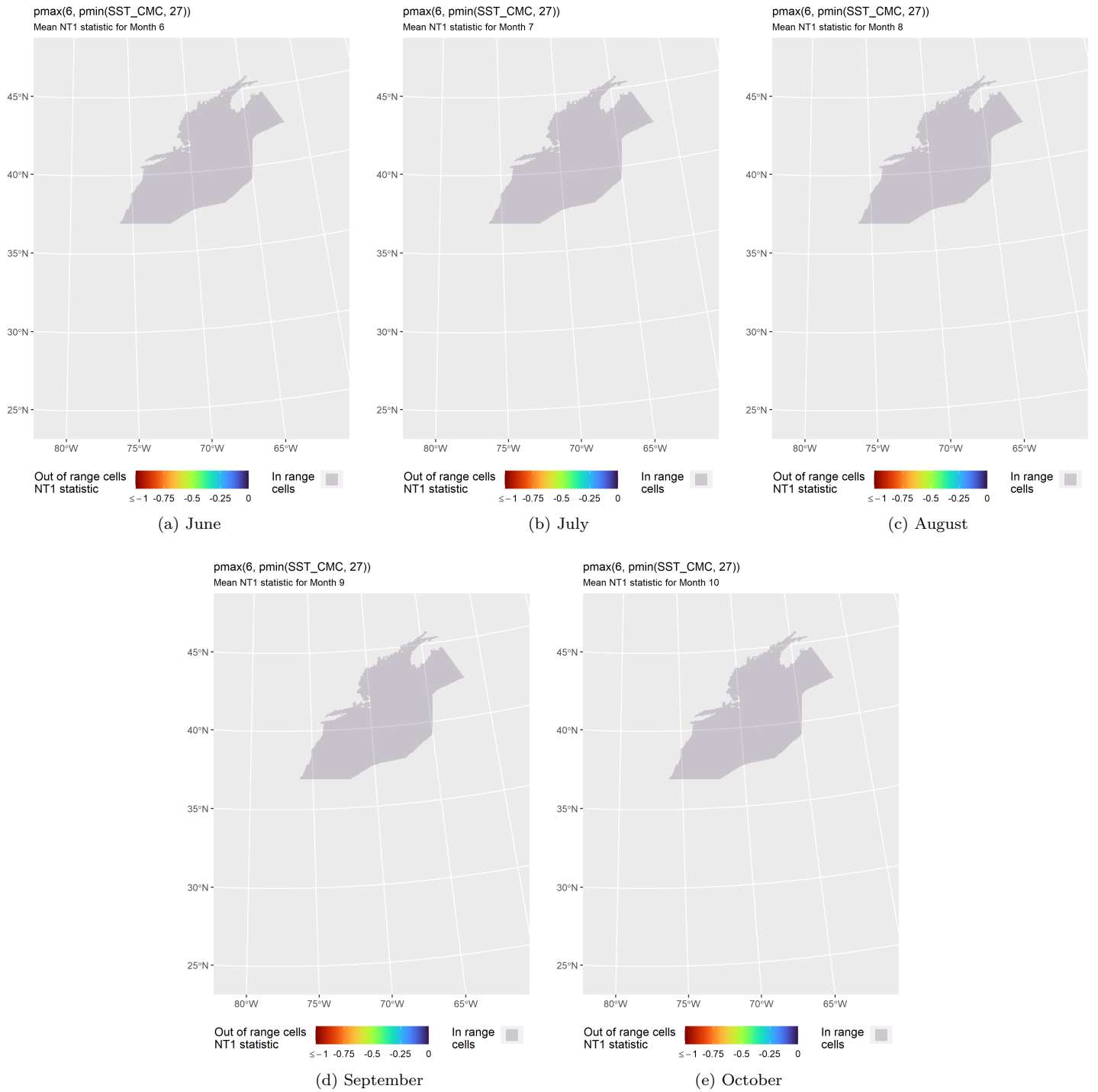
(a) June   (b) July   (c) August

(d) September   (e) October
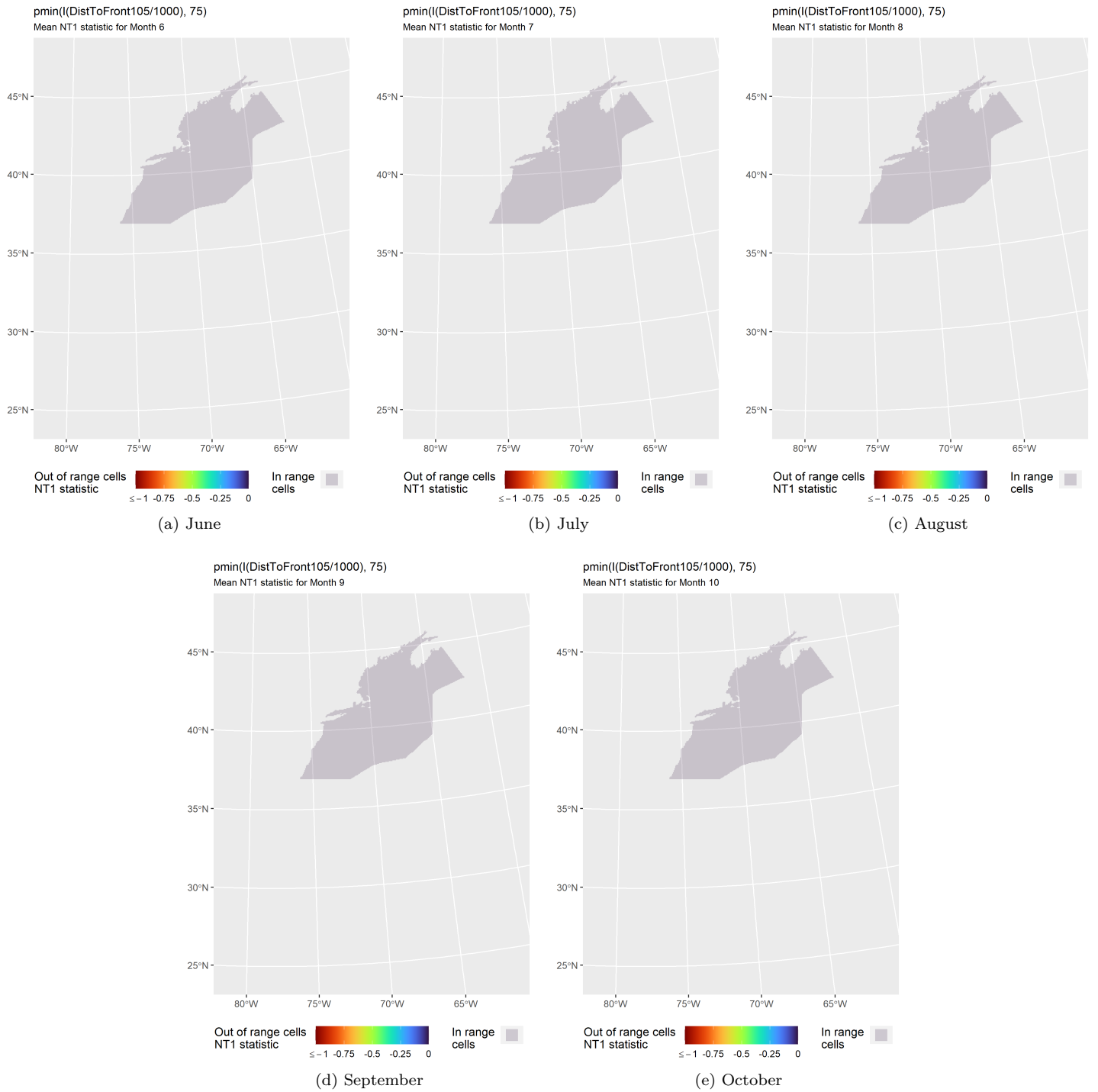
Figure 31: NT1 statistic (Mesgaran et al. (2014)) for the DistToFront105 covariate in the model for the region Chesapeake Bay to Halifax for Summer. Areas outside the sampled range of a covariate appear in color, indicating univariate extrapolation of that covariate occurred there during the month. Areas within the sampled range appear in gray, indicating it did not occur.
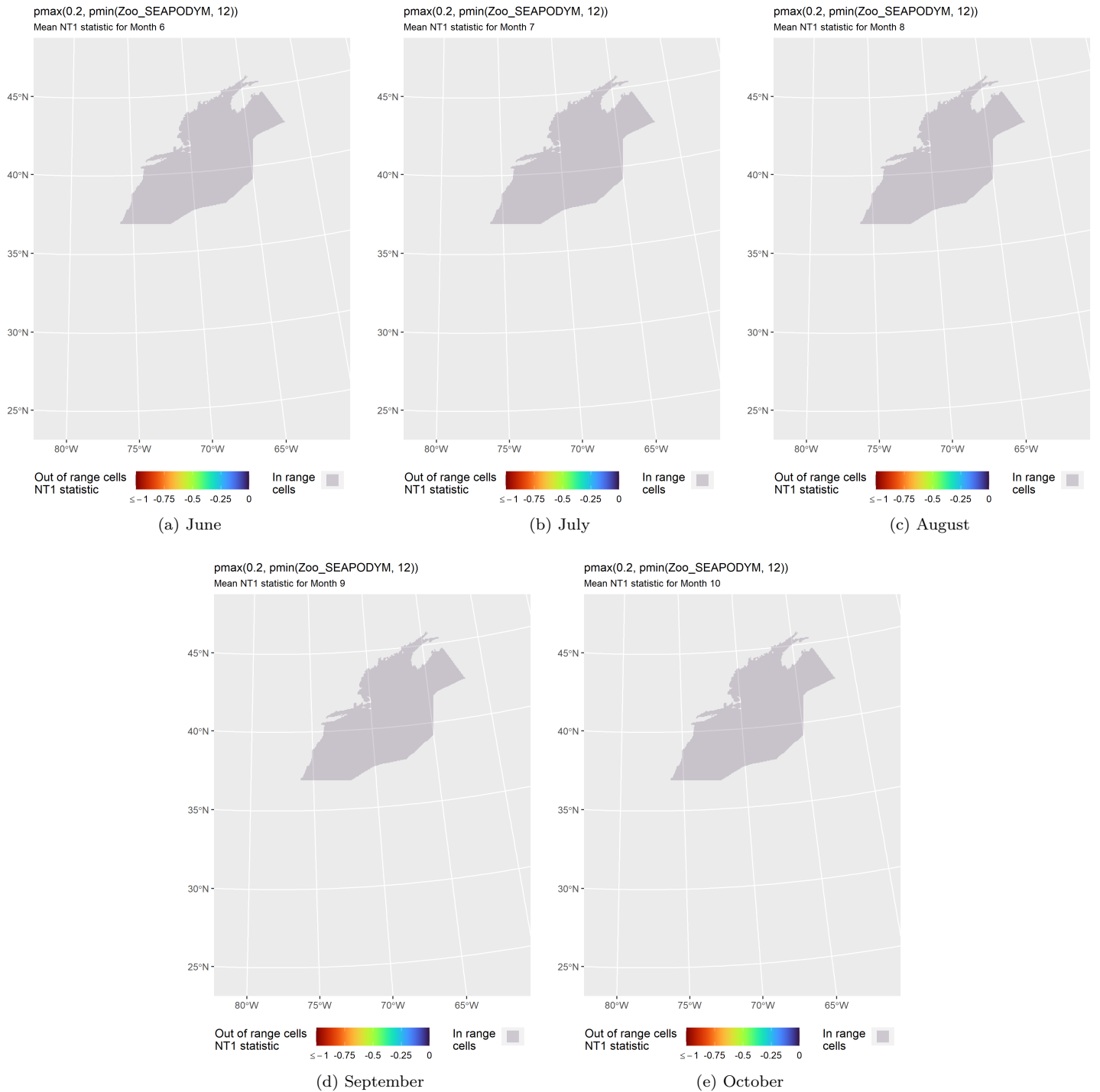
(a) June   (b) July   (c) August

(d) September   (e) October
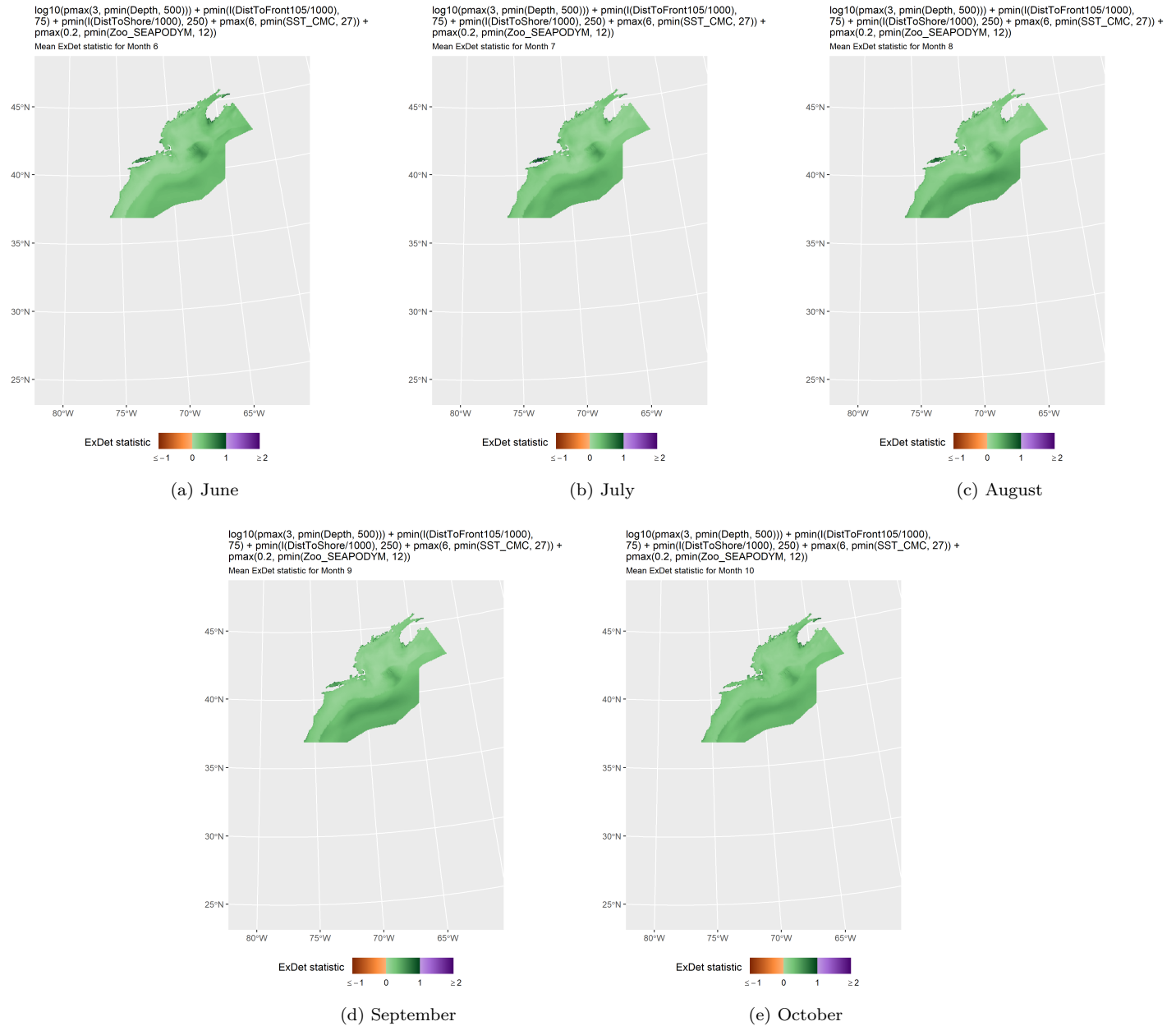
Figure 32: NT1 statistic (Mesgaran et al. (2014)) for the SST_CMC covariate in the model for the region Chesapeake Bay to Halifax for Summer. Areas outside the sampled range of a covariate appear in color, indicating univariate extrapolation of that covariate occurred there during the month. Areas within the sampled range appear in gray, indicating it did not occur.

(a) June

(b) July

(c) August

(d) September

(e) October

Figure 33: NT1 statistic (Mesgaran et al. (2014)) for the Zoo_SEAPODYM covariate in the model for the region Chesapeake Bay to Halifax for Summer. Areas outside the sampled range of a covariate appear in color, indicating univariate extrapolation of that covariate occurred there during the month. Areas within the sampled range appear in gray, indicating it did not occur.

4.1.3.2 Multivariate Extrapolation

(a) June

(b) July

(c) August

(d) September

(e) October

Figure 34: ExDet statistic (Mesgaran et al. (2014)) for all of the covariates used in the model for the region Chesapeake Bay to Halifax for Summer. Areas in orange (ExDet < 0) required univariate extrapolation of one or more covariates (see previous section). Areas in purple (ExDet > 1), did not require univariate extrapolation but did require multivariate extrapolation, by virtue of having novel combinations of covariates not represented in the survey data, according to the NT2 statistic (Mesgaran et al. (2014)). Areas in green ($0 \geq$ ExDet ≤ 1) did not require either type of extrapolation.

4.2 Winter Model

For the Winter (November-May) season, we modeled the entire study area except for the Scotian Shelf and upper Bay of Fundy—we lacked sufficient data to confidently model these areas—and coastal waters from the southern half of Onslow Bay, North Carolina south to Florida, where we assumed seals were absent. We caution that seals are known to very occasionally appear on southern beaches—for example, between 1994-2004, 20 live seals and 6 dead seals were sighted in South Carolina (Wayne E. McFee and Eric S. Zolman, unpublished data)—but when we included this area in our model, it predicted unrealistically high density in several areas. Given the known rarity of seals there, it was more appropriate to assume they were absent than to use the aberrant predictions.

The surveys incorporated into the model, spanning November-May of 1997/98-2019/20, reported over 900 sightings (Figure 35). Most were concentrated southeast of Cape Cod and elsewhere in southern New England. A substantial number were scattered evenly across the Gulf of Maine and Georges Bank. The southernmost sightings occurred along the New Jersey coastline, reported by the 2008-2009 NJDEP surveys.

The model selection procedure was straightforward. When ranked by REML score (Wood 2011), the highest ranked model with contemporaneous covariates, which we selected as our final choice, outranked that with climatological covariates, and explained 1% more deviance, 18.8% vs. 17.8%.

The model included two static covariates and four dynamic covariates (Table 14). Similar to the summer model, the functional relationship for depth (Figure 38) indicated a positive effect in waters shallower than 80 m (about 1.9 in $\log_{10}$ scale), but the relationship for distance to shore was positive closer than 70 km to shore and the slope of the line was much less steep than for the summer model, indicating a more even distribution of density in winter, that reached substantially farther from shore. This reflects the scattering of sightings across the Gulf of Maine and Georges Bank, and is consistent with Moxley's (2016) finding of gray seals conducting distant foraging excursions in winter months.

Turning to the dynamic covariates, the relationship for SST showed a flat positive effect for all temperatures lower than about 12.5 °C and a steady drop as temperature increased beyond that value, with the relationship turning negative at about 14 °C. The overall effect indicates a preference for cool to cold waters, consistent with reports that both species inhabit ice-forming regions of the Gulf of St. Lawrence in winter (Lesage and Hammill 2001; Lesage et al. 2004). Similar to summer, the relationship for distance to SST fronts was positive within 30 km of a front and negative beyond it. The relationship for net primary productivity, as estimated by the Vertically Generalized Production Model (VGPM) (Behrenfeld and Falkowski 1997), showed a peak at relatively high values, corresponding to inshore areas and the region around Nantucket Shoals. Finally, the relationship for sea surface salinity was hump-shaped, with a positive effect for values in the range 32.7-33.1 PSU, indicating a preference for northerly shelf waters.

The NT1 univariate extrapolation diagnostic indicated values of the primary productivity covariate were slightly beyond the sampled range in several regions (Figure 46a-46g), particularly offshore in the south at the beginning and end of the season, where productivity is relatively low. In all of these cases, covariate values were slightly below the minimum sampled value and were Winsorized up to that minimum. Given that the relationship was trending down on the left side, it is possible that densities were slightly overpredicted in these places in these months. However, the resulting densities, inclusive of this effect, were very low (Figures 56-62), so this is probably not a cause for concern for most users of the predictions.
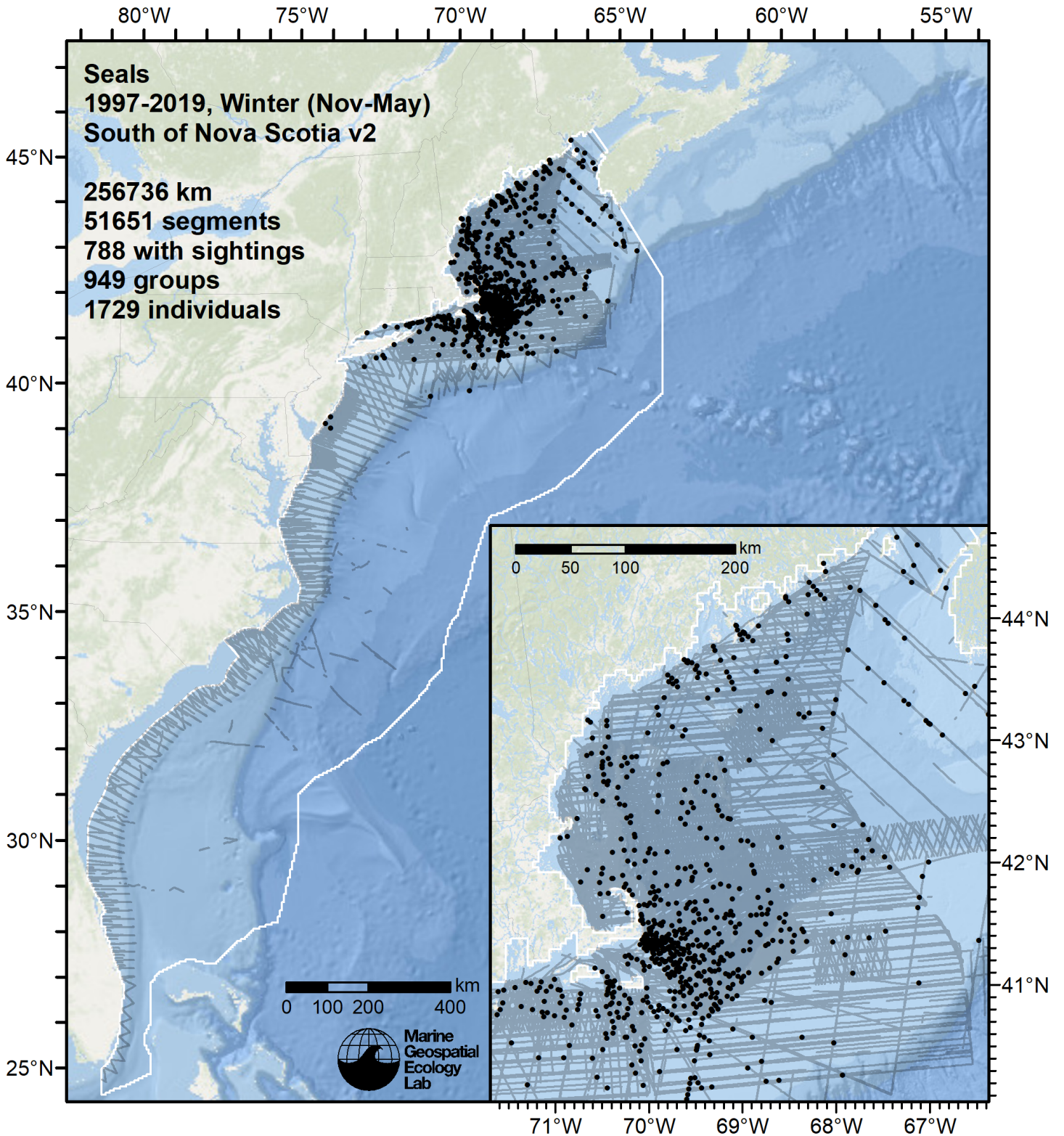
Figure 35: Survey segments used to fit the model for the region South of Nova Scotia v2 for Winter. Black points indicate segments with observations.
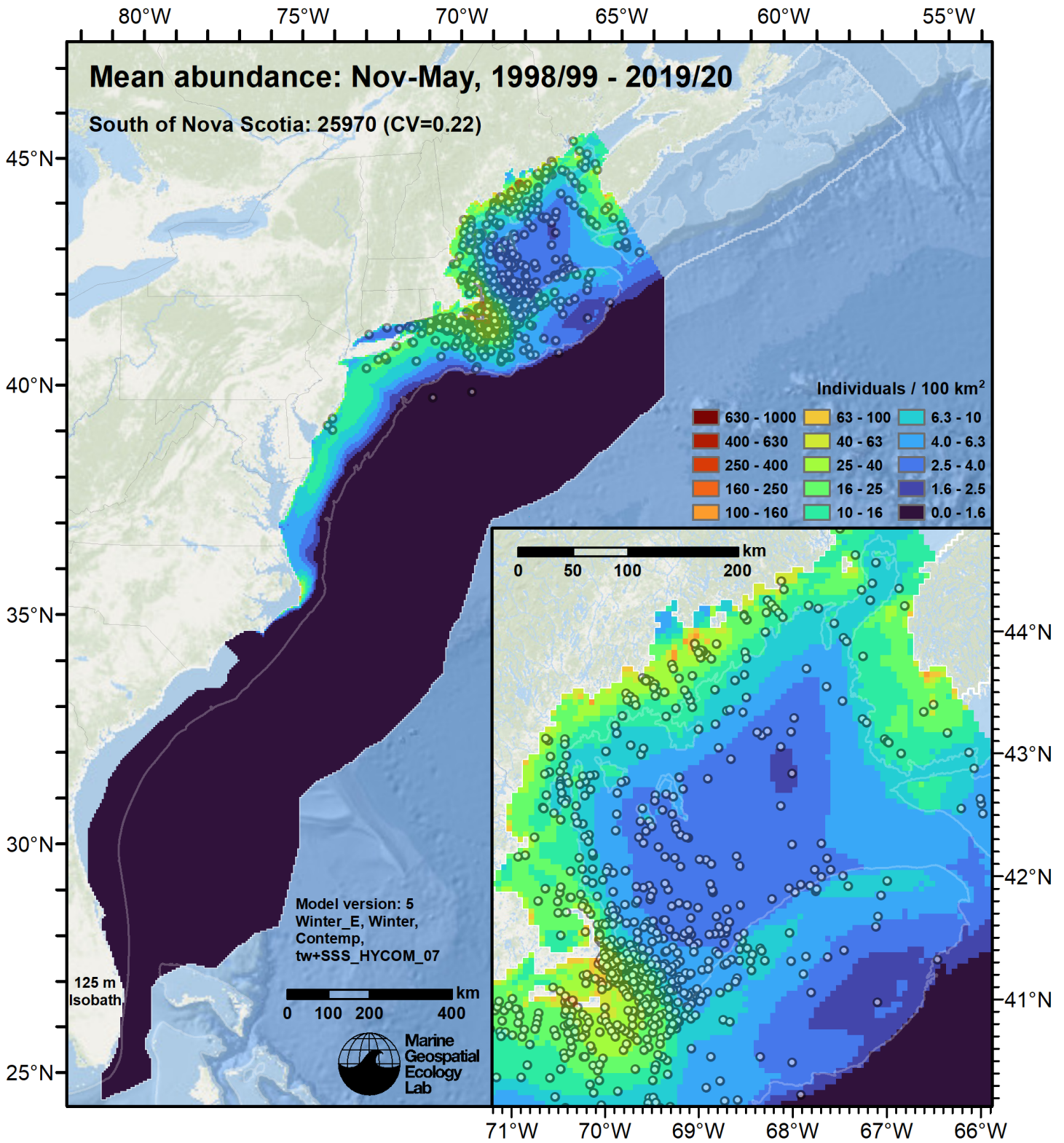
Figure 36: Seals mean density for the indicated period, as predicted by the model for the region South of Nova Scotia v2 for Winter. Open circles indicate segments with observations. Mean total abundance and its coefficient of variation (CV) are given in the subtitle. Variance was estimated with the analytic approach given by Miller et al. (2022), Appendix S1, and accounts both for uncertainty in model parameter estimates and for seasonal and interannual variability in dynamic covariates.
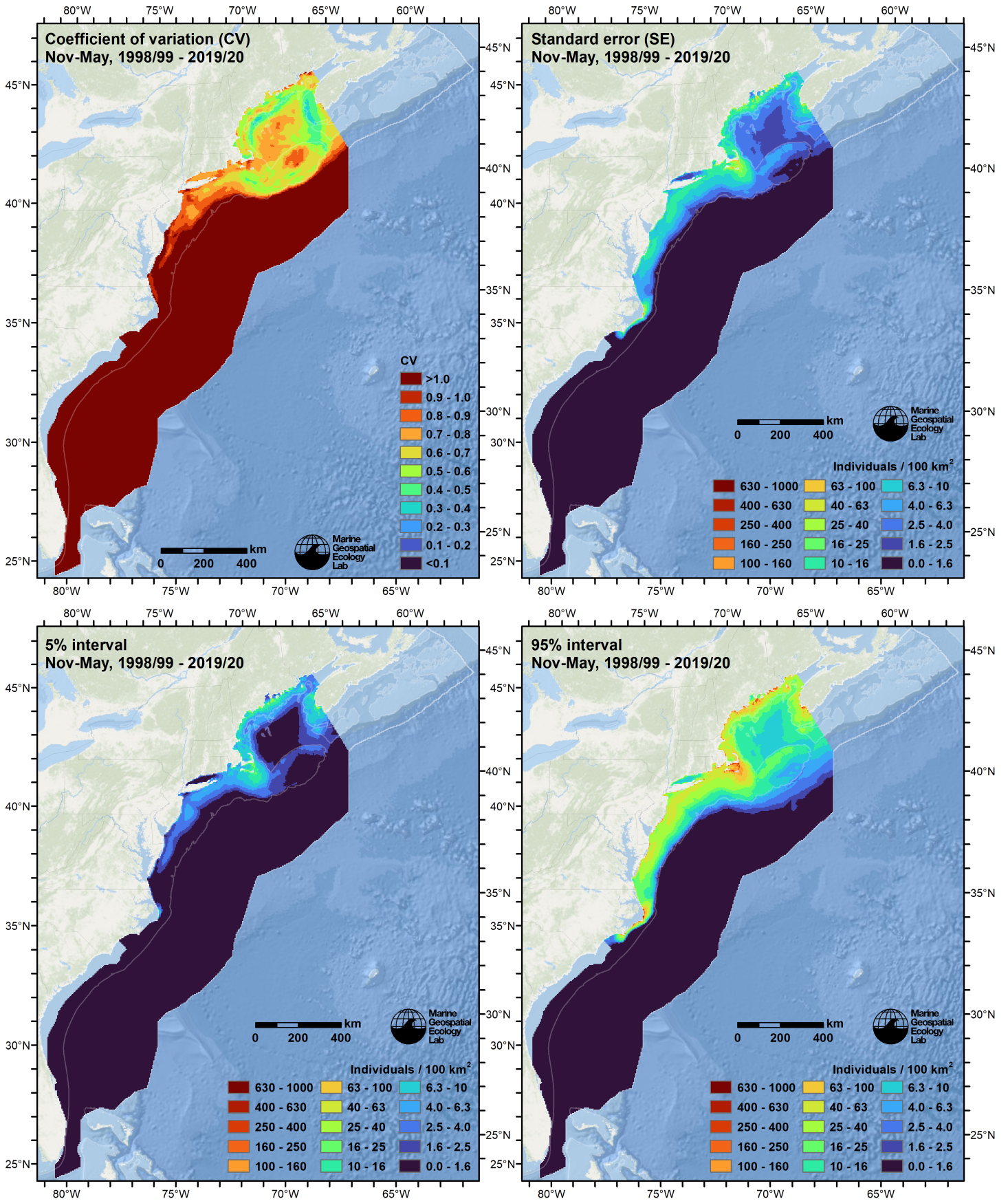
Figure 37: Uncertainty statistics for the seals mean density surface (Figure 36) predicted by the model for the region South of Nova Scotia v2 for Winter. Variance was estimated with the analytic approach given by Miller et al. (2022), Appendix S1, and accounts both for uncertainty in model parameter estimates and for seasonal and interannual variability in dynamic covariates.

Statistical output for this model:

```
Family: Tweedie(p=1.234)
Link function: log

Formula:
IndividualsCorrected ~ offset(log(SegmentArea)) + s(pmin(I(DistToShore/1000),
    275), bs = "ts", k = 5) + s(log10(pmax(3, pmin(Depth, 500)))),
    bs = "ts", k = 5) + s(pmax(2, pmin(SST_CMC, 22)), bs = "ts",
    k = 5) + s(pmin(I(DistToFront063/1000), 75), bs = "ts", k = 5) +
    s(pmax(30, pmin(SSS_HYCOM, 35.5)), bs = "ts", k = 5) + s(pmax(200,
    pmin(PP_VGPM, 3500)), bs = "ts", k = 5)

Parametric coefficients:
            Estimate Std. Error t value Pr(>|t|)
(Intercept) -19.5795     0.6163  -31.77   <2e-16 ***
---
Signif. codes:  0 '***' 0.001 '**' 0.01 '*' 0.05 '.' 0.1 ' ' 1

Approximate significance of smooth terms:
                                     edf Ref.df      F  p-value
s(pmin(I(DistToShore/1000), 275))  1.141      4 11.135  < 2e-16 ***
s(log10(pmax(3, pmin(Depth, 500)))) 3.531     4 20.555  < 2e-16 ***
s(pmax(2, pmin(SST_CMC, 22)))      3.792      4  6.564 1.73e-05 ***
s(pmin(I(DistToFront063/1000), 75)) 3.737     4 46.168  < 2e-16 ***
s(pmax(30, pmin(SSS_HYCOM, 35.5))) 3.621      4 13.277  < 2e-16 ***
s(pmax(200, pmin(PP_VGPM, 3500)))  3.724      4 17.647  < 2e-16 ***
---
Signif. codes:  0 '***' 0.001 '**' 0.01 '*' 0.05 '.' 0.1 ' ' 1

R-sq.(adj) =  0.0106   Deviance explained = 18.8%
-REML = 6818.5  Scale est. = 30.889    n = 51651

Method: REML   Optimizer: outer newton
full convergence after 15 iterations.
Gradient range [-0.004923718,0.001524371]
(score 6818.532 & scale 30.88938).
Hessian positive definite, eigenvalue range [0.3620682,3839.723].
Model rank =  25 / 25

Basis dimension (k) checking results. Low p-value (k-index<1) may
indicate that k is too low, especially if edf is close to k'.

                                     k'  edf k-index p-value
s(pmin(I(DistToShore/1000), 275))  4.00 1.14    0.83   0.230
s(log10(pmax(3, pmin(Depth, 500)))) 4.00 3.53   0.83   0.105
s(pmax(2, pmin(SST_CMC, 22)))      4.00 3.79    0.82   0.020 *
s(pmin(I(DistToFront063/1000), 75)) 4.00 3.74   0.81   0.035 *
s(pmax(30, pmin(SSS_HYCOM, 35.5))) 4.00 3.62    0.81   0.030 *
s(pmax(200, pmin(PP_VGPM, 3500)))  4.00 3.72    0.84   0.575
---
Signif. codes:  0 '***' 0.001 '**' 0.01 '*' 0.05 '.' 0.1 ' ' 1
```

(a) Seafloor depth (m)

(b) Distance to SST front (km)

(c) Distance to shore (km)

(d) Net primary productivity (mg C m^{-2} day^{-1}) (VGPM)

(e) Sea surface salinity (PSU)
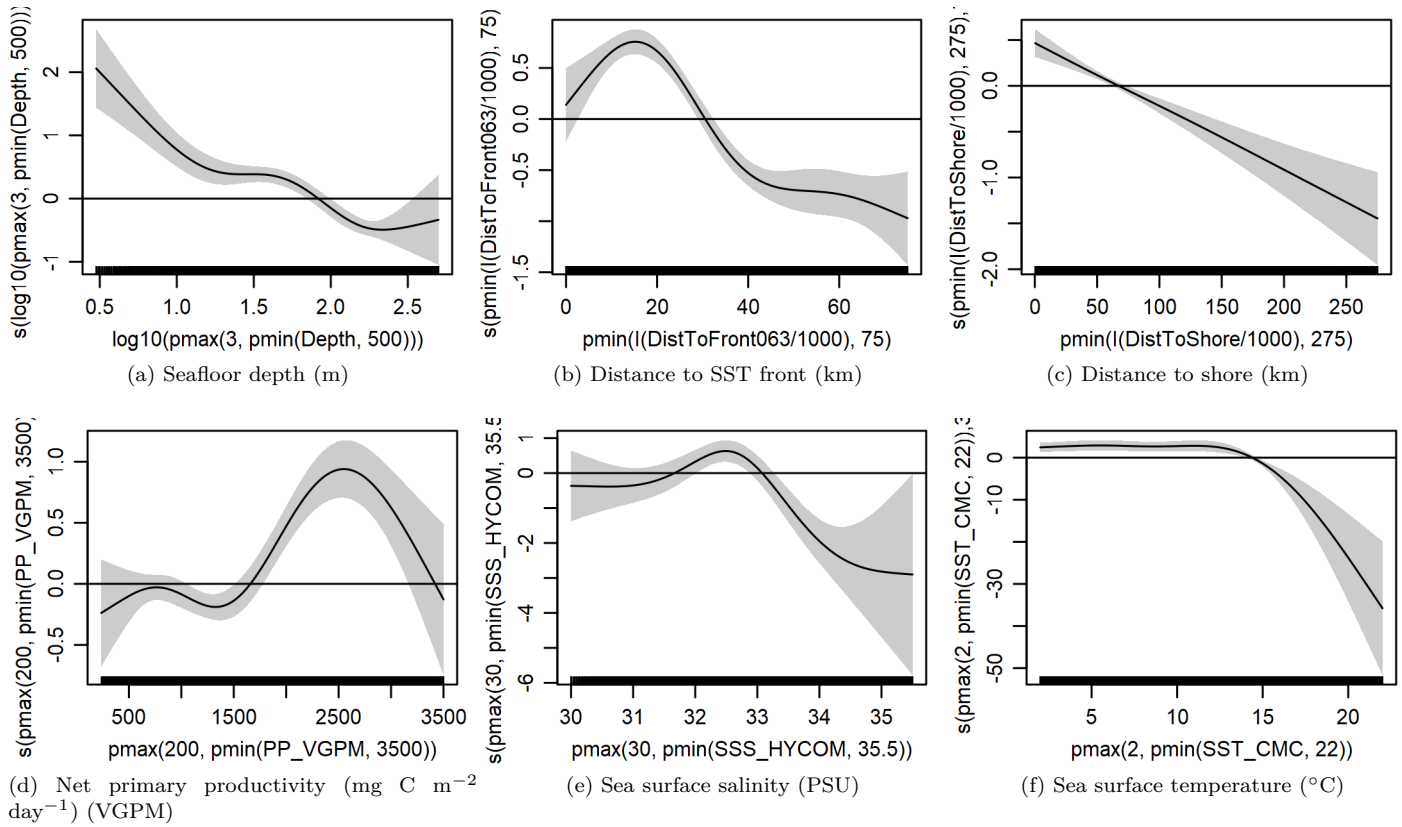
(f) Sea surface temperature (°C)

Figure 38: Functional plots for the final model for the region South of Nova Scotia v2 for Winter. Transforms and other treatments are indicated in axis labels. *log10* indicates the covariate was $\log_{10}$ transformed. *pmax* and *pmin* indicate the covariate's minimum and maximum values, respectively, were Winsorized to the values shown. Winsorization was used to prevent runaway extrapolations during prediction when covariates exceeded sampled ranges, or for ecological reasons, depending on the covariate. */1000* indicates meters were transformed to kilometers for interpretation convenience.

Table 14: Covariates used in the final model for the region South of Nova Scotia v2 for Winter.

| Covariate	Description
Depth	Depth (m) of the seafloor, from SRTM30_PLUS (Becker et al. (2009))
DistToFront063	Monthly mean distance (km) to the closest sea surface temperature front detected in daily GHRSST Level 4 CMC0.2deg and CMC0.1deg images (Brasnett (2008); Canada Meteorological Center (2012); Meissner et al. (2016); Canada Meteorological Center (2016)) with MGET's implementation of the Canny edge detector (Roberts et al. (2010); Canny (1986))
DistToShore	Distance (km) to shore excluding Bermuda and Sable Island, derived from SRTM30_PLUS (Becker et al. (2009))
PP_VGPM	Monthly mean net primary productivity (mg C m^{-2} day^{-1}) from the Vertically Generalized Production Model (VGPM) (Behrenfeld and Falkowski (1997))
SSS_HYCOM	Monthly mean sea surface salinity (PSU) from the HYCOM GOFS 3.1 1/12° ocean model (Chassignet et al. (2009))
SST_CMC	Monthly mean sea surface temperature (°C) from GHRSST Level 4 CMC0.2deg and CMC0.1deg (Brasnett (2008); Canada Meteorological Center (2012); Meissner et al. (2016); Canada Meteorological Center (2016))

4.2.2 Diagnostic Plots
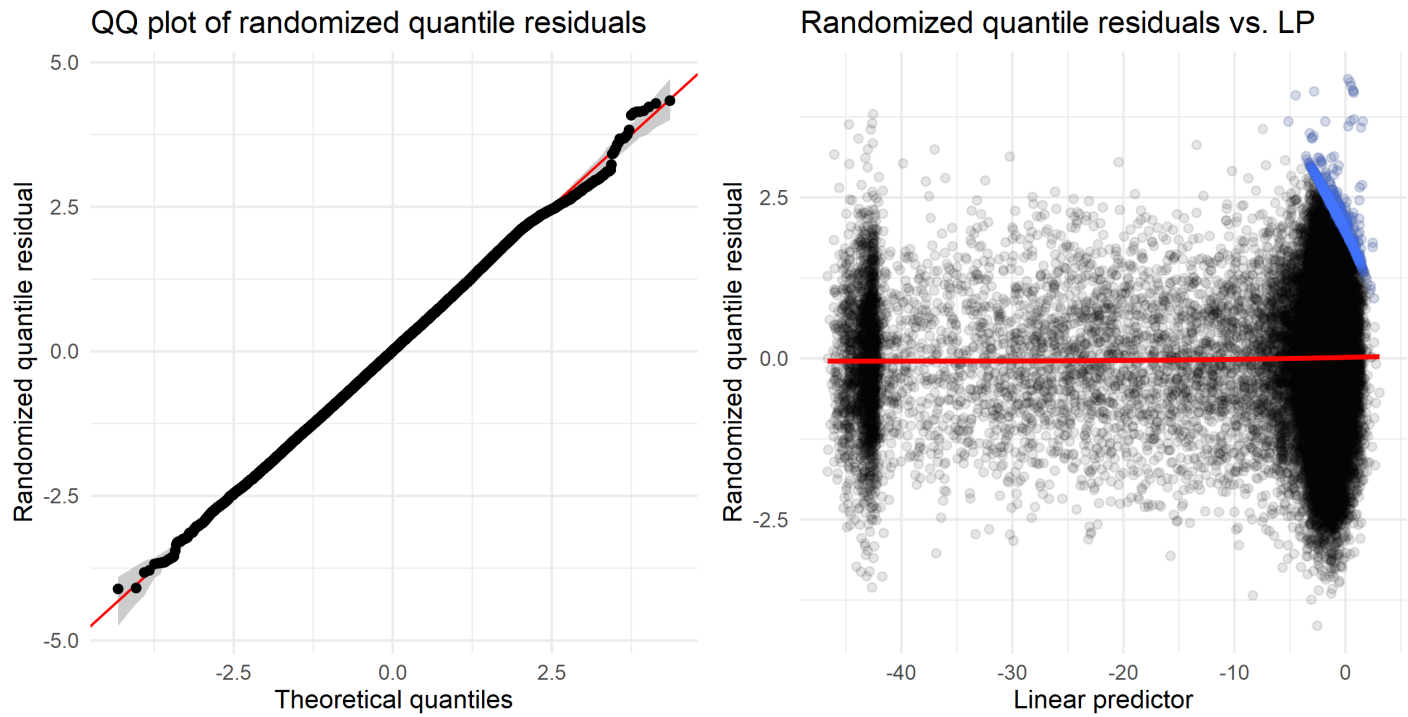
Figure 39: Residual plots for the final model for the region South of Nova Scotia v2 for Winter.
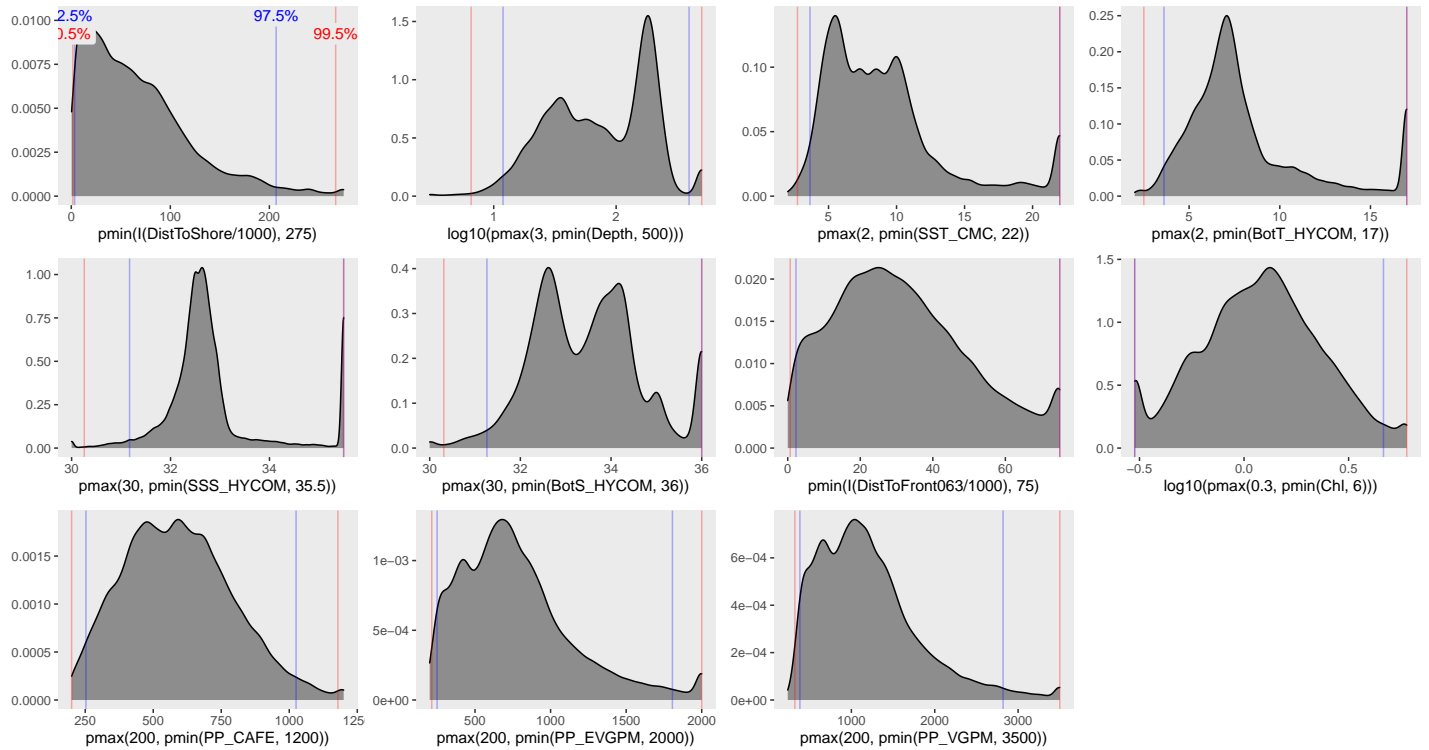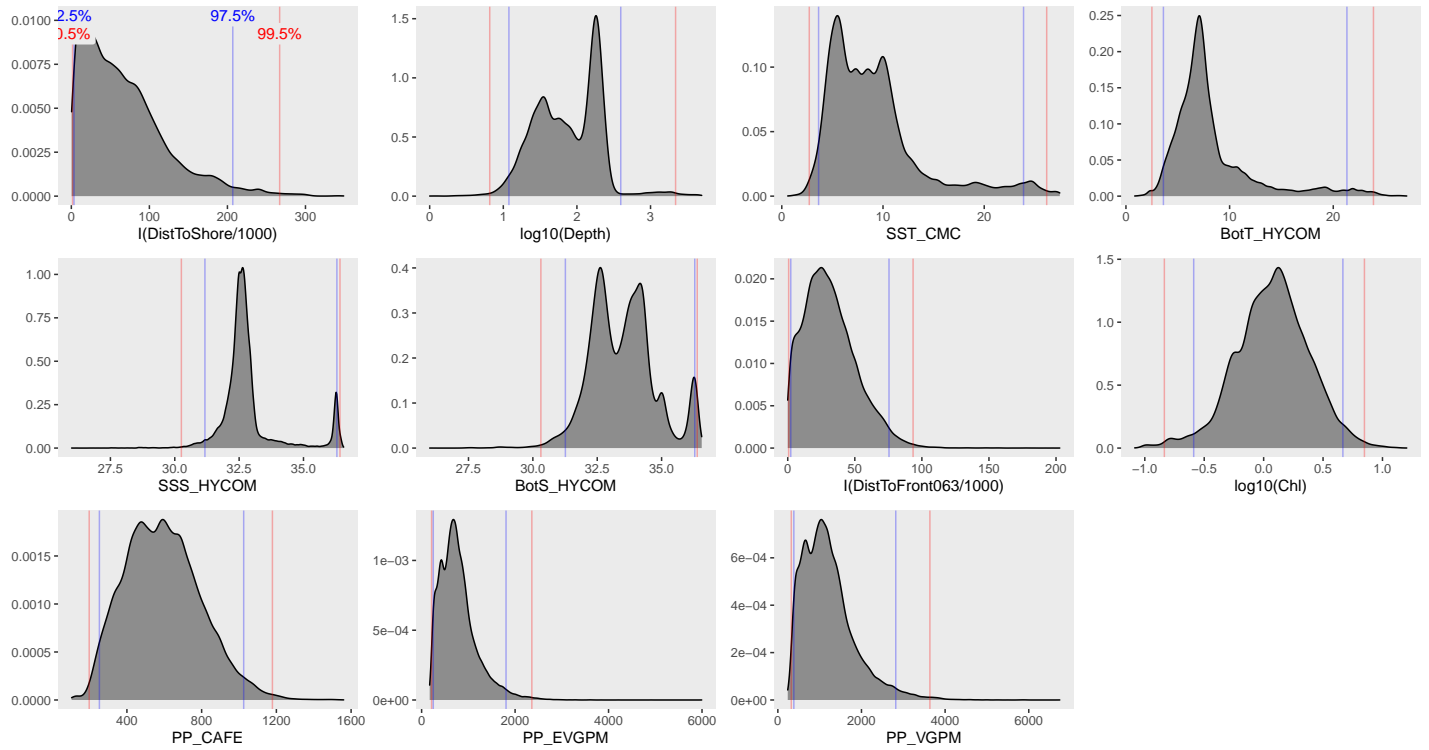
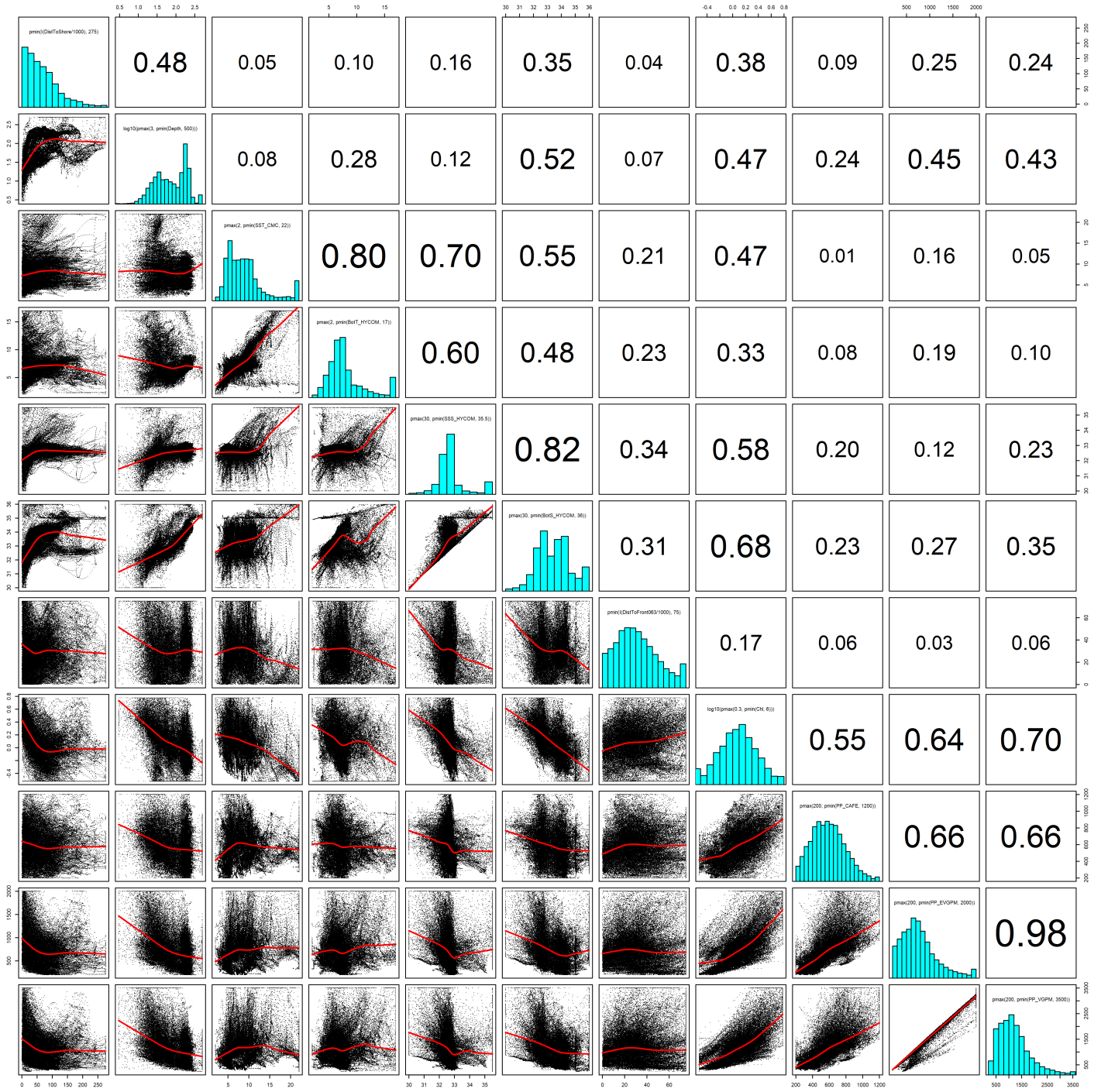Figure 40: Density histograms showing the distributions of the covariates considered during the final model selection step. The final model may have included only a subset of the covariates shown here (see Figure 38), and additional covariates may have been considered in preceding selection steps. Red and blue lines enclose 99% and 95% of the distributions, respectively. Transforms and other treatments are indicated in axis labels. *log10* indicates the covariate was $\log_{10}$ transformed. *pmax* and *pmin* indicate the covariate's minimum and maximum values, respectively, were Winsorized to the values shown. Winsorization was used to prevent runaway extrapolations during prediction when covariates exceeded sampled ranges, or for ecological reasons, depending on the covariate. */1000* indicates meters were transformed to kilometers for interpretation convenience.

Figure 41: Density histograms shown in Figure 40 replotted without Winsorization, to show the full range of sampling represented by survey segments.
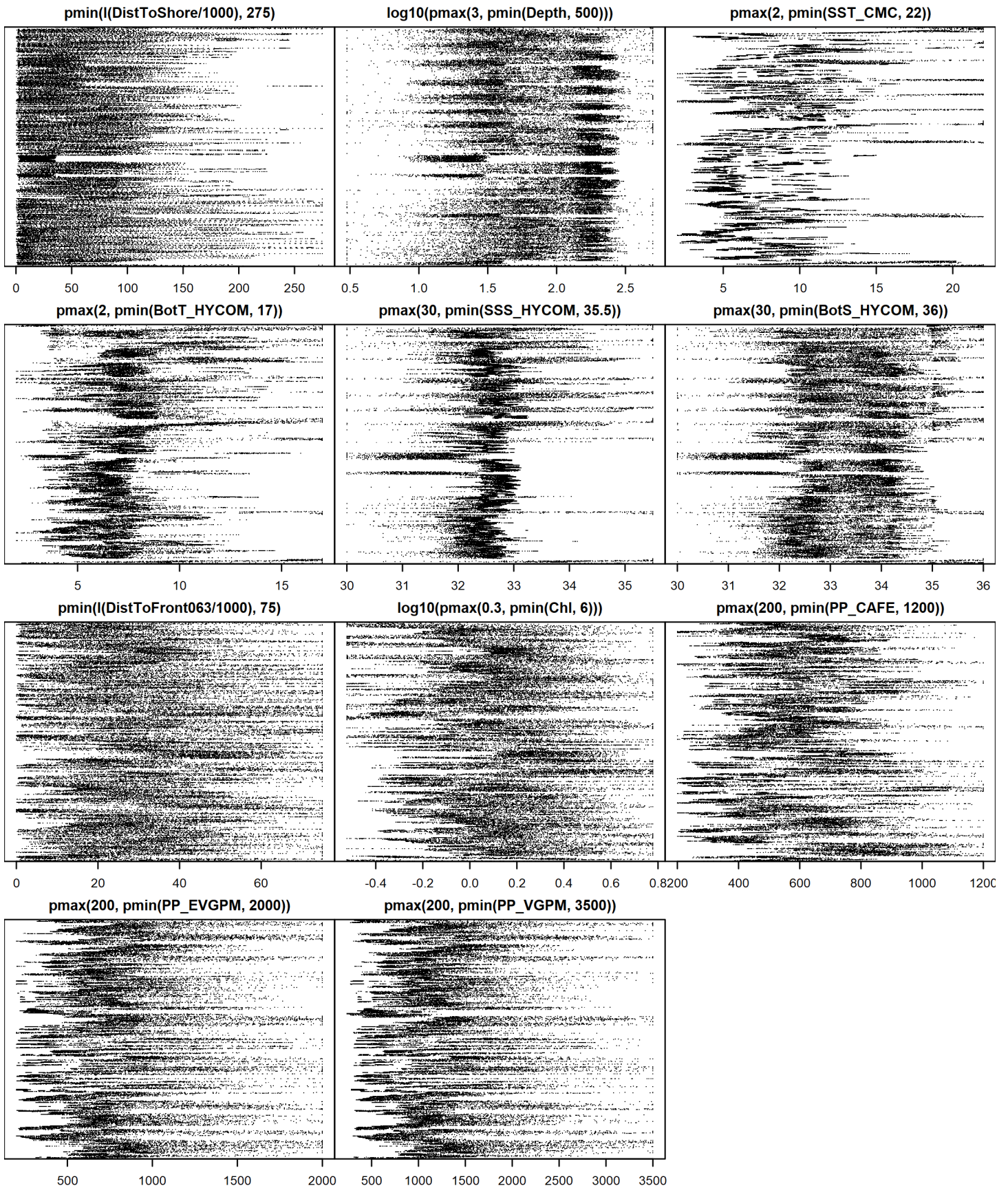
Figure 42: Scatterplot matrix of the covariates considered during the final model selection step. The final model may have included only a subset of the covariates shown here (see Figure 38), and additional covariates may have been considered in preceding selection steps. Covariates are transformed and Winsorized as shown in Figure 40. This plot is used to check simple correlations between covariates (via pairwise Pearson coefficients above the diagonal) and visually inspect for concurvity (via scatterplots and red lowess curves below the diagonal).

Figure 43: Dotplot of the covariates considered during the final model selection step. The final model may have included only a subset of the covariates shown here (see Figure 38), and additional covariates may have been considered in preceding selection steps. Covariates are transformed and Winsorized as shown in Figure 40. This plot is used to check for suspicious patterns and outliers in the data. Points are ordered vertically by segment ID, sequentially in time.

4.2.3 Extrapolation Diagnostics

4.2.3.1 Univariate Extrapolation

(a) Depth covariate

(b) DistToShore covariate
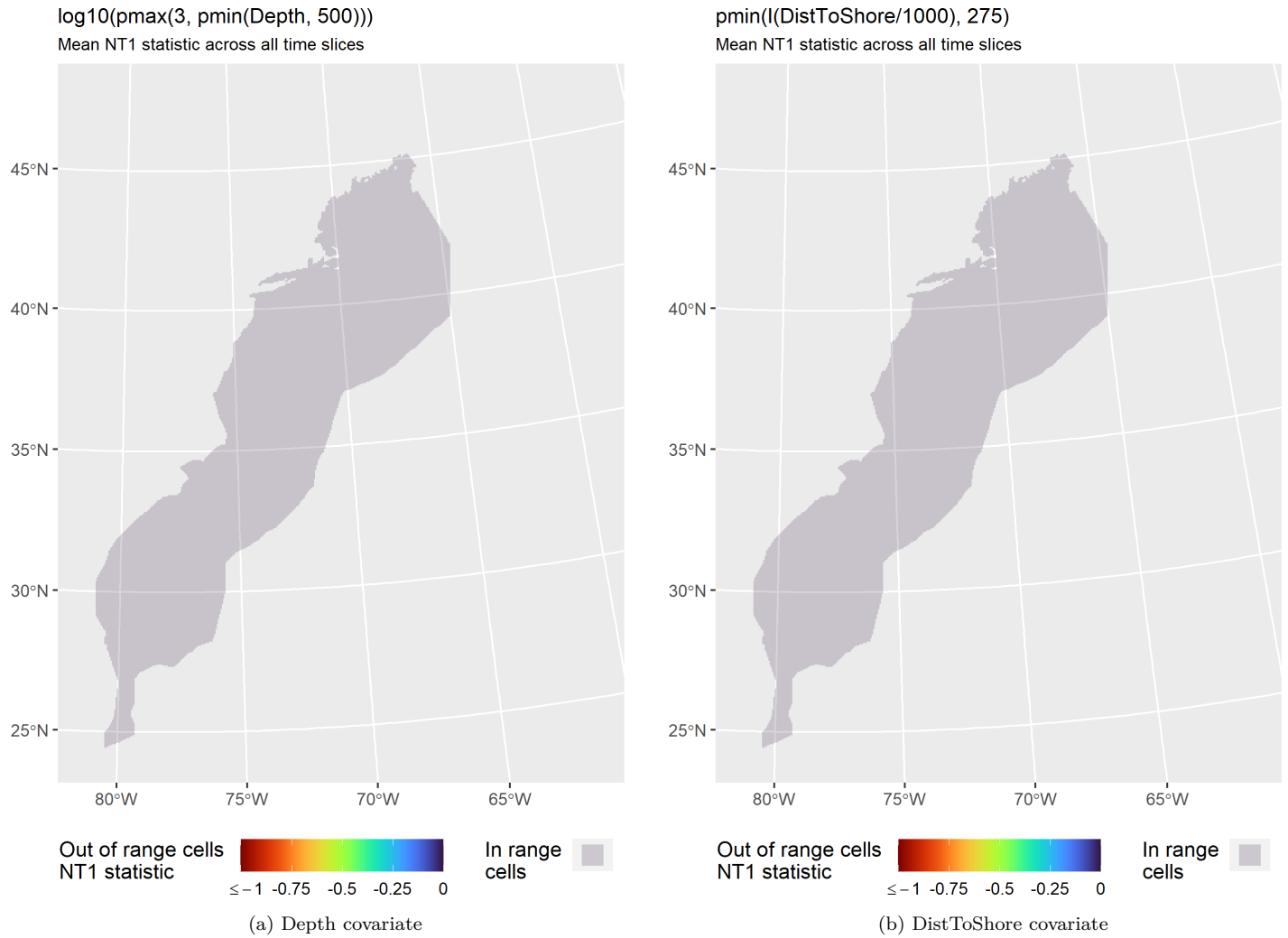
Figure 44: NT1 statistic (Mesgaran et al. (2014)) for static covariates used in the model for the region South of Nova Scotia v2 for Winter. Areas outside the sampled range of a covariate appear in color, indicating univariate extrapolation of that covariate occurred there. Areas within the sampled range appear in gray, indicating it did not occur.
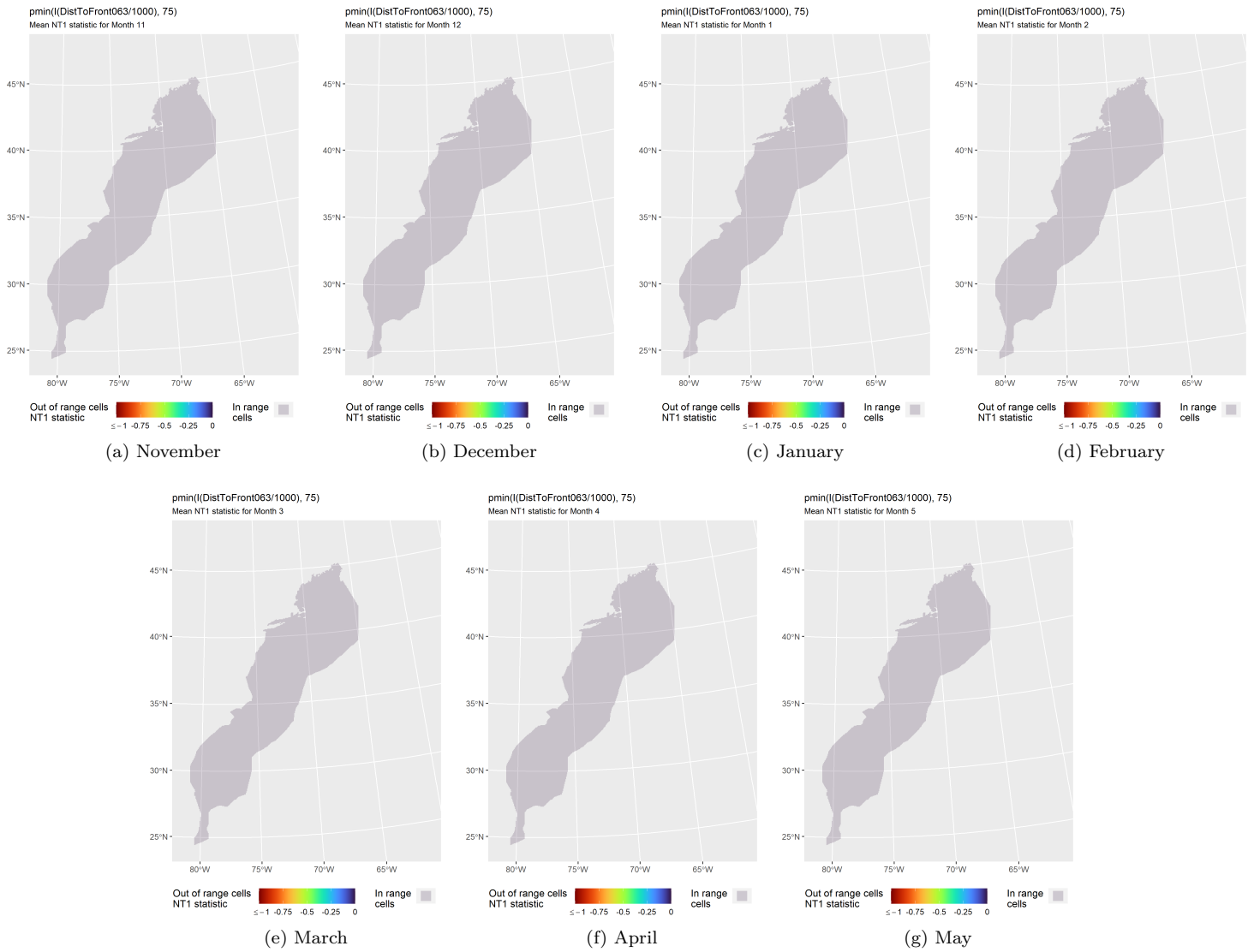
Figure 45: NT1 statistic (Mesgaran et al. (2014)) for the DistToFront063 covariate in the model for the region South of Nova Scotia v2 for Winter. Areas outside the sampled range of a covariate appear in color, indicating univariate extrapolation of that covariate occurred there during the month. Areas within the sampled range appear in gray, indicating it did not occur.
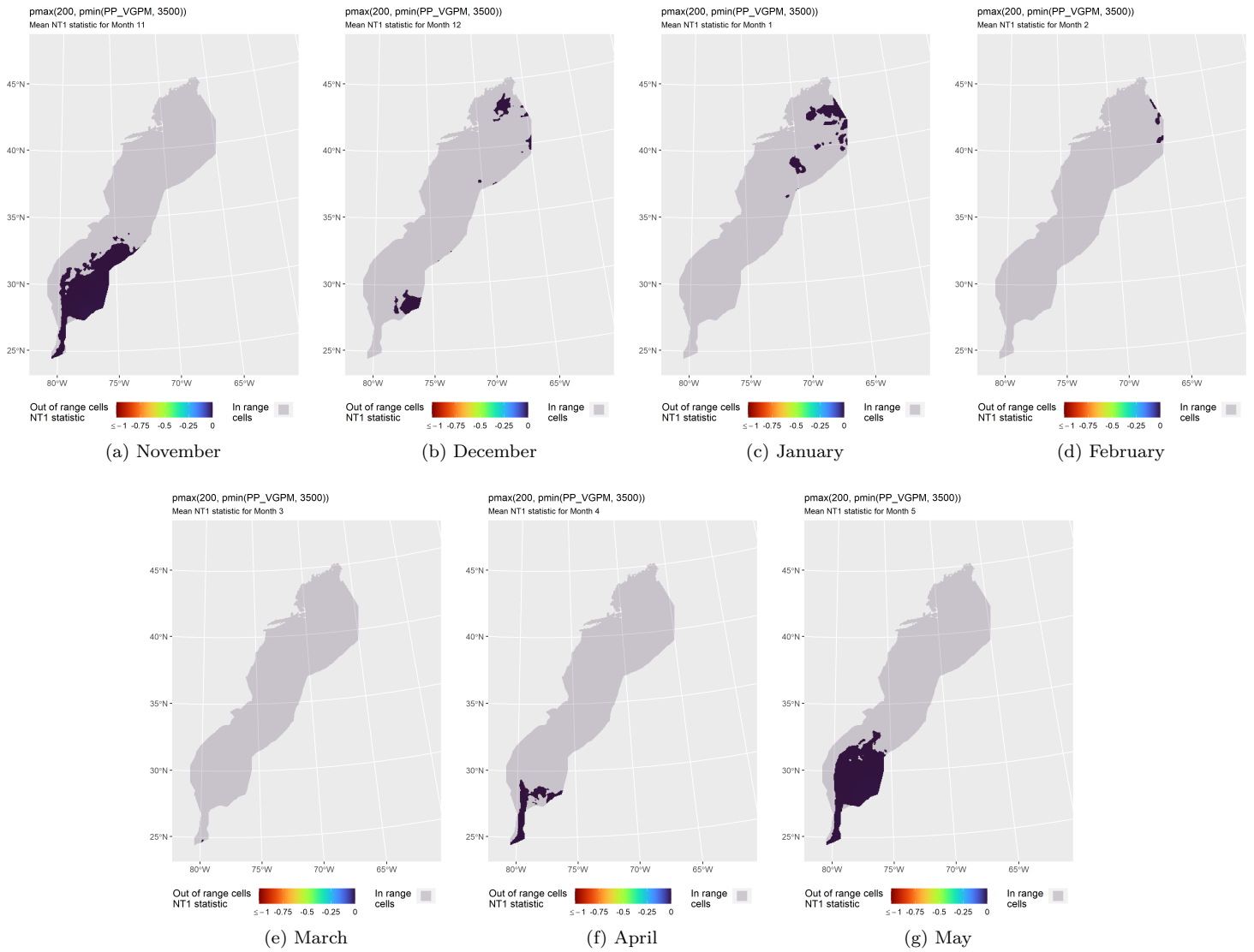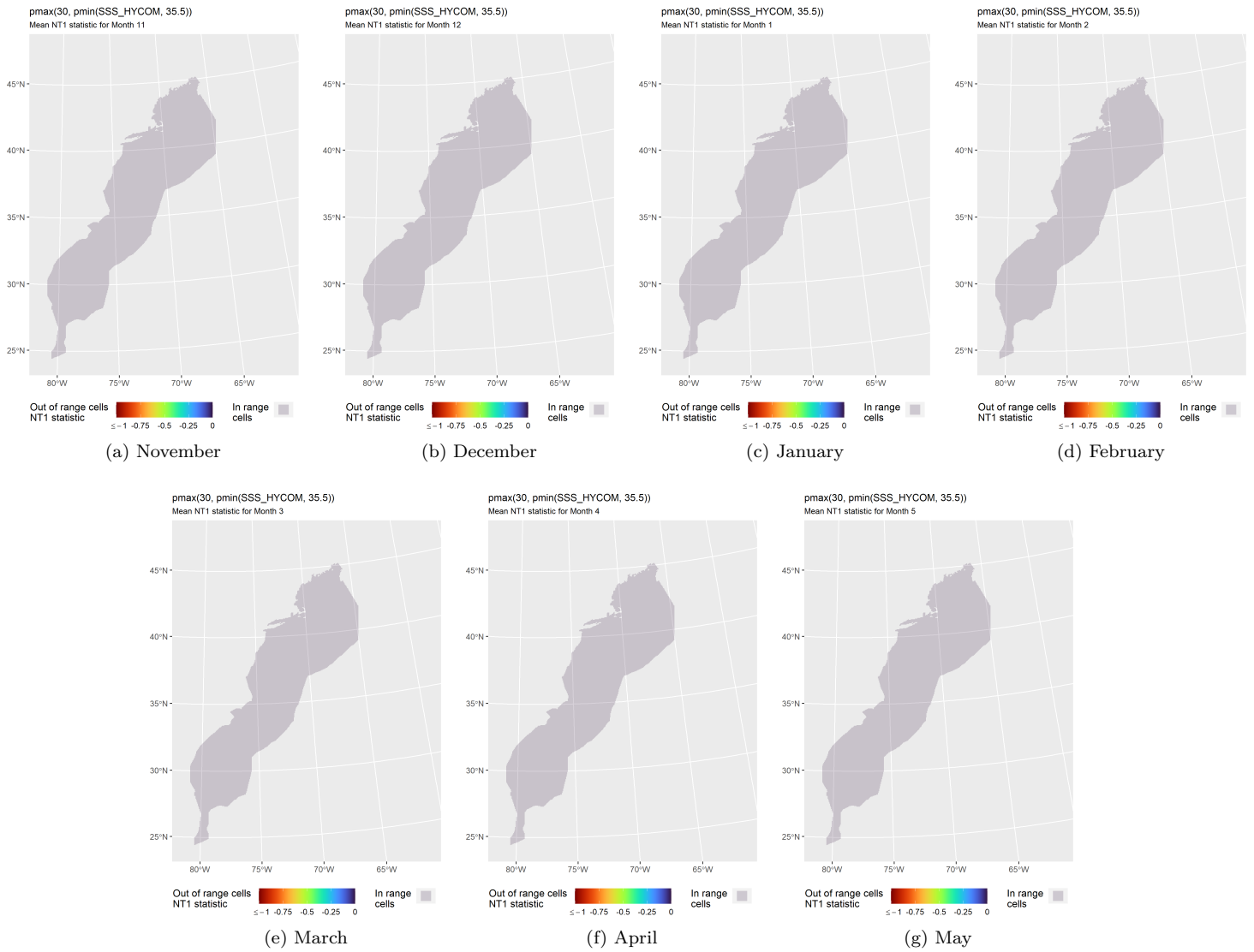
Figure 46: NT1 statistic (Mesgaran et al. (2014)) for the PP_VGPM covariate in the model for the region South of Nova Scotia v2 for Winter. Areas outside the sampled range of a covariate appear in color, indicating univariate extrapolation of that covariate occurred there during the month. Areas within the sampled range appear in gray, indicating it did not occur.

Figure 47: NT1 statistic (Mesgaran et al. (2014)) for the SSS_HYCOM covariate in the model for the region South of Nova Scotia v2 for Winter. Areas outside the sampled range of a covariate appear in color, indicating univariate extrapolation of that covariate occurred there during the month. Areas within the sampled range appear in gray, indicating it did not occur.
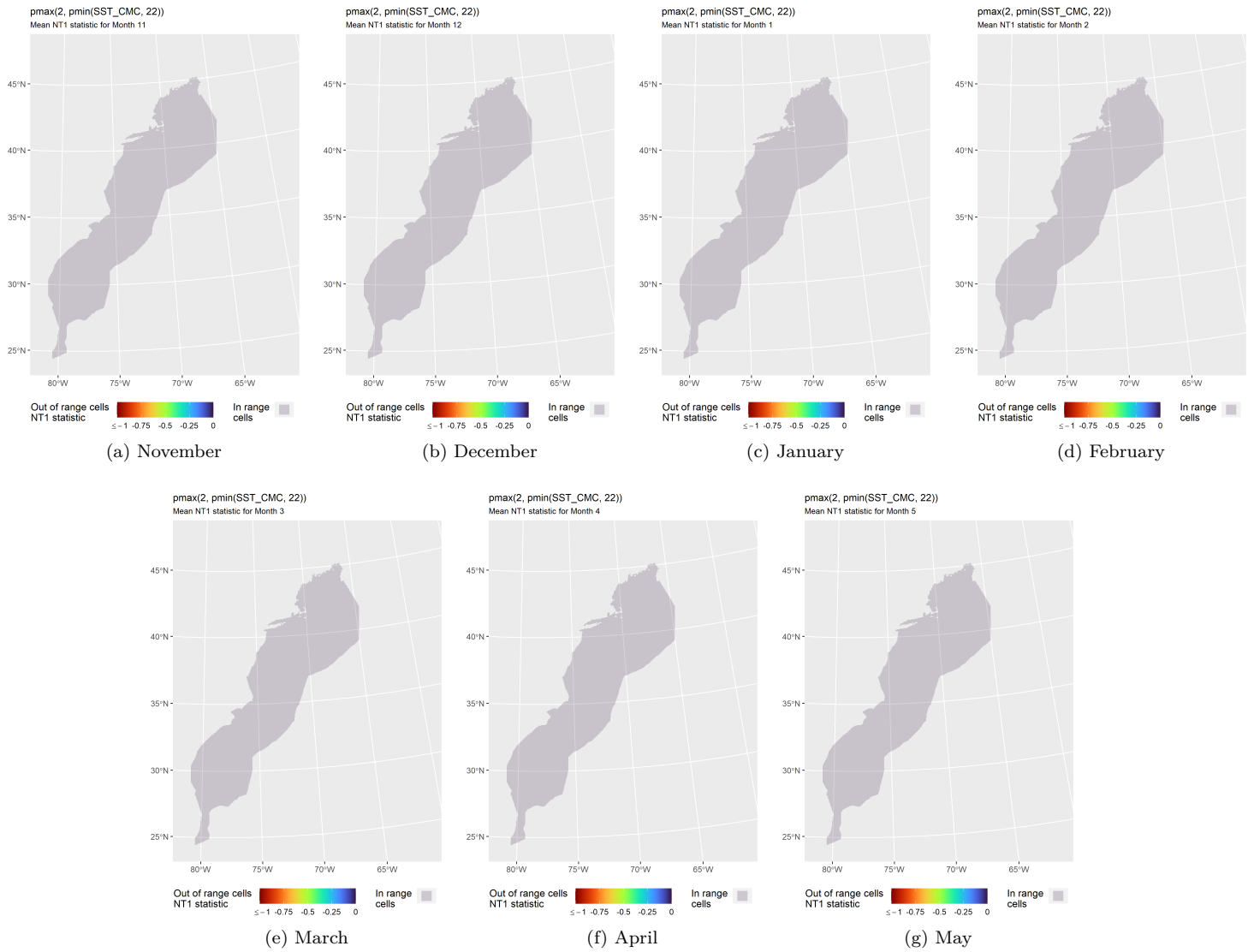
Figure 48: NT1 statistic (Mesgaran et al. (2014)) for the SST_CMC covariate in the model for the region South of Nova Scotia v2 for Winter. Areas outside the sampled range of a covariate appear in color, indicating univariate extrapolation of that covariate occurred there during the month. Areas within the sampled range appear in gray, indicating it did not occur.

4.2.3.2 Multivariate Extrapolation

(a) November (b) December (c) January (d) February
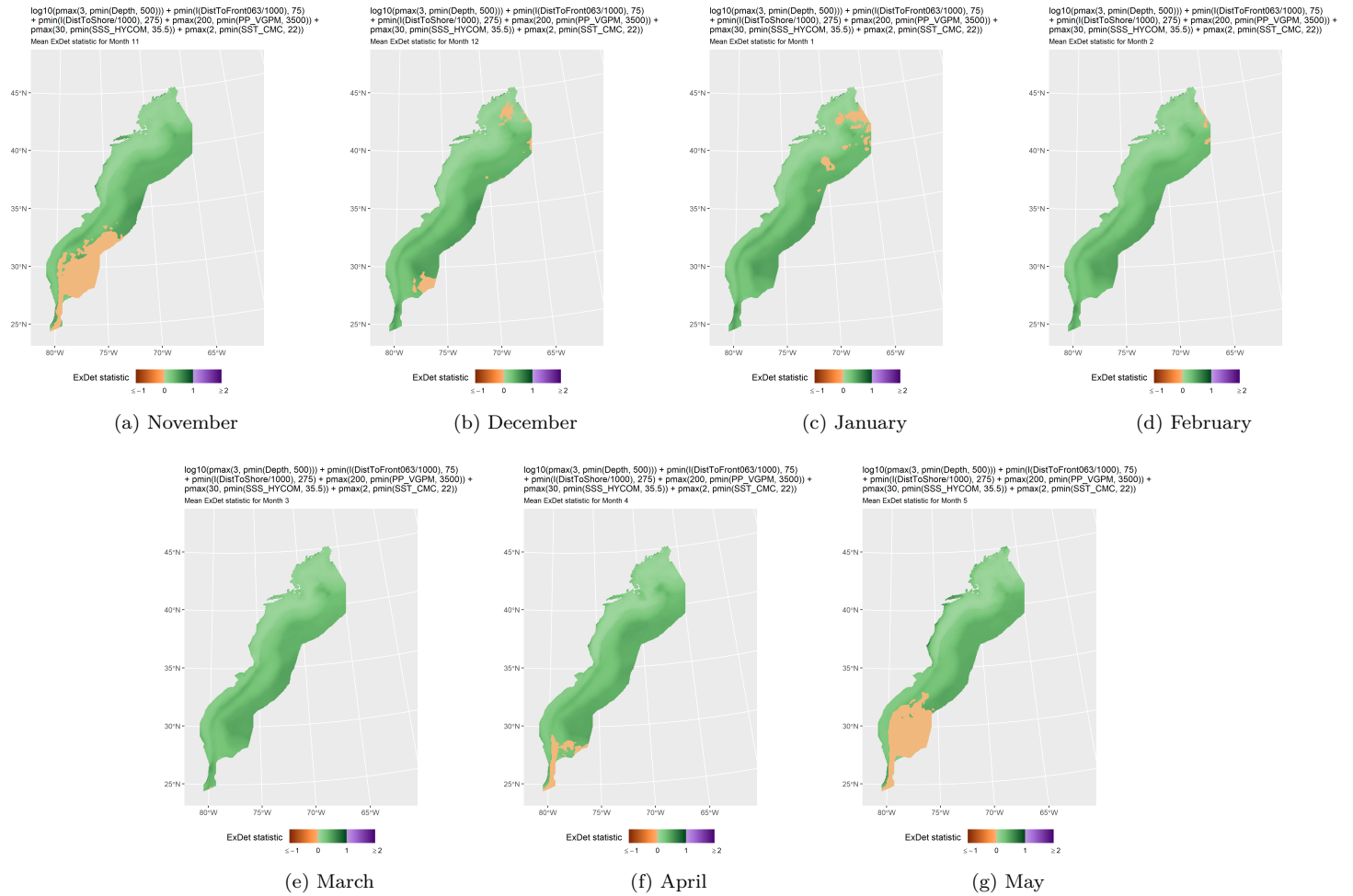

(e) March (f) April (g) May

Figure 49: ExDet statistic (Mesgaran et al. (2014)) for all of the covariates used in the model for the region South of Nova Scotia v2 for Winter. Areas in orange (ExDet < 0) required univariate extrapolation of one or more covariates (see previous section). Areas in purple (ExDet > 1), did not require univariate extrapolation but did require multivariate extrapolation, by virtue of having novel combinations of covariates not represented in the survey data, according to the NT2 statistic (Mesgaran et al. (2014)). Areas in green (0 ≥ ExDet ≤ 1) did not require either type of extrapolation.

5 Predictions

Based on our evaluation of this model in the context of what is known of this taxon (see Section 6), we summarized its predictions into monthly climatological density and uncertainty surfaces, shown in the maps below.
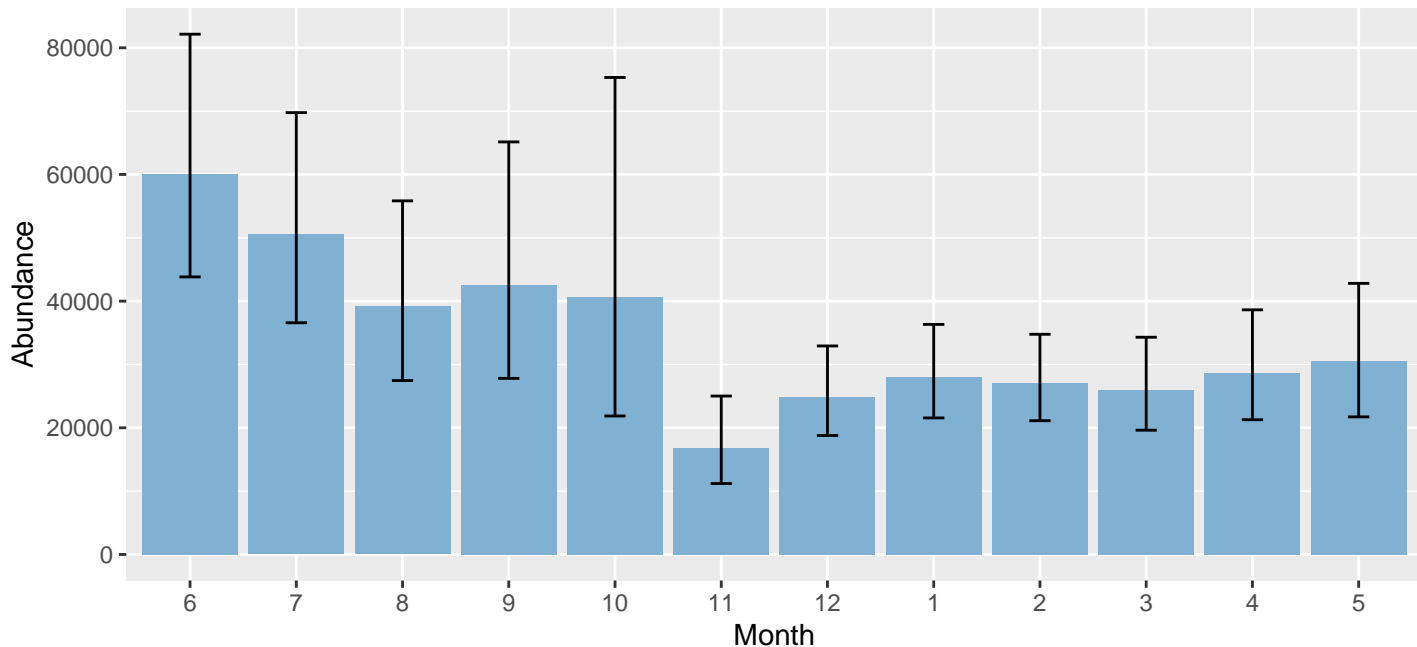
5.1 Summarized Predictions

Figure 50: Mean monthly abundance for the prediction area for June 1998 - May 2020. Note that the prediction area was not the same for all months (see Table 15 below and maps following). Error bars are a 95% interval, made with a log-normal approximation using the prediction's CV. The CV was estimated with the analytic approach given by Miller et al. (2022), Appendix S1, and accounts both for uncertainty in model parameter estimates and for temporal variability in dynamic covariates.

Table 15: Mean monthly abundance and density for the prediction area for June 1998 - May 2020. CV and intervals estimated as described for the previous figure.

| Month	Abundance	CV	95% Interval	Area (km^2)	Density (individuals / 100 km^2)
6	59,998	0.161	43,822 - 82,144	1,154,825	5.20
7	50,522	0.166	36,587 - 69,763	1,154,825	4.37
8	39,153	0.183	27,458 - 55,830	1,154,825	3.39
9	42,554	0.220	27,801 - 65,134	1,154,825	3.68
10	40,579	0.324	21,864 - 75,313	1,154,825	3.51
11	16,736	0.207	11,196 - 25,017	1,088,850	1.54
12	24,866	0.144	18,780 - 32,924	1,088,850	2.28
1	27,984	0.134	21,558 - 36,325	1,088,850	2.57
2	27,098	0.128	21,120 - 34,767	1,088,850	2.49
3	25,941	0.143	19,620 - 34,299	1,088,850	2.38
4	28,668	0.153	21,276 - 38,629	1,088,850	2.63
5	30,496	0.174	21,726 - 42,806	1,088,850	2.80
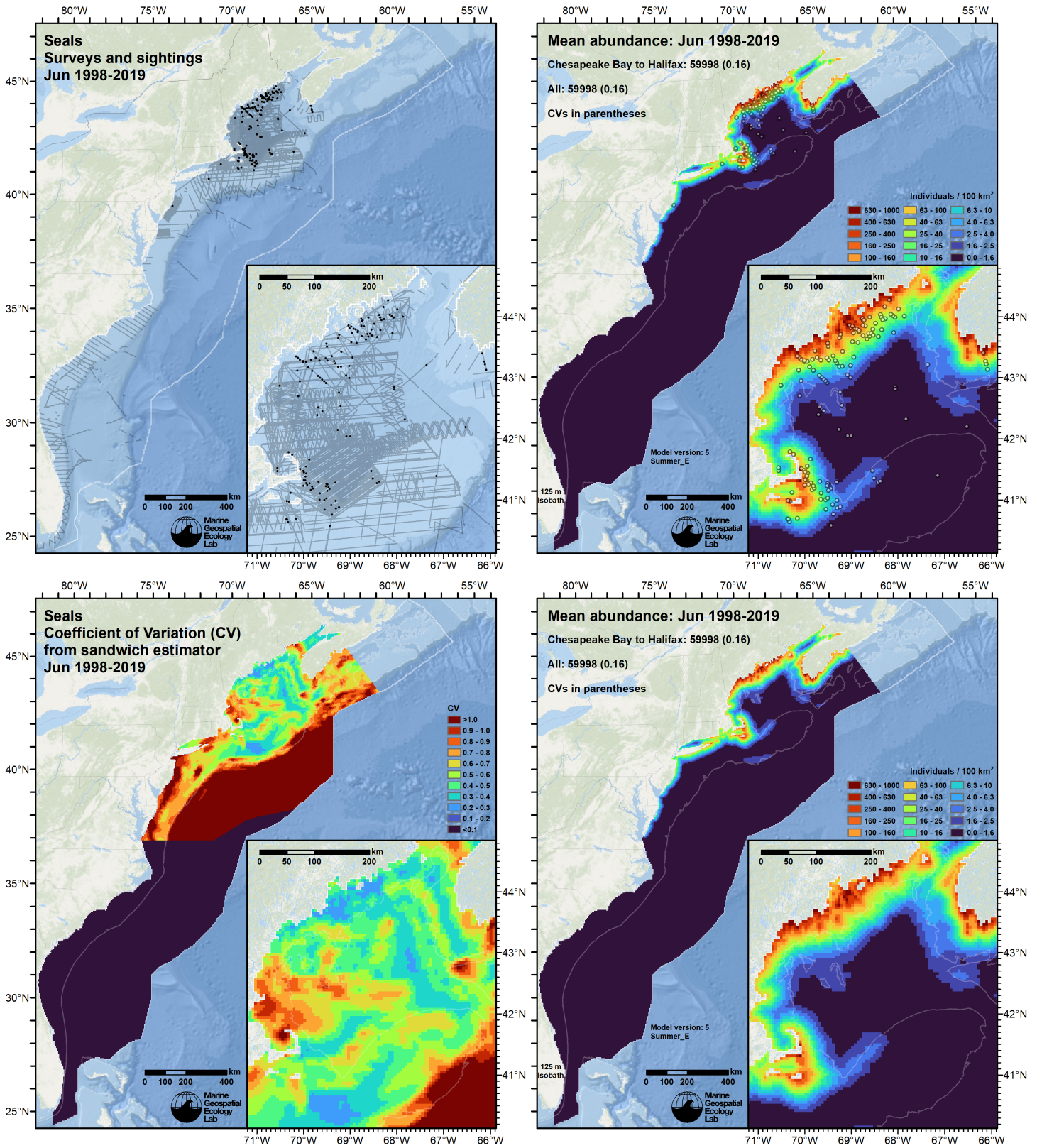
Figure 51: Survey effort and observations (top left), predicted density with observations (top right), predicted density without observations (bottom right), and coefficient of variation of predicted density (bottom left), for the month of June for the given era. Variance was estimated with the analytic approach given by Miller et al. (2022), Appendix S1, and accounts both for uncertainty in model parameter estimates and for temporal variability in dynamic covariates.
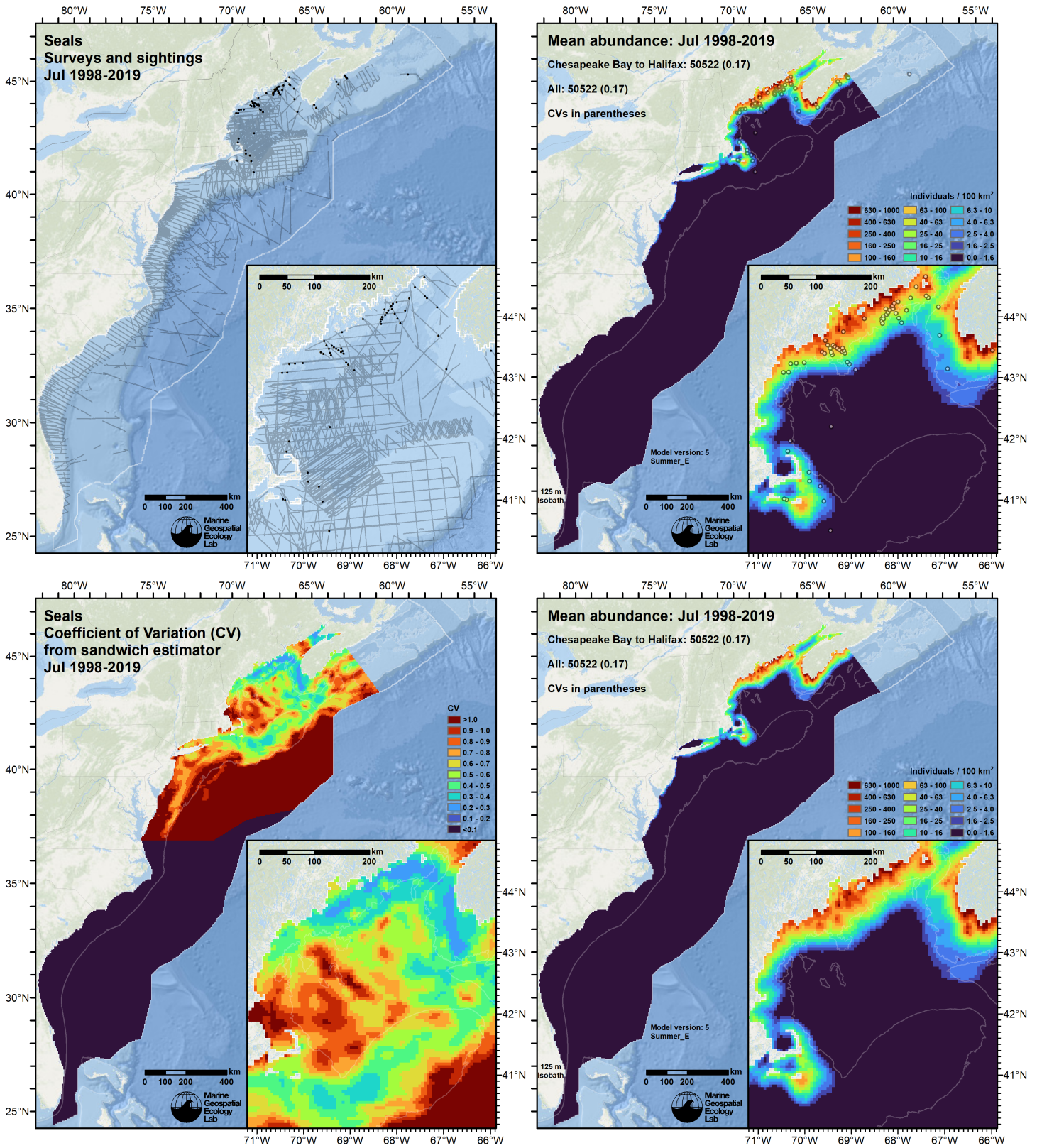
64

Figure 52: Survey effort and observations (top left), predicted density with observations (top right), predicted density without observations (bottom right), and coefficient of variation of predicted density (bottom left), for the month of July for the given era. Variance was estimated with the analytic approach given by Miller et al. (2022), Appendix S1, and accounts both for uncertainty in model parameter estimates and for temporal variability in dynamic covariates.
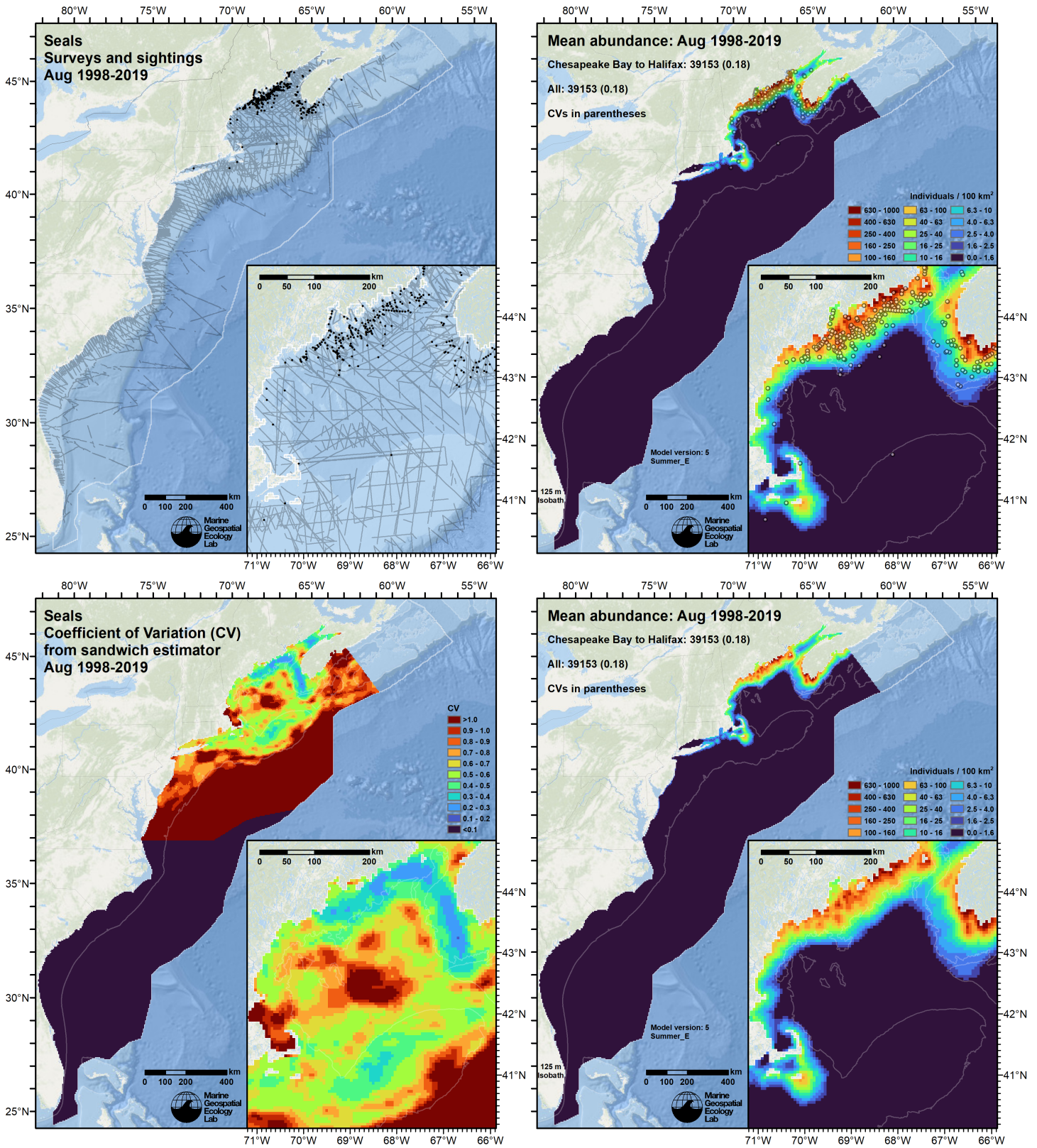
Figure 53: Survey effort and observations (top left), predicted density with observations (top right), predicted density without observations (bottom right), and coefficient of variation of predicted density (bottom left), for the month of August for the given era. Variance was estimated with the analytic approach given by Miller et al. (2022), Appendix S1, and accounts both for uncertainty in model parameter estimates and for temporal variability in dynamic covariates.
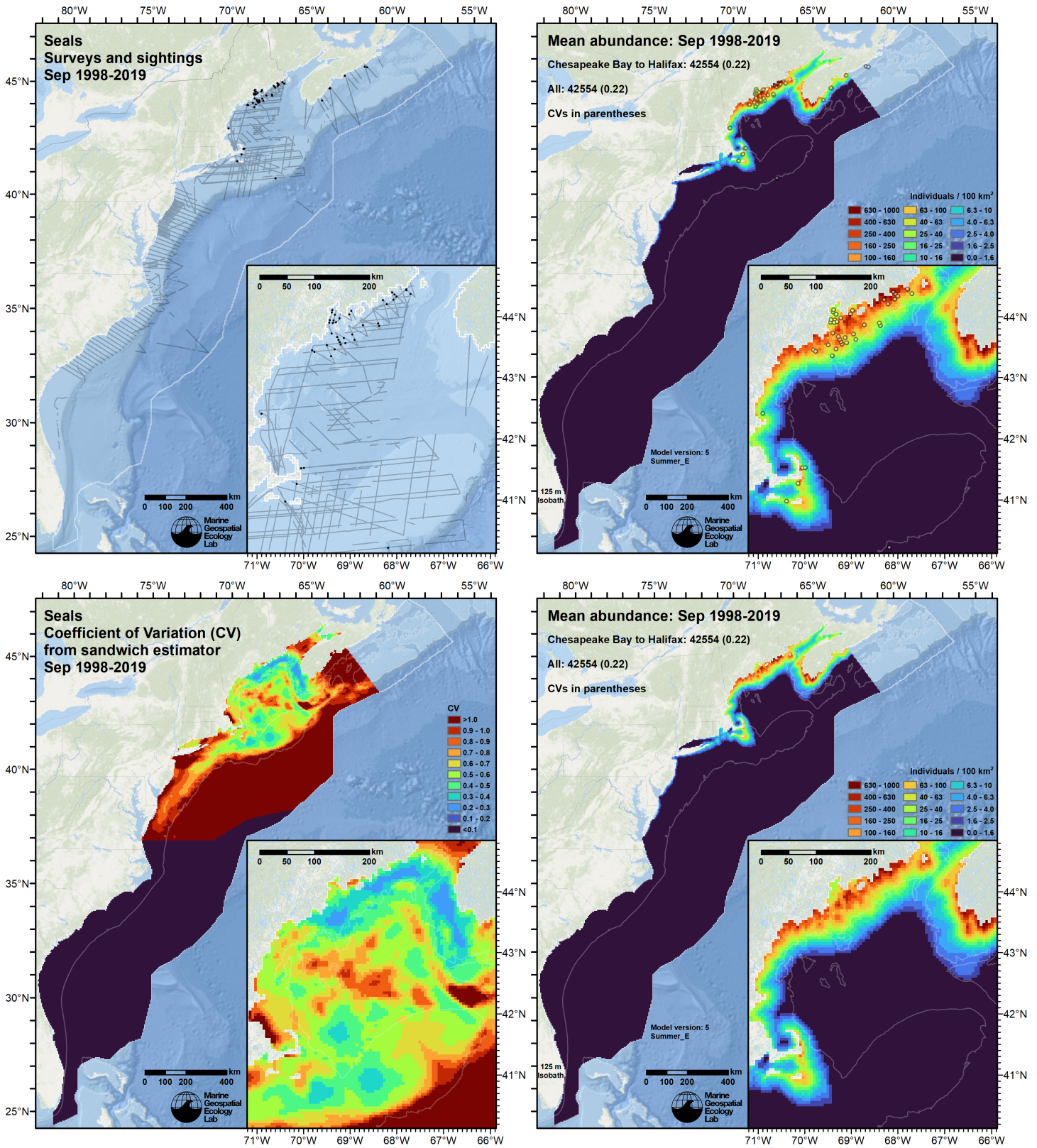
Figure 54: Survey effort and observations (top left), predicted density with observations (top right), predicted density without observations (bottom right), and coefficient of variation of predicted density (bottom left), for the month of September for the given era. Variance was estimated with the analytic approach given by Miller et al. (2022), Appendix S1, and accounts both for uncertainty in model parameter estimates and for temporal variability in dynamic covariates.
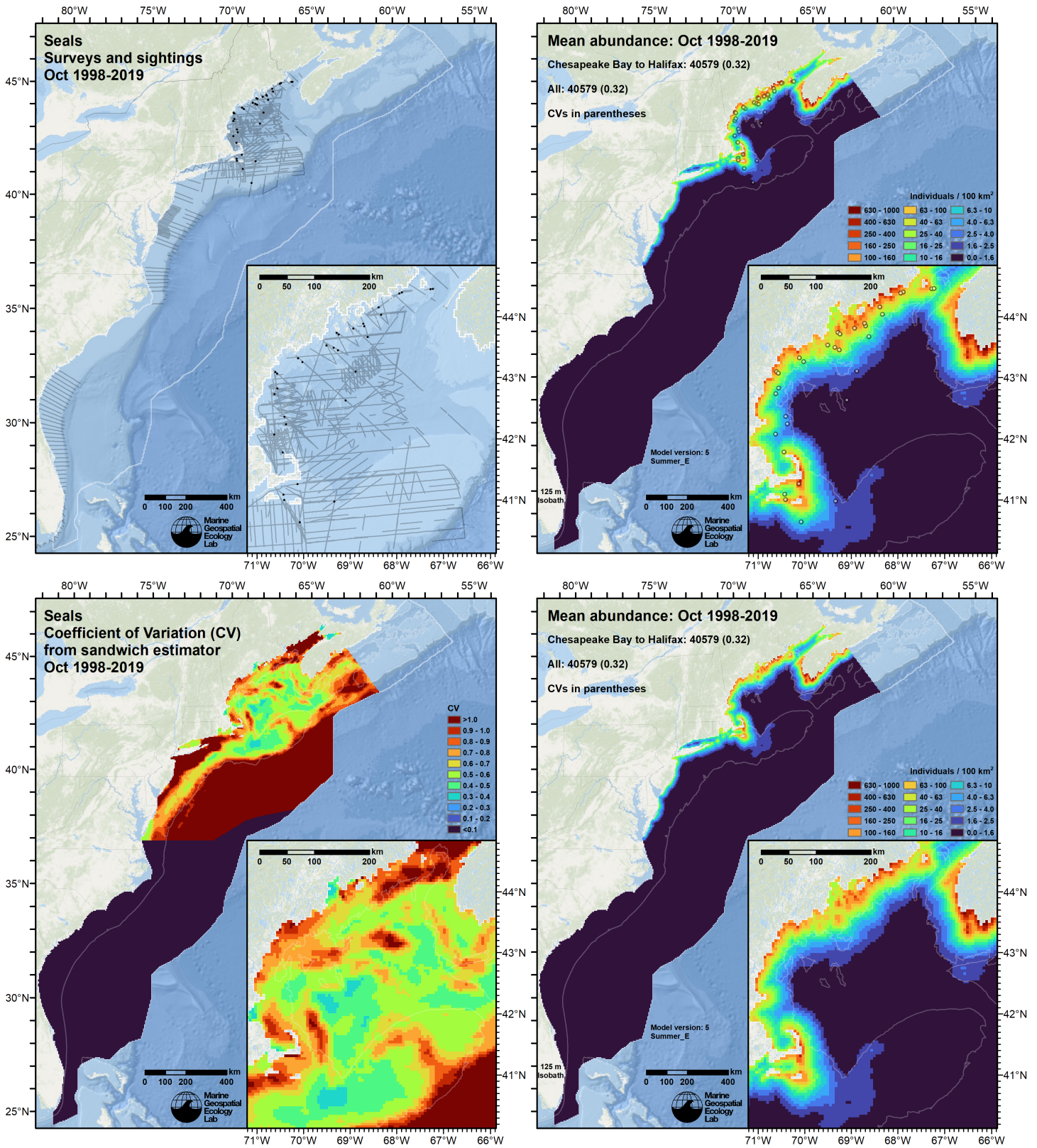
Figure 55: Survey effort and observations (top left), predicted density with observations (top right), predicted density without observations (bottom right), and coefficient of variation of predicted density (bottom left), for the month of October for the given era. Variance was estimated with the analytic approach given by Miller et al. (2022), Appendix S1, and accounts both for uncertainty in model parameter estimates and for temporal variability in dynamic covariates.
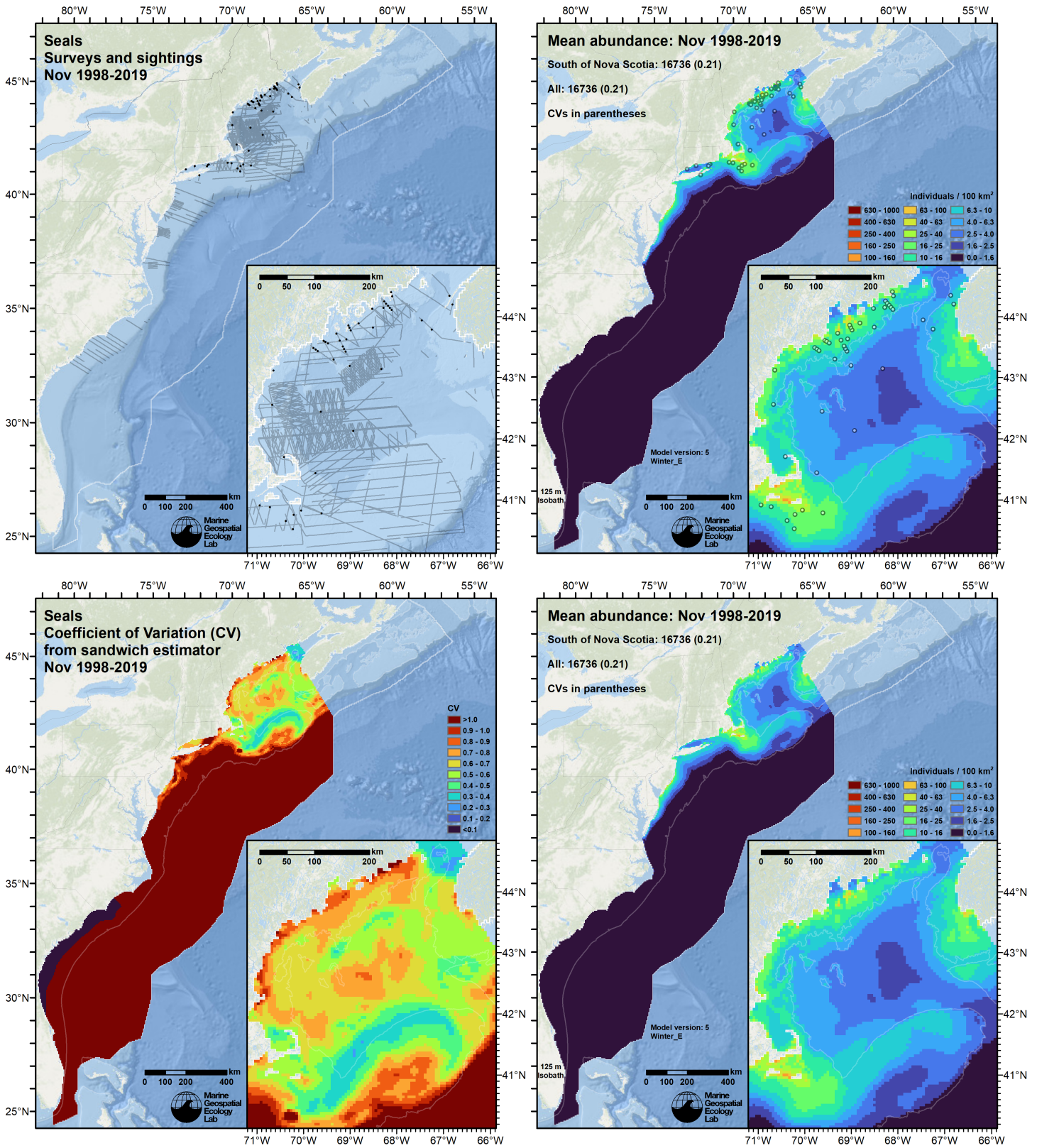
Figure 56: Survey effort and observations (top left), predicted density with observations (top right), predicted density without observations (bottom right), and coefficient of variation of predicted density (bottom left), for the month of November for the given era. Variance was estimated with the analytic approach given by Miller et al. (2022), Appendix S1, and accounts both for uncertainty in model parameter estimates and for temporal variability in dynamic covariates.

Figure 57: Survey effort and observations (top left), predicted density with observations (top right), predicted density without observations (bottom right), and coefficient of variation of predicted density (bottom left), for the month of December for the given era. Variance was estimated with the analytic approach given by Miller et al. (2022), Appendix S1, and accounts both for uncertainty in model parameter estimates and for temporal variability in dynamic covariates.
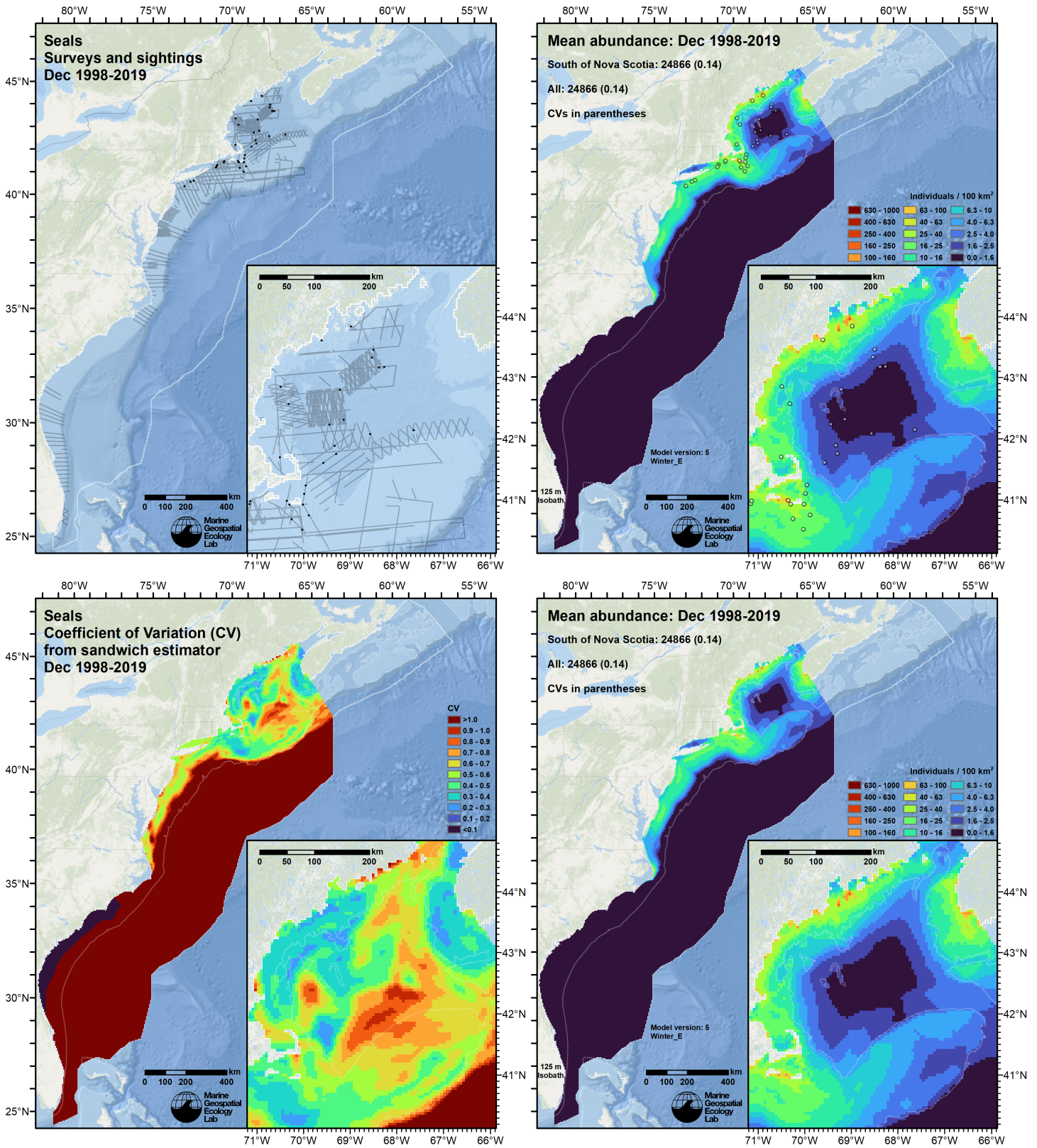
Figure 58: Survey effort and observations (top left), predicted density with observations (top right), predicted density without observations (bottom right), and coefficient of variation of predicted density (bottom left), for the month of January for the given era. Variance was estimated with the analytic approach given by Miller et al. (2022), Appendix S1, and accounts both for uncertainty in model parameter estimates and for temporal variability in dynamic covariates.
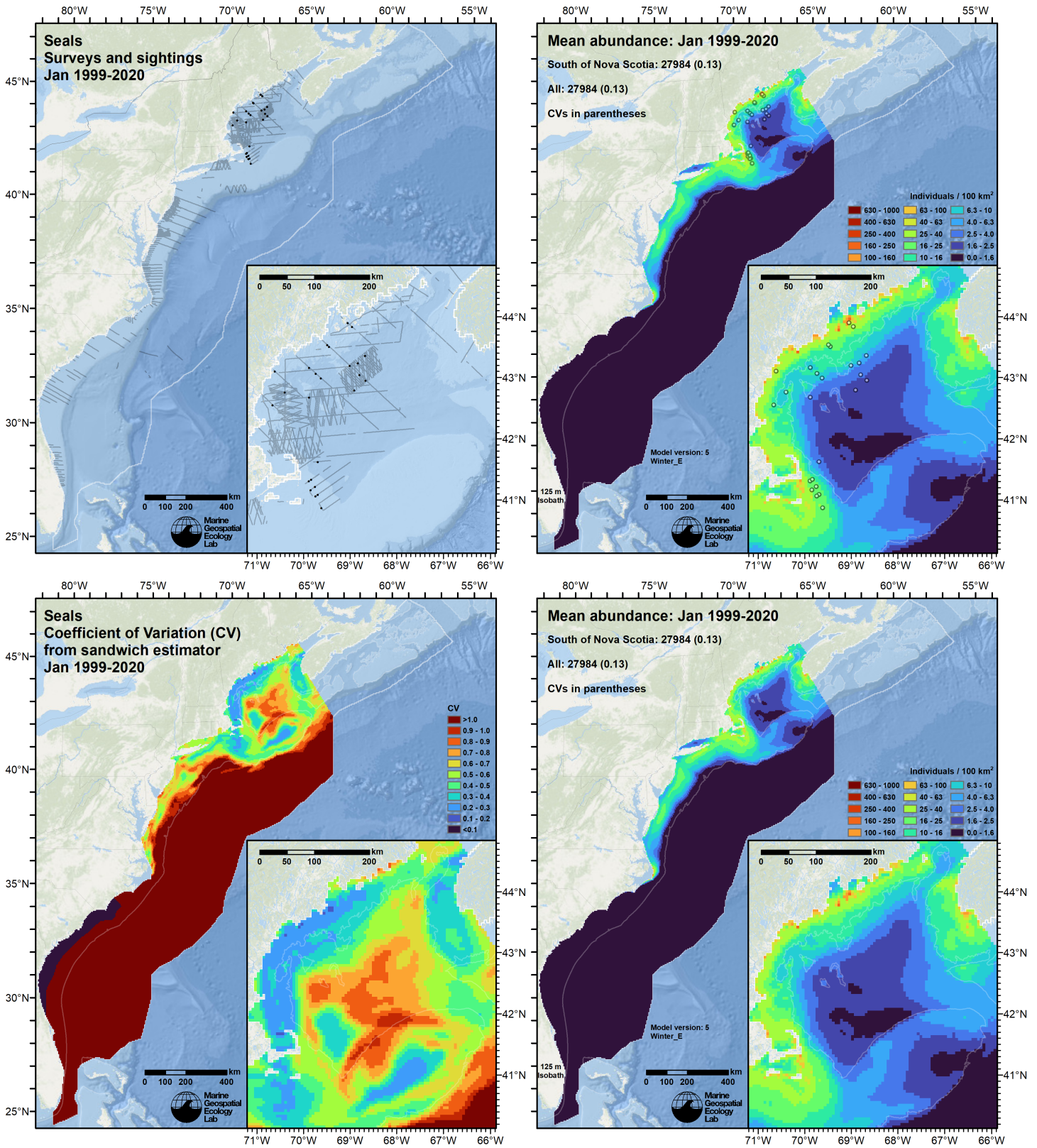
Figure 59: Survey effort and observations (top left), predicted density with observations (top right), predicted density without observations (bottom right), and coefficient of variation of predicted density (bottom left), for the month of February for the given era. Variance was estimated with the analytic approach given by Miller et al. (2022), Appendix S1, and accounts both for uncertainty in model parameter estimates and for temporal variability in dynamic covariates.

Figure 60: Survey effort and observations (top left), predicted density with observations (top right), predicted density without observations (bottom right), and coefficient of variation of predicted density (bottom left), for the month of March for the given era. Variance was estimated with the analytic approach given by Miller et al. (2022), Appendix S1, and accounts both for uncertainty in model parameter estimates and for temporal variability in dynamic covariates.
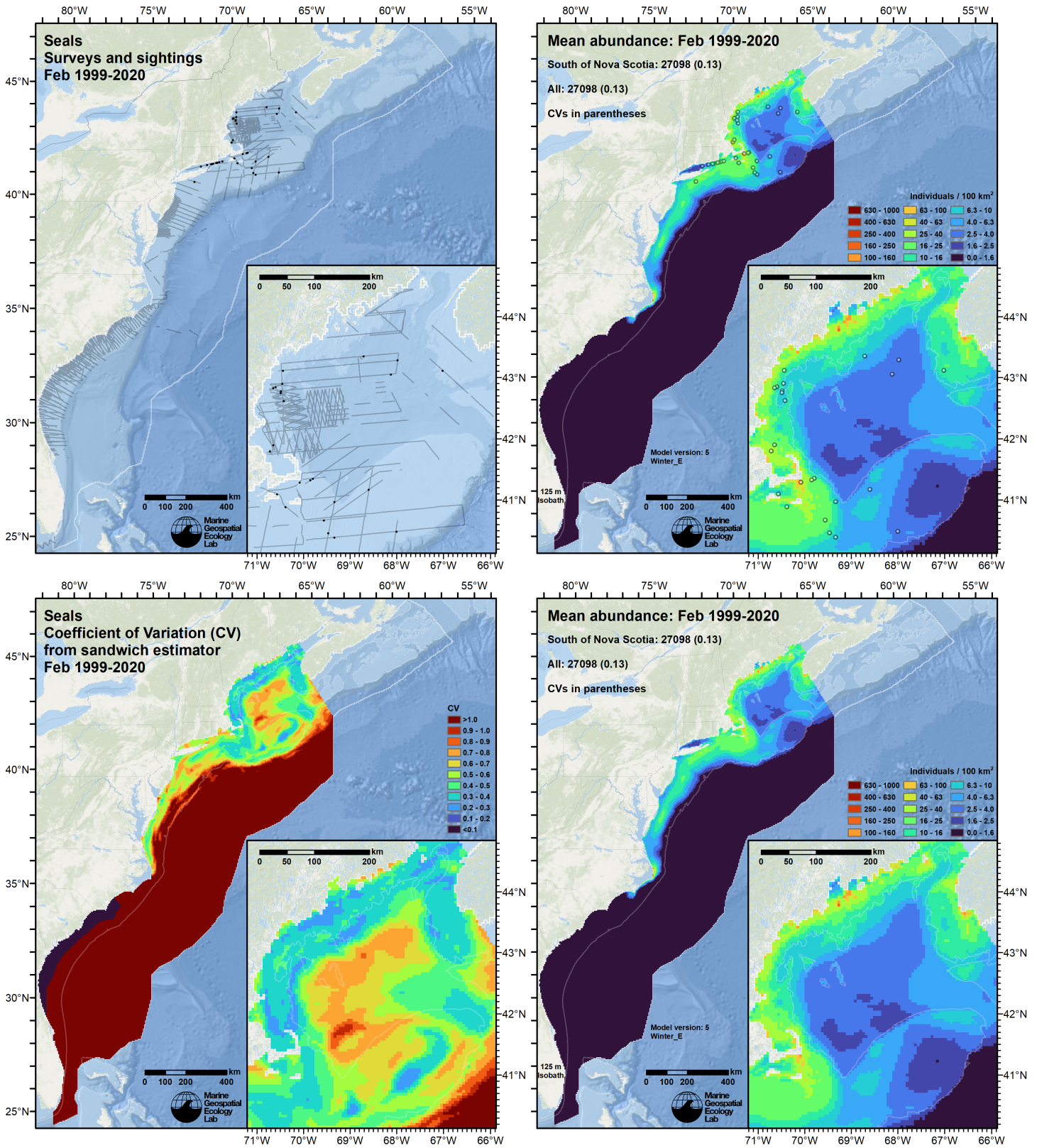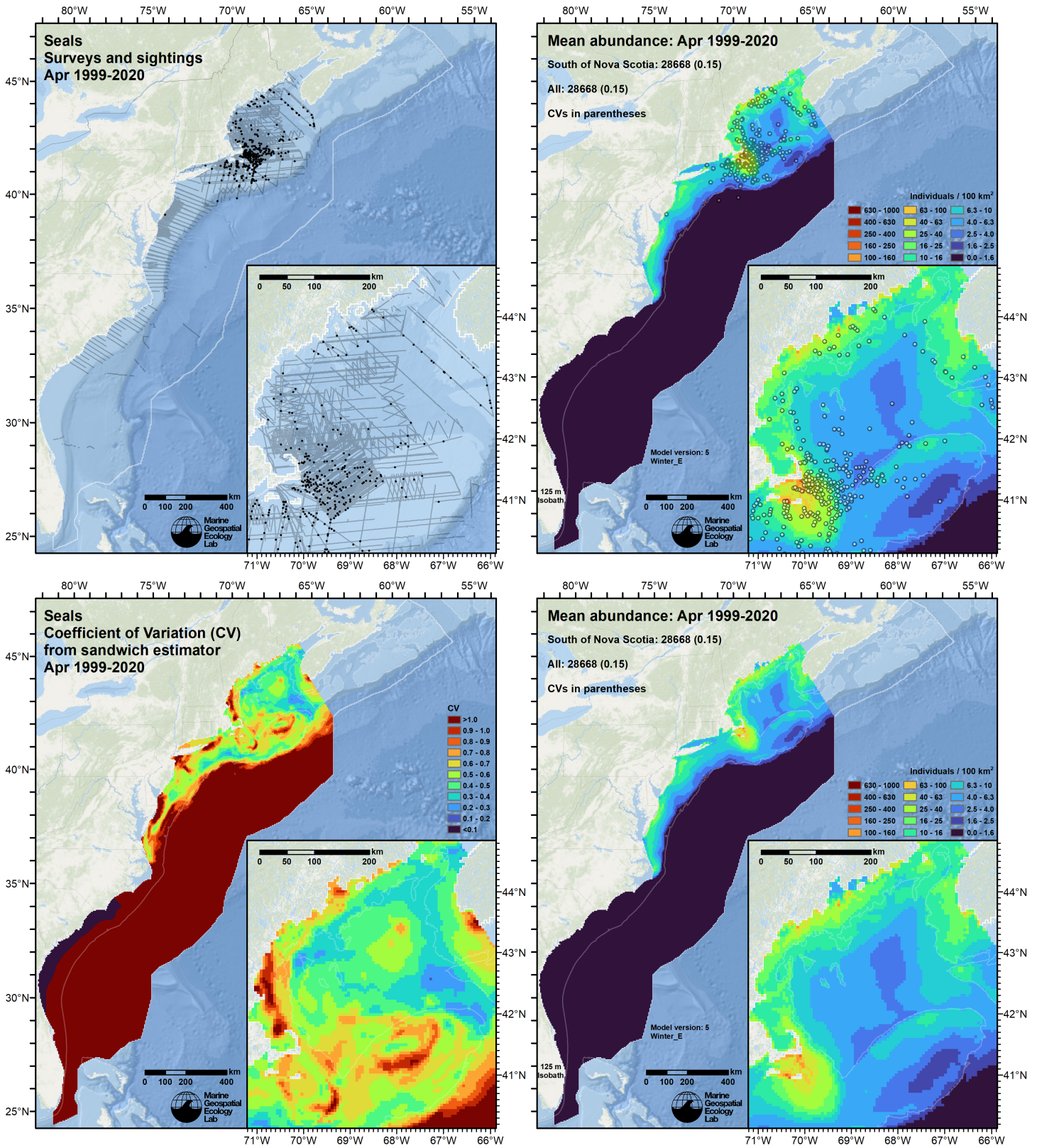
Figure 61: Survey effort and observations (top left), predicted density with observations (top right), predicted density without observations (bottom right), and coefficient of variation of predicted density (bottom left), for the month of April for the given era. Variance was estimated with the analytic approach given by Miller et al. (2022), Appendix S1, and accounts both for uncertainty in model parameter estimates and for temporal variability in dynamic covariates.
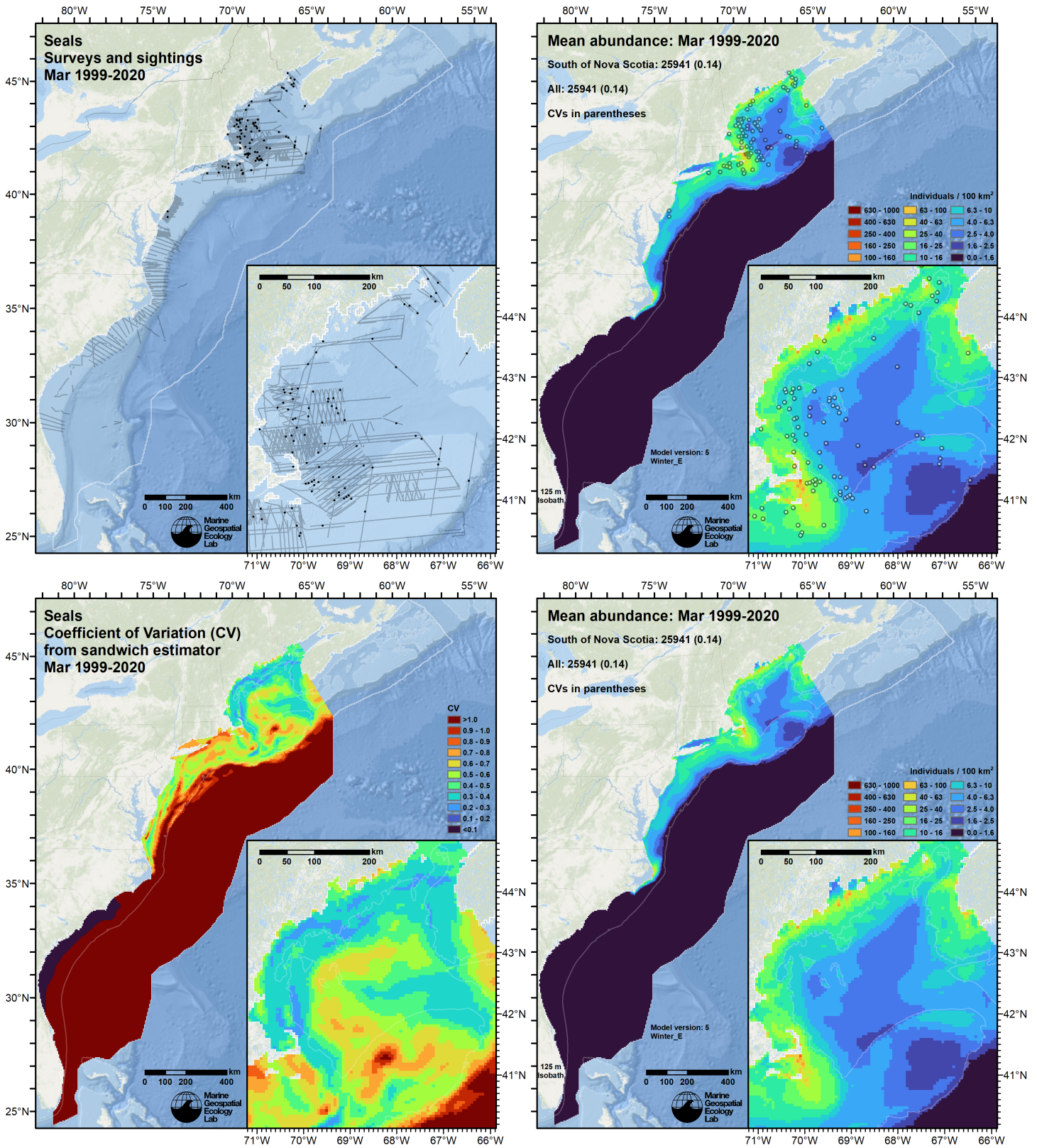
Figure 62: Survey effort and observations (top left), predicted density with observations (top right), predicted density without observations (bottom right), and coefficient of variation of predicted density (bottom left), for the month of May for the given era. Variance was estimated with the analytic approach given by Miller et al. (2022), Appendix S1, and accounts both for uncertainty in model parameter estimates and for temporal variability in dynamic covariates.
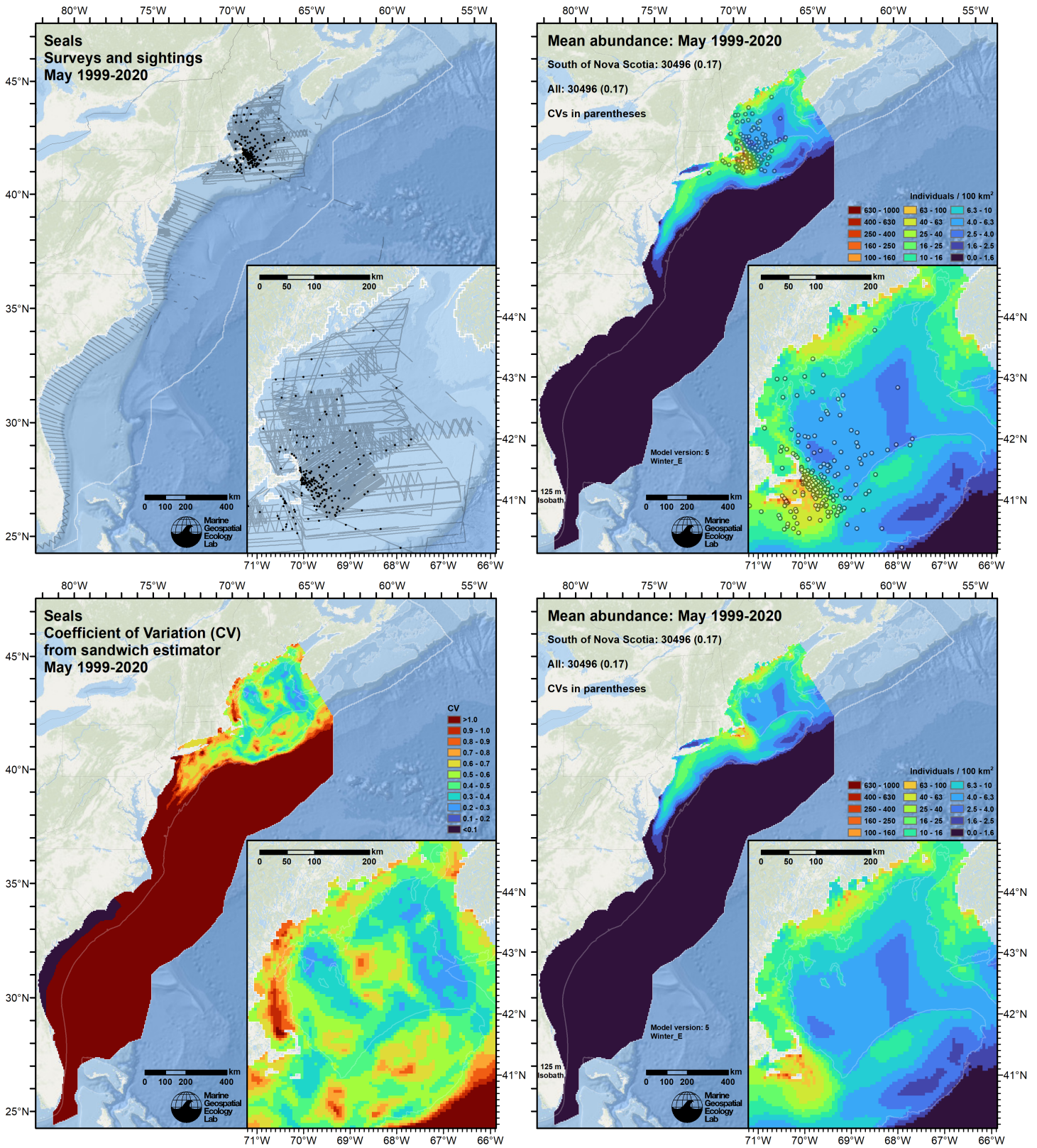
5.2 Abundance Comparisons

5.2.1 NOAA Stock Assessment Reports

Table 16: Comparison of regional abundance estimates from the NOAA Stock Assessment Reports (SARs) to estimates from this density model, extracted for comparable zones from the multi-year mean density surfaces we provide to model users (Section 5.1).

NOAA Stock Assessment Report			Density Model		
Month/Year	Stock and Area	N_{est}	Period	Zone	Abundance
May-Jun 2018	Harbor seal, Maine coast[a]	61,336			
2016	Gray seal, U.S. population[b]	27,131			
			May-Jun 1998-2020	U.S. EEZ, in water[c]	33,695
			May-Jun 1998-2020	U.S. EEZ, hauled out[d]	50,542
2016-2018	Total	88,636	May-Jun 1998-2020	Total	84,238

[a] Estimate originally from Sigourney et al. (2022) and referenced in the 2022 SAR, Hayes et al. (2022).

[b] Estimate originally from the 2020 SAR, Hayes et al. (2021), which derived it from the 2016 pup count at known pupping sites in U.S. waters reported by Wood et al. (2020) (see their Table 2). (Note that the SAR refers to this publication as being from 2019, the year it was first made available online; it first appeared in print in 2020.)

[c] Two-month mean abundance of in-water seals within the U.S. Exclusive Economic Zone, extracted from our monthly density surfaces for May (Figure 62) and June (Figure 51).

[d] Two-month mean abundance of hauled-out seals within the U.S. Exclusive Economic Zone, estimated from the in-water abundance above, under the assumption that 60% of the population is hauled out (Sigourney et al. (2022)).

5.2.2 Previous Density Model

Figure 63: Comparison of the mean density predictions from the previous model (left) released by Roberts et al. (2018) to those from this model (right) for the Summer season.
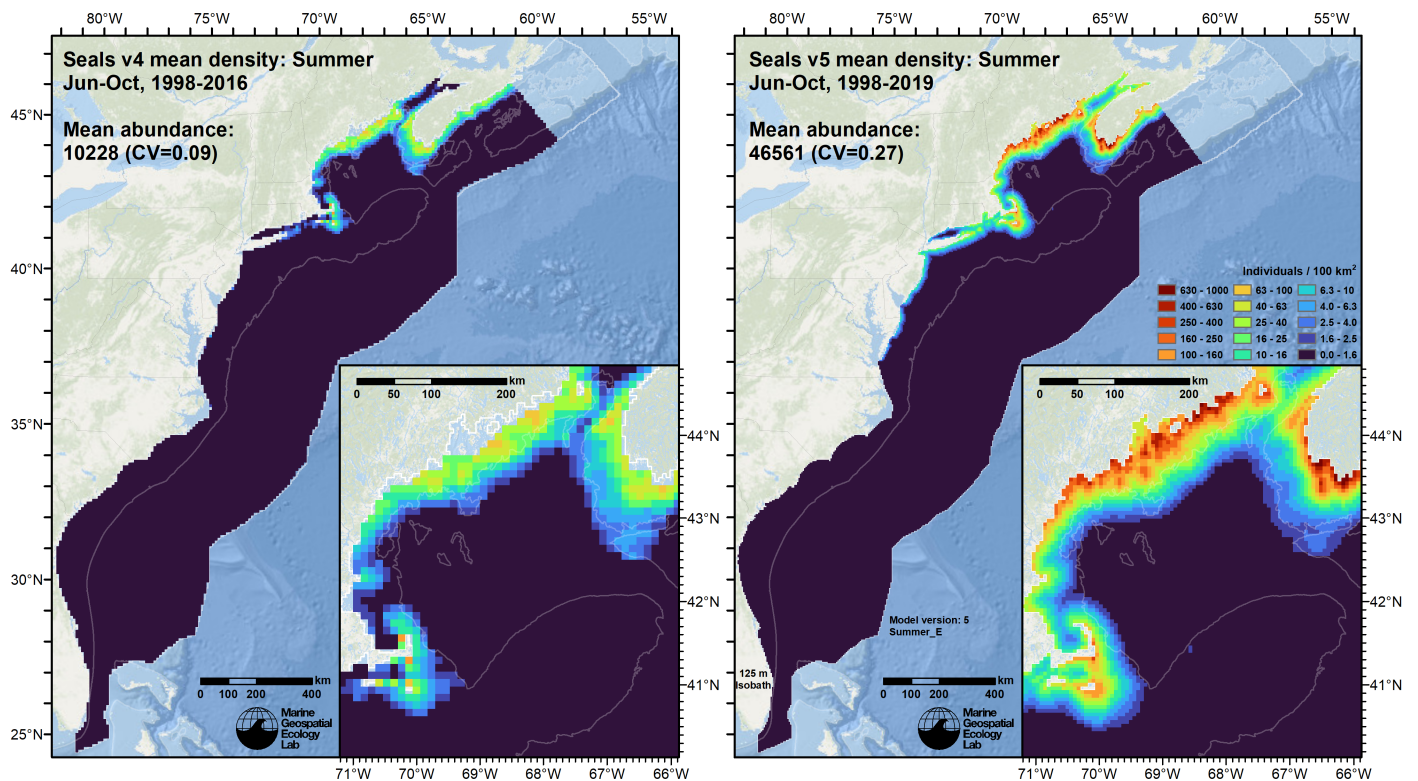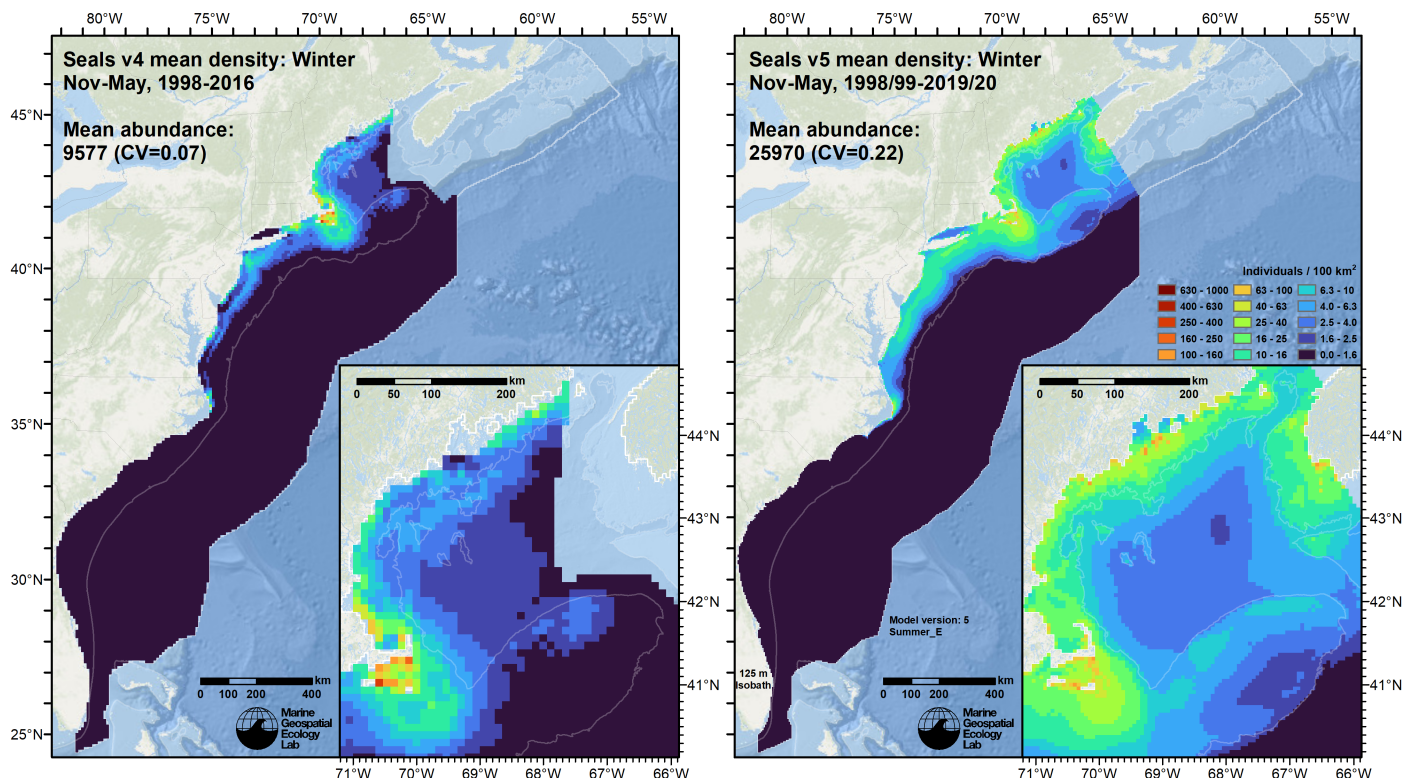
Figure 64: Comparison of the mean density predictions from the previous model (left) released by Roberts et al. (2018) to those from this model (right) for the Winter season.

6   Discussion

When summarized across the modeled period (June 1998 - May 2020), mean monthly density maps (Figures 51-62) generally agreed with the overall distributions and seasonal patterns of harbor seals and gray seals described in the literature. In the height of summer, July-September, the bulk of density was concentrated along coastal Maine and Canada, with lower but appreciable values extending down through southern New England to the northeastern tip of Long Island. In October, density began to shift south, extending down the mid-Atlantic states, and in November, out to offshore waters of the Gulf of Maine and Georges Bank. By December, some density was predicted off North Carolina and across the mid-shelf waters of the mid-Atlantic. From January-March, low to moderate densities were predicted across the shelf from Cape Lookout, North Carolina through to Canada. In April, density began shifting north, culminating in high values in southern New England and coastal Maine and Canada by June.

Comparison of our model's abundance estimates to those of the most recent NOAA Stock Assessment Reports (SARs) (Table 16) is complicated by differences in what was estimated. We estimated the abundance of all seals in the water, as a guild, while NOAA estimated the abundance of each species, accounting both for seals in the water and those hauled-out. NOAA's total estimate of harbor seals and gray seals together was 88,636. Our estimate of all seals in the water, during the May-June period in which NOAA made it's harbor seal estimate, was 33,685. Using Sigourney et al.'s (2022) estimate that 60% of the harbor seal population is hauled-out during pupping season (see their Section 3.3), we obtained a total abundance of seals in the water and hauled-out of 84,238, about 5% lower than NOAA's.

Although this small difference suggests confidence in our result, we advise caution, as there are two important caveats: First, NOAA's estimate was made for a single year for each species, while ours was an average over the 1998-2020 period. Over that period, the harbor seal population fluctuated but overall was stable or slightly declined (Sigourney et al. 2022), while the gray seal population, as assessed through pup counts, increased substantially, as much as 26.3% per annum at Monomoy Island, the fastest growing site (Wood et al. 2020). Our model does not explicitly account for growth.

Second, our method for estimating the abundance of hauled-out seals was to scale our estimate of seals in the water using Sigourney et al.'s (2022) estimated proportion (0.60) of harbor seals that were hauled-out during the May-June pupping season. Our abundance estimate for hauled-out seals is highly sensitive to that proportion, and Sigourney et al. noted that prior estimates for it ranged from 0.43 to 0.84. Furthermore, we do not know if Sigourney's estimate is transferable to gray seals. Moxley (2016) estimated from seven tagged seals that during the month of June at one site (Chatham, Massachusetts), the proportion of seals hauled-out at low tide was about 0.50, but that foraging was primarily occurring at night, which

Moxley suggested was to avoid predation by white sharks. It may be that that in May-June, considerably more than 50% of gray seals haul out during daytime, when our visual line-transect surveys occurred. If so, we should have estimated a larger number of seals hauled-out.

Returning to our predictions of seals in the water, we also advise caution with our winter season (November-May). Although the mean abundance estimated for winter (25,970) excluded Canada while summer's estimate did not, the winter estimate was disproportionately smaller, at only 56% of the estimate for summer (46,561). During winter, harbor seals move south from Maine and Canada to southern New England and spend reduced time hauled-out (Pace et al. 2019). Conversely, gray seals pup in December-February and molt in March-June, periods in which they should spend increased time hauled-out (Pace et al. 2019). Therefore, in winter, we would expect the abundance of harbor seals in the water to be higher and gray seals to be lower. It is hard to guess whether the combined effect would yield a lower total abundance. Complicating this are Moxley's (2016) results, which showed that gray seals spent roughly twice as much time hauled-out in June-October than they did in November-March, which runs contrary to Pace et al.'s description of December-June being a period of longer haul-outs for pupping and molting.

It is also possible that our lower abundances in winter months result from incorrectly modeled or unaddressed seasonal variability in detection probability, perception bias, or avilability bias. For example, the detection functions for the two largest sources of seal sightings, the NEFSC AMAPPS and 2003-2016 NARWSS aerial surveys, both retained season as a detectability covariate. The detection function for the AMAPPS program, which flew at 600 ft., had a belly port observer, and employed a protocol specifically designed to sight both large and small mammals, estimated that detection probability was substantially higher in winter and spring than in summer and fall (Figure 6). Conversely, the detection function for the 2003-2016 NARWSS program, which flew at 750 ft., did not use a belly port observer, and targeted large whales while still recording seals, estimated that detection probability was lower in fall and winter than in spring and summer (Figure 11). Although we consider AMAPPS to have the more robust survey protocol and field methods for surveying small mammals, the result of higher detection probability in winter and spring, when there is less light and worse weather, seems suspicious. If we removed this covariate from the AMAPPS detection model, it would likely push summer abundance down and winter abundance up, reducing the difference between them.

As another possiblity, although NARWSS seemed to have the seasonal effect that we expected, it might be that we still overestimated winter detection probability. There was clear evidence that NARWSS observers were missing seals close to the trackline, by virtue of the wide left-truncation distance required for the detection function (Figure 8). After left and right truncation, only about 100 seals were sighted in fall-winter, compared to about 690 in spring-summer. This is a much greater disparity than for AMAPPS, which sighted about 250 in winter-spring and 280 in summer-fall. This suggests NARWSS might be significantly worse at detecting seals in winter than in summer, although further investigation is required to rule out that the disparity might result from seasonal heterogeneity in survey effort instead. In any case, the diagnosis of differences between summer and winter density and abundance estimates should remain a focus of future updates to this model.

There are two final concerns to mention about the winter model. First, the model predicts relatively high density along the North Carolina coastline from December-March (Figures 57-60). Although seals occur regularly occur in North Carolina during this time—for example, there was an average of 9 strandings per year during 1997-2008 (Byrd et al. 2014)—it is unlikely that the coastal waters of the Outer Banks sustain the same density as southern New England. Model uncertainty is high here (as shown on the CV maps), and we believe the model likely overestimated density, probably because covariate values here during December-March were surprisingly similar to those in parts of New England where numerous sightings occurred. To correct this, we explored adding Latitude to the model as a univariate smoothed term. This very strongly reduced densities for all waters south of New Jersey, where the southernmost sightings were reported by our collaborators. Because it is well known that seals inhabit waters between North Carolina and New Jersey in winter (Ampela et al. 2021; Jones and Rees 2022), we opted against including Latitude in the model, as a precaution against underestimating density south of New Jersey.

The other final concern about the winter model involves two sightings made far offshore, beyond the continental shelf break in fairly deep waters, southeast of Long Island, both in the month of April. These sightings occur well beyond the region for which non-negigible density was predicted (Figure 61). We caution that the winter model included relatively little effort beyond the continental shelf and slope (Figure 35). Although we doubt that these coastal species occur beyond the shelf break in appreciable numbers, this cannot be ruled out until more comprehensive surveying is conducted in November-May in those offshore waters.

Given the general match between the model's predictions and what has been reported in the literature, the concerns above notwithstanding, we elected to offer density predictions for this species at monthly temporal resolution, as we did for our prior model. This model estimated about 4.5 times higher abundance in summer and 2.7 times higher abundance in winter than the prior model (Figures 63, 64). The large increase in density and abundance likely results from a combination of factors:

In the prior model we did not correct for availability bias on aerial surveys, but we did so for this model, with the bulk of corrections ranging from 0.37 to 0.40 (Figure 20). All else being equal, this change alone would more than double the density

and abundance of the prior model. Another imporant change was that for this model and the others in the 2022 modeling cycle, we expanded the study area further inshore, particularly around Maine, mainly to assist NOAA with management needs related to right whales. This added prime seal habitat that was not included in the prior model, boosting total abundance. Finally, this model included NEFSC AMAPPS aerial surveys of nearshore Maine in 2016, 2017, and 2019 which sighted particularly large numbers of seals. These surveys were not available for the prior model.

Given these differences, we do not consider the higher density and abundances predicted by the new model to be problematic. Rather, we conclude that the prior model underestimated density and abundance. Finally, we note that the prior model's CVs of its mean abundance estimates were substantially lower than those of the new model. The CVs of the prior model were unrealistically low because that model only accounted for uncertainty in model parameter estimates, while the new model also accounts for seasonal and interannual variability in predictions.

References

Ampela K, DeAngelis M, DiGiovanni R, Lockhart GG (2019) Seal Tagging and Tracking in Virginia: 2017–2018. HDR, Inc., submitted to Naval Facilities Engineering Command Atlantic, prepared for U.S. Fleet Forces Command under Contract No. N62470-15-8006, Virginia Beach, VA

Ampela K, Bort J, DeAngelis M, Jr RD, DiMatteo A (2021) Seal Tagging and Tracking in Virginia: 2019-2020. HDR, Inc., submitted to Naval Facilities Engineering Command Atlantic, prepared for U.S. Fleet Forces Command under Contract No. N62470-15-8006, Task Order 19F4147, Virginia Beach, VA

Barco SG, Burt L, DePerte A, Digiovanni R Jr. (2015) Marine Mammal and Sea Turtle Sightings in the Vicinity of the Maryland Wind Energy Area July 2013-June 2015, VAQF Scientific Report #2015-06. Virginia Aquarium & Marine Science Center Foundation, Virginia Beach, VA

Becker JJ, Sandwell DT, Smith WHF, Braud J, Binder B, Depner J, Fabre D, Factor J, Ingalls S, Kim S-H, Ladner R, Marks K, Nelson S, Pharaoh A, Trimmer R, Von Rosenberg J, Wallace G, Weatherall P (2009) Global Bathymetry and Elevation Data at 30 Arc Seconds Resolution: SRTM30_PLUS. Marine Geodesy 32:355–371. doi: 10.1080/01490410903297766

Behrenfeld MJ, Falkowski PG (1997) Photosynthetic rates derived from satellite-based chlorophyll concentration. Limnology and oceanography 42:1–20. doi: 10.4319/lo.1997.42.1.0001

Bowen WD, McMillan J, Mohn R (2003) Sustained exponential population growth of grey seals at Sable Island, Nova Scotia. ICES Journal of Marine Science 60:1265–1274. doi: 10.1016/S1054-3139(03)00147-4

Brasnett B (2008) The impact of satellite retrievals in a global sea-surface-temperature analysis. Quarterly Journal of the Royal Meteorological Society 134:1745–1760. doi: 10.1002/qj.319

Breed GA, Bowen WD, McMillan JI, Leonard ML (2006) Sexual segregation of seasonal foraging habitats in a non-migratory marine mammal. Proc R Soc B 273:2319–2326. doi: 10.1098/rspb.2006.3581

Buckland ST, Anderson DR, Burnham KP, Laake JL, Borchers DL, Thomas L (2001) Introduction to Distance Sampling: Estimating Abundance of Biological Populations. Oxford University Press, Oxford, UK

Burt ML, Borchers DL, Jenkins KJ, Marques TA (2014) Using mark-recapture distance sampling methods on line transect surveys. Methods in Ecology and Evolution 5:1180–1191. doi: 10.1111/2041-210X.12294

Byrd BL, Harms CA, Hohn AA, McLellan WA, Lovewell GN, Moore KT, Altman KM, Rosel PE, Barco SG, Thayer VG, Friedlaender A (2014) Strandings as indicators of marine mammal biodiversity and human interactions off the coast of North Carolina. Fishery Bulletin 112:1–23. doi: 10.7755/FB.112.1.1

Canada Meteorological Center (2012) GHRSST Level 4 CMC0.2deg Global Foundation Sea Surface Temperature Analysis Version 2.0. PODAAC, CA, USA. doi: 10.5067/GHCMC-4FM02

Canada Meteorological Center (2016) GHRSST Level 4 CMC0.1deg Global Foundation Sea Surface Temperature Analysis Version 3.0. PODAAC, CA, USA. doi: 10.5067/GHCMC-4FM03

Canny JF (1986) A computational approach to edge detection. IEEE Transactions on Pattern Analysis and Machine Intelligence 8:679–698. doi: 10.1016/B978-0-08-051581-6.50024-6

Chassignet E, Hurlburt H, Metzger EJ, Smedstad O, Cummings J, Halliwell G, Bleck R, Baraille R, Wallcraft A, Lozano C, Tolman H, Srinivasan A, Hankin S, Cornillon P, Weisberg R, Barth A, He R, Werner F, Wilkin J (2009) US GODAE: Global Ocean Prediction with the HYbrid Coordinate Ocean Model (HYCOM). Oceanog 22:64–75. doi: 10.5670/oceanog.2009.39

Cole T, Gerrior P, Merrick RL (2007) Methodologies of the NOAA National Marine Fisheries Service Aerial Survey Program for Right Whales (Eubalaena glacialis) in the Northeast U.S., 1998-2006. U.S. Department of Commerce, Woods Hole, MA

den Heyer CE, Bowen WD, Dale J, Gosselin J, Hammill MO, Johnston DW, Lang SLC, Murray KT, Stenson GB, Wood SA (2021) Contrasting trends in gray seal (*Halichoerus Grypus*) pup production throughout the increasing northwest Atlantic metapopulation. Mar Mam Sci 37:611–630. doi: 10.1111/mms.12773

Garrison LP, Martinez A, Maze-Foley K (2010) Habitat and abundance of cetaceans in Atlantic Ocean continental slope waters off the eastern USA. Journal of Cetacean Research and Management 11:267–277.

Geo-Marine, Inc. (2010) New Jersey Department of Environmental Protection Baseline Studies Final Report Volume III: Marine Mammal and Sea Turtle Studies. Geo-Marine, Inc., Plano, TX

Gilbert JR, Waring GT, Wynne KM, Guldager N (2005) Changes in Abundance of Harbor Seals in Maine, 1981–2001. Marine Mammal Science 21:519–535. doi: 10.1111/j.1748-7692.2005.tb01246.x

Haverkamp H, Chang H, Newcomb E, Doughty L, Walk D, Seton R, Jones LS, Todd S, Cammen KM (2023) A retrospective socio-ecological analysis of seal strandings in the Gulf of Maine. Marine Mammal Science 39:232–250. doi: 10.1111/mms.12975

Hayes SA, Josephson E, Maze-Foley K, Rosel PE, Byrd B, Chavez-Rosales S, Cole TVN, Garrison LP, Hatch JM, Henry A, Horstman SC, Litz J, Lyssikatos MC, Mullin KD, Orphanides C, Pace RM, Palka DL, Powell J, Wenzel FW (2019) US Atlantic and Gulf of Mexico Marine Mammal Stock Assessments - 2018. NOAA National Marine Fisheries Service, Northeast Fisheries Science Center, Woods Hole, MA

Hayes SA, Josephson EA, Maze-Foley K, Rosel PE, Turek J, Byrd B, Chavez-Rosales S, Cole TVN, Garrison LP, Hatch J, Henry A, Horstman SC, Litz J, Lyssikatos MC, Mullin KD, Orphanides C, Ortega-Ortiz J, Pace RM, Palka DL, Powell J, Rappucci G, Wenzel FW (2021) US Atlantic and Gulf of Mexico Marine Mammal Stock Assessments 2020. NOAA National Marine Fisheries Service, Northeast Fisheries Science Center, Woods Hole, MA

Hayes SA, Josephson E, Maze-Foley K, Rosel PE, Wallace J, Brossard A, Chavez-Rosales S, Cole TVN, Garrison LP, Hatch J, Henry A, Horstman SC, Litz J, Lyssikatos MC, Mullin KD, Murray K, Orphanides C, Ortega-Ortiz J, Pace RM, Palka DL, Powell J, Rappucci G, Soldevilla M, Wenzel FW (2022) US Atlantic and Gulf of Mexico Marine Mammal Stock Assessments 2021. NOAA National Marine Fisheries Service, Northeast Fisheries Science Center, Woods Hole, MA

Johnston DW, Frungillo J, Smith A, Moore K, Sharp B, Schuh J, Read AJ (2015) Trends in Stranding and By-Catch Rates of Gray and Harbor Seals along the Northeastern Coast of the United States: Evidence of Divergence in the Abundance of Two Sympatric Phocid Species? PLOS ONE 10:e0131660. doi: 10.1371/journal.pone.0131660

Jones DV, Rees DR (2022) Haul-out Counts and Photo-Identification of Pinnipeds in Chesapeake Bay and Eastern Shore, Virginia: 2020/2021 Annual Progress Report. Naval Facilities Engineering Command Atlantic, prepared for U.S. Fleet Forces Command, Norfolk, VA

Laake JL, Calambokidis J, Osmek SD, Rugh DJ (1997) Probability of Detecting Harbor Porpoise From Aerial Surveys: Estimating g(0). Journal of Wildlife Management 61:63–75. doi: 10.2307/3802415

Lehodey P, Senina I, Murtugudde R (2008) A spatial ecosystem and populations dynamics model (SEAPODYM)–Modeling of tuna and tuna-like populations. Progress in Oceanography 78:304–318. doi: 10.1016/j.pocean.2008.06.004

Lehodey P, Conchon A, Senina I, Domokos R, Calmettes B, Jouanno J, Hernandez O, Kloser R (2015) Optimization of a micronekton model with acoustic data. ICES Journal of Marine Science 72:1399–1412. doi: 10.1093/icesjms/fsu233

Lesage V, Hammill MO (2001) The status of the grey seal, Halichoerus grypus, in the Northwest Atlantic. Canadian Field-Naturalist 115:653–666.

Lesage V, Hammill MO, Kovacs KM (1999) Functional classification of harbor seal (Phoca vitulina) dives using depth profiles, swimming velocity, and an index of foraging success. Can J Zool 77:74–87. doi: 10.1139/z98-199

Lesage V, Hammill MO, Kovacs KM (2004) Long-distance movements of harbour seals (*Phoca Vitulina*) from a seasonally ice-covered area, the St. Lawrence River estuary, Canada. Can J Zool 82:1070–1081. doi: 10.1139/z04-084

Marsh H, Sinclair DF (1989) Correcting for Visibility Bias in Strip Transect Aerial Surveys of Aquatic Fauna. The Journal of Wildlife Management 53:1017. doi: 10.2307/3809604

McLellan WA, McAlarney RJ, Cummings EW, Read AJ, Paxton CGM, Bell JT, Pabst DA (2018) Distribution and abundance of beaked whales (Family Ziphiidae) Off Cape Hatteras, North Carolina, U.S.A. Marine Mammal Science. doi: 10.1111/mms.12500

Meissner T, Wentz FJ, Scott J, Vazquez-Cuervo J (2016) Sensitivity of Ocean Surface Salinity Measurements From Spaceborne L-Band Radiometers to Ancillary Sea Surface Temperature. IEEE Trans Geosci Remote Sensing 54:7105–7111. doi: 10.1109/TGRS.2016.2596100

Mesgaran MB, Cousens RD, Webber BL (2014) Here be dragons: A tool for quantifying novelty due to covariate range and correlation change when projecting species distribution models. Diversity Distrib 20:1147–1159. doi: 10.1111/ddi.12209

Miller DL, Becker EA, Forney KA, Roberts JJ, Cañadas A, Schick RS (2022) Estimating uncertainty in density surface models. PeerJ 10:e13950. doi: 10.7717/peerj.13950

Moxley JH (2016) The Abundance and Behavioral Ecology of Cape Cod Gray Seals Under Predation Risk from White Sharks. PhD thesis, Duke University

Mullin KD, Fulling GL (2003) Abundance of cetaceans in the southern U.S. North Atlantic Ocean during summer 1998. Fishery Bulletin 101:603–613.

Pace R, Josephson E, Wood SA, Murray K, Waring G (2019) Trends and Patterns of Seal Abundance at Haul-out Sites in a Gray Seal Recolonization Zone, NOAA Technical Memorandum NMFS-NE-251. NOAA National Marine Fisheries Service, Northeast Fisheries Science Center, Woods Hole, MA

Palka D, Aichinger Dias L, Broughton E, Chavez-Rosales S, Cholewiak D, Davis G, DeAngelis A, Garrison L, Haas H, Hatch J, Hyde K, Jech M, Josephson E, Mueller-Brennan L, Orphanides C, Pegg N, Sasso C, Sigourney D, Soldevilla M, Walsh H (2021) Atlantic Marine Assessment Program for Protected Species: FY15 – FY19 (OCS Study BOEM 2021-051). U.S. Deptartment of the Interior, Bureau of Ocean Energy Management, Washington, DC

Palka DL (2006) Summer abundance estimates of cetaceans in US North Atlantic navy operating areas (NEFSC Reference Document 06-03). U.S. Department of Commerce, Northeast Fisheries Science Center, Woods Hole, MA

Palka DL, Chavez-Rosales S, Josephson E, Cholewiak D, Haas HL, Garrison L, Jones M, Sigourney D, Waring G, Jech M, Broughton E, Soldevilla M, Davis G, DeAngelis A, Sasso CR, Winton MV, Smolowitz RJ, Fay G, LaBrecque E, Leiness JB, Dettloff K, Warden M, Murray K, Orphanides C (2017) Atlantic Marine Assessment Program for Protected Species: 2010-2014 (OCS Study BOEM 2017-071). U.S. Deptartment of the Interior, Bureau of Ocean Energy Management, Washington, DC

Payne PM, Selzer LA (1989) The Distribution, Abundance and Selected Prey of the Harbor Seal, Phoca Vitulina Concolor, in Southern New England. Marine Mammal Science 5:173–192. doi: 10.1111/j.1748-7692.1989.tb00331.x

Reay N (2005) Estimation of g(0) for bottlenose dolphin, grey seal, and harbour porpoise in Cardigan Bay SAC. Master's thesis, University of Wales, Bangor

Roberts JJ, Best BD, Dunn DC, Treml EA, Halpin PN (2010) Marine Geospatial Ecology Tools: An integrated framework for ecological geoprocessing with ArcGIS, Python, R, MATLAB, and C++. Environmental Modelling & Software 25:1197–1207. doi: 10.1016/j.envsoft.2010.03.029

Roberts JJ, Best BD, Mannocci L, Fujioka E, Halpin PN, Palka DL, Garrison LP, Mullin KD, Cole TVN, Khan CB, McLellan WA, Pabst DA, Lockhart GG (2016) Habitat-based cetacean density models for the U.S. Atlantic and Gulf of Mexico. Scientific Reports 6:22615. doi: 10.1038/srep22615

Roberts JJ, Mannocci L, Schick RS, Halpin PN (2018) Final Project Report: Marine Species Density Data Gap Assessments and Update for the AFTT Study Area, 2017-2018 (Opt. Year 2), Document Version 1.2. Duke University Marine Geospatial Ecology Lab, Durham, NC

Roberts JJ, Yack TM, Halpin PN (2023) Marine mammal density models for the U.S. Navy Atlantic Fleet Training and Testing (AFTT) study area for the Phase IV Navy Marine Species Density Database (NMSDD), Document Version 1.3. Duke University Marine Geospatial Ecology Lab, Durham, NC

Robertson FC, Koski WR, Brandon JR, Thomas TA, Trites AW (2015) Correction factors account for the availability of bowhead whales exposed to seismic operations in the Beaufort Sea. Journal of Cetacean Research and Management 15:35–44.

Ryan C, Boisseau O, Cucknell A, Romagosa M, Moscrop A, McLanaghan R (2013) Final report for trans-Atlantic research passages between the UK and USA via the Azores and Iceland, conducted from R/V Song of the Whale 26 March to 28 September 2012. Marine Conservation Research International, Essex, UK

Sigourney DB, Murray KT, Gilbert JR, Ver Hoef JM, Josephson E, DiGiovanni RA (2022) Application of a Bayesian hierarchical model to estimate trends in Atlantic harbor seal (*Phoca Vitulina Vitulina*) abundance in Maine, U.S.A., 1993–2018. Marine Mammal Science 38:500–516. doi: 10.1111/mms.12873

Toth J, Evert S, Zimmermann E, Sullivan M, Dotts L, Able KW, Hagan R, Slocum C (2018) Annual Residency Patterns and Diet of Phoca vitulina concolor (Western Atlantic Harbor Seal) in a Southern New Jersey Estuary. Northeastern Naturalist 25:611. doi: 10.1656/045.025.0407

Vance HM, Hooker SK, Mikkelsen L, van Neer A, Teilmann J, Siebert U, Johnson M (2021) Drivers and constraints on offshore foraging in harbour seals. Scientific Reports 11:14. doi: 10.1038/s41598-021-85376-2

Whitt AD, Powell JA, Richardson AG, Bosyk JR (2015) Abundance and distribution of marine mammals in nearshore waters off New Jersey, USA. Journal of Cetacean Research and Management 15:45–59.

Wood SA, Murray KT, Josephson E, Gilbert J (2020) Rates of increase in gray seal (Halichoerus grypus atlantica) pupping at recolonized sites in the United States, 1988–2019. Journal of Mammalogy 101:121–128. doi: 10.1093/jmammal/gyz184

Wood SN (2011) Fast stable restricted maximum likelihood and marginal likelihood estimation of semiparametric generalized linear models. Journal of the Royal Statistical Society: Series B (Statistical Methodology) 73:3–36. doi: 10.1111/j.1467-9868.2010.00749.x